National Technical University of Athens
School of Civil Engineering
Geotechnical Division

Εθνικό Μετσόβιο Πολυτεχνείο
Σχολή Πολιτικών Μηχανικών
Τομέας Γεωτεχνικής

Diploma Thesis by

Panopoulos Vasileios

Supervised by

N. Gerolymos

DEVELOPMENT OF AN ALGORITHM FOR COMPUTATION AND VISUALIZATION OF INTERNAL FORCES IN 3D STRUCTURAL ELEMENTS: APPLICATION TO THE NON-LINEAR LATERAL RESPONSE OF PILES

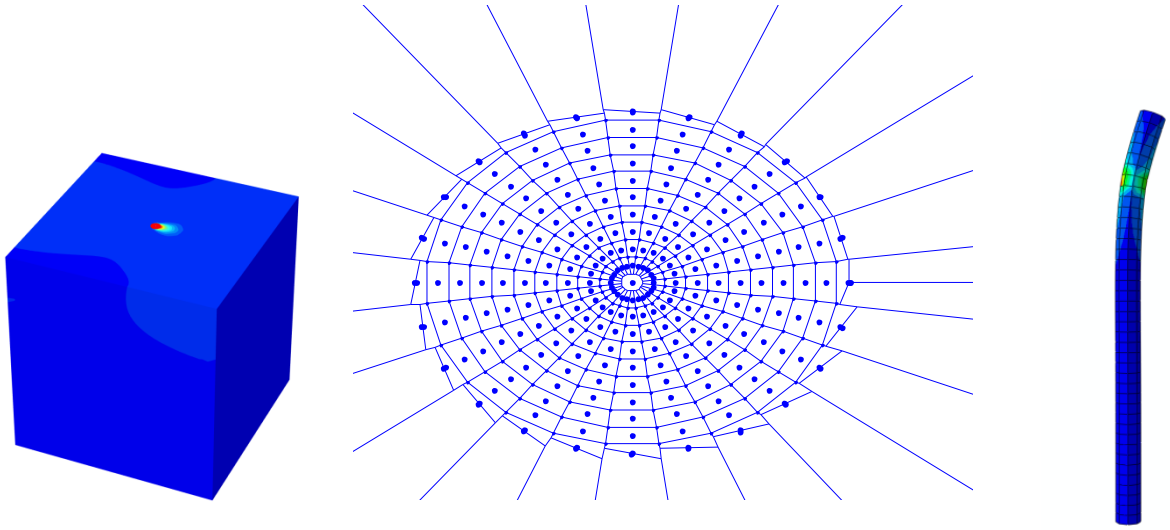

ΑΛΓΟΡΙΘΜΟΣ ΓΙΑ ΤΟΝ ΥΠΟΛΟΓΙΣΜΟ ΚΑΙ ΤΗΝ ΑΠΕΙΚΟΝΙΣΗ ΕΝΤΑΤΙΚΩΝ ΜΕΓΕΘΩΝ ΣΕ ΤΡΙΔΙΑΣΤΑΤΑ ΔΟΜΙΚΑ ΣΤΟΙΧΕΙΑ: ΕΦΑΡΜΟΓΗ ΣΤΗ ΜΗ-ΓΡΑΜΜΙΚΗ ΕΓΚΑΡΣΙΑ ΑΠΟΚΡΙΣΗ ΠΑΣΣΑΛΟ-ΟΜΑΔΑΣ

Διπλωματική Εργασία

Πανόπουλου Βασίλειου

Επιβλέπων

Ν. Γερόλυμος

Μάϊος 2014

Acknowledgements

Upon completing my diploma thesis, I feel the need to thank the people that supported and encouraged me throughout my work.

This thesis would not have been possible without my supervisor, assistant Professor N. Gerolymos, to whom I owe my respectful gratitude not only for the inspiration provided, but also for his guidance, help and patience. His contribution to solving the challenging obstacles that arised throughout this thesis was really considerable.

I would also like to express my deepest appreciation and gratitude to Professor G. Gazetas, for his valuable guidance throughout my studies. He has been an endless source of inspiration and has greatly contributed to the love that I have developed towards Engineering in general and Geotechnical Engineering in particular.

I would like to thank assistant Professor I. Anastasopoulos for the interest shown and all the people of the Geotechnical Department and Soil Mechanics laboratory for their kind embrace as well as my fellow students and friends for the experiences we shared.

Finally, above all, I feel the need to thank my family for their consistent support and encouragement.

Table of Contents

Chapter 1

Introduction

1 Introduction

1.1 Scope

The purpose of this thesis is to investigate the behaviour of pile foundations under combined axial, horizontal and moment loading. Assuming undrained conditions, primary goal is the proposition of a new method, which utilizes the results of the Finite Element Analysis so as to calculate the structural forces of the pile. This is attempted in a way so as to overcome the drawbacks of the existing methods and take fully into consideration the 3-D geometry of the pile, the interaction between the piles and the interaction between the internal forces. To capture the accurate pile behaviour, it is used a new macroscopic approach that was developed in Papakyriakopoulos' thesis. The validity of this approach is examined in an alternative scope, so as to both corroborate its results and also extract the pile forces. The method of the internal forces calculation is implemented in various types of loading, soil profiles and border conditions. The pile forces of a single pile are examined in the first stage and, in addition, the interaction of piles in Pile-group is studied. Emphasis is given to the interaction between the pile axial force and its moment capacity and moment distribution. Although this method is implemented to piles, its use can be further extended to any other structural element and provide a tool that could be proven effective for various applications of civil engineer.

1.2 Use of Pile Foundations

Fig 1.1 presents a rough categorization of the types of foundations that are generally used in order to support structural systems. Surface or shallow embedded foundations are distinguished by small slenderness ratios, while pile foundations are generally more slender elements. Caisson foundations lie somewhere in between in terms of slenderness or embedment; yet their limits are vague. The compressibility of the soil and the structural element should also be taken into consideration for a more realistic distinction of different foundation types.

Pile foundations are typically made from steel or reinforced concrete and possibly timber. They are principally used to transfer the loads from a superstructure, through weak, compressible strata or water onto stronger, more compact, less compressible and stiffer soil or rock at depth, increasing the effective size of a foundation and resisting horizontal loads (Tomlinson & Woodward, 2007). They are used in very large buildings, off-shore structures, bridge piers and in situations where the soil under the superstructure is not suitable to prevent excessive settlement. Piles can be classified by their function:

- End bearing piles are those where most of the friction is developed at the toe.

- Friction piles are those where most of the pile bearing capacity is developed by shear stresses along the sides of the pile (Atkinson, 2007).

There are two types of pile foundation installations: driven piles and bored piles:

- Driven piles are normally made from pre-cast concrete which is then hammered into the ground once on site.

- Bored piles are cast in situ; the soil is bored out of the ground, under reaming is performed and then the concrete is poured into the hole. Alternatively, boring of the soil and pouring of the concrete can take place simultaneously, in which case the piles are called continuous fight augured (CFA) piles.

The choice of pile used depends on the location and type of structure, the ground conditions, durability of the materials in the environment and cost. Most piles use some end bearing and some friction, in order to resist the action of loads. Driven piles are useful in offshore applications, are stable in soft squeezing soils and can densify loose soil. However, bored piles are more popular in urban areas as there is

minimal vibration, they can be used where headroom is limited, there is no risk of heave and it is easy to vary their length. Deeply embedded foundations have been consistently used in major offshore structures, where the study of their response under combined vertical, shear and moment loading is of great importance.

1.3 Piles under lateral loading

In Pile foundations the lateral loads are applied principally in two ways:

- Horizontal static and dynamic loads in the head of the piles, e.g. due to wind, earthquake, forces from the superstructure, sea waves etc.
- Horizontal loads along the length of the pile-side, e.g. in piled walls, bridge pier foundations, piles for soil improvement. These piles are usually vertical and in special circumstances inclined.

The vertical piles undertake horizontal loads with simultaneous bending and lateral displacement, activating in this way not only their resistance but that of the surrounding soil too.

The control of the ultimate capacity in horizontal loading must contain:

- The ultimate capacity of the surrounding soil
- The pile resistance as carrying member in bending due to lateral stresses
- The maximum displacement of the pile head, i.e. acceptable from the superstructure.

The behavior of the piles in horizontal loads depends on many factors as the relative stiffness of the pile soil system, the stress-strain relation (pile and soil), the soil resistance and the fixity conditions of the pile head.
The head of the pile, depending on whether the pile is single, belongs to a pile group, or in other special fixity conditions, might be considered free, pined, or fully fixed.
With respect to the forms of the horizontal loads- displacement diagrams of the total pile, the piles might be considered as

- Rigid in the case that they rotate around a specific pivot point, without their significant deformation.
- Flexible in case that their response can be simulated by an elastic beam in elastic soil.

The piles can be categorized also in respect to the ratio L/D (L=length, D=diameter). A short pile behaves and rotates as a rigid body under lateral loads and has a ratio L/D<10. When vertical loads are applied, the loads transferred to the tip of the pile are a percentage of the total. In the case of the long pile (L/D>10), after a certain length (active length l_c) the rest of the pile remains inactive under lateral loading. Under vertical loading the forces are received by the friction of the pile walls at full length.

The active Length l_c is the minimum length after which the displacement at the pile head under a certain lateral load remains unaffected.

- $L \geq l_c : flexible$
- $l_c/_2 < L < l_c : stiff$
- $L \leq l_c/_2 : rigid$

According to Gazetas (1991) the equations that determine the active length in an elastic half-space, are dependent of the soil elastic modulus distribution (Fig 1.2.a – 1.2.c).

$$l_c \approx 1.5\, d \left(\frac{E_p}{E_s}\right)^{0.25}, for\ uniform\ distribution$$

$$l_c \approx 1.5\, d \left(\frac{E_p}{\widetilde{E_s}}\right)^{0.22}, for\ linear\ increase\ of\ E_s\ with\ depth$$

$$l_c \approx 1.5\, d \left(\frac{E_p}{\widetilde{E_s}}\right)^{0.20}, for\ parabolic\ increase\ of\ E_s\ with\ depth$$

1.4 Beam on Winkler foundation

The Winkler model uses the beam elements to simulate the pile and adopts an infinite number of closely spaced unconnected springs to model the soil reactions. Thus the displacement at any point is directly related to the contact pressure at that point. The stiffness of these springs is uniquely defined by the foundation modulus k. Later, improved theories have been introduced on refinement of Winkler's model, by visualizing various types of interconnections such as shear layers among the Winkler springs. These theories have been attempted to find an applicable and simple representation of foundation materials at the contact area. All these models are mathematically equivalent, but they differ only in definition of the foundation parameters. The foundation modeling methods, including the usage of formal expansions, show that the first order approximation corresponds to the compressibility term of an improved approximation, including the effect of the shear interactions. Bernoulli-Euler beam theory, Timoshenko beam theory and refined beam theory (Reddy's simplified third-order beam theory) are the mainly used beam theories for bending analysis.

The Winkler model is frequently adopted to describe and simulate the soil behavior. Its simplicity allows closed-form solutions to be found for various problems. However, regardless the validity of the soil response, the Winkler model is generally founded on the method of calibration of the spring coefficients, the dashpot coefficients and their set-up. Physics of the soil, its constitutive model that describes the properties of the soil, its plastic flow rule and its interaction with the pile, are not examined thoroughly. Instead, the proposed approach offers a more technical solution that is case sensitive and do not apply at all ranges of pile loading. Furthermore, the beam elements are one dimensional, so they are not able to reproduce the pile interaction with other elements, owed to its dimensions. Finally, the beam elements of the pile, may respond well to moment – shear force combination, but this is not the case with moment - axial force combination. Elastic theories are not taking into account the interaction between axial force and the pile bearing capacity, thus neither the beneficial contribution of the compression force nor the disadvantageous influence of the tension force are considered.

1.5 Beam – Plate hybrid in 3-D soil elements

This method proposes a linear viscoelastic pile. It is represented with a series of 3D Euler-Bernoulli beam elements. The connection of the beam nodes with the corresponding peripheral soil nodes is established through appropriate kinematic constraints in order to properly model the pile geometry. In this way, each pile section behaves as a rigid disk: rotation is allowed on the condition that the disk remains always perpendicular to the beam axis, but stretching cannot occur. Finally, full-bonding conditions are assumed at pile-soil interface, which is a simplification of reality.

However, a number of drawbacks stem when extracting pile capacity and pile internal forces from this approach. First, the aforementioned method is widely used in commercially available codes, as the moment-curvature or axial force – strain constitutive laws work only with beam elements. Furthermore, the interplay between axial and bending responses is either not taken into account or is captured in an oversimplified manner, as mentioned above, on beam on Winkler foundation.

In addition, modeling piles with beam elements is a crude approximation of reality which may lead erroneous results. This is attributed to the one-dimensional nature of beams (their thickness, or diameter in case of circular piles, is geometrically zero) that fails to reproduce the lateral capacity of the pile (which is directly proportional to pile diameter). Moreover, the pile-to-pile interaction in the case of a pile group depends on the pile spacing ratio s/d. Since diameter (d) is zero, this ratio cannot be defined and its influence is not taken into account.

Moreover, the effect of soil confining pressure on the increase of the bending moment capacity of the pile is totally neglected when the latter is modeled with beam elements. This effect is amplified in lateral loading due to the development of large passive pressures on the pile opposed to the direction of its movement.

Finally, any benefits that stem from the -up to a point- 3-D functionality of the pile due to the rigid disks, perpendicular to the beam along the pile length, they have limited value to the enhanced validity of the results. This is because the Beam - Plate hybrid response resembles to the Euler - Bernoulli beam, as the cross sections are perpendicular to the bending line. This assumption is not true and may produce results that deviate from the accurate solution, especially in dynamic problems.

1.6 Embedded pile

An embedded pile consists of beam elements with embedded interface elements to describe the interaction with the soil at the pile skin and at the pile foot (bearing capacity). The material parameters of the embedded pile distinguish between the parameters of the beam and the parameters of the skin resistance and foot resistance. The beam elements are considered to be linear elastic and are defined by the same material parameters as a regular beam element. The interaction of the pile with the soil at the skin of the pile is described by linear elastic behaviour with a finite strength and is defined by the parameter T_{max}, the maximum traction allowed at the skin of the embedded pile and can vary along the pile. An embedded pile is a pile composed of beam elements that can be placed in arbitrary direction in the sub-soil and interacts with the sub-soil by means of special interface elements. The interaction may involve a skin resistance as well as a foot resistance. Although an embedded pile does not occupy volume, a particular volume around the pile (elastic zone) is assumed, in which plastic soil behaviour is excluded. The size of this zone is based on the (equivalent) pile diameter according to the corresponding embedded pile material data set. This makes the pile almost behave like a volume pile. However, installation effects of piles are not taken into account and the pile-soil interaction is modelled at the center rather than at the circumference. The installation effects of the embedded pile cannot be considered, so this option should be primarily used for pile types that cause a limited disturbance of the surrounding soil during installation, such as some types of bored piles, but obviously not driven piles or soil displacement piles.

An embedded pile consists of beam elements with special interface elements providing the interaction between the beam and the surrounding soil. The beam elements are 3-node line elements with six degrees of freedom (u_x, u_y and u_z) and three rotational degrees of freedom (ϕ_x, ϕ_y and ϕ_z). Element stiffness matrices are integrated from the four Gaussian points. The element allows for beam deflections sue to shearing as well as bending. In addition, the element can change length when an axial force is applied.

The special interface elements are different from the regular interface elements as used along walls or volume piles. Therefore, at the position of the beam element nodes, virtual nodes are created in the soil volume element from the element shape functions. The special interface forms a connection between the beam element nodes and these virtual nodes, and thus with all nodes of the soil volume element. Pile forces are evaluated at the beam element integration points and extrapolated to the beam element nodes.

As described about the aforementioned beam, the case with the embedded pile is that, regardless the satisfying interaction with the adjacent soil due to the unique interface elements, its geometry and its constitutive model cannot describe well the physics and the actual response of the three-dimensional pile. Specifically, the one-dimensional beam is not able to take into consideration the real interaction between the soil and the pile, because the pile dimension is neglected

Figures

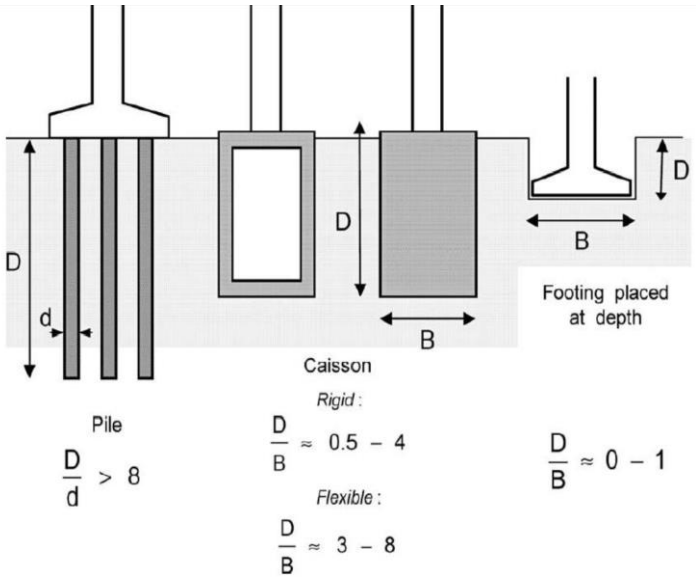

Figure 1.1. *A rough categorization of different foundation types based on their slenderness or embedment ratio D/B. From the left to the right we can distinguish (a) piles, (b) deeply embedded foundations and (c) shallow foundations. (after Gerolymos & Gazetas, 2006)*

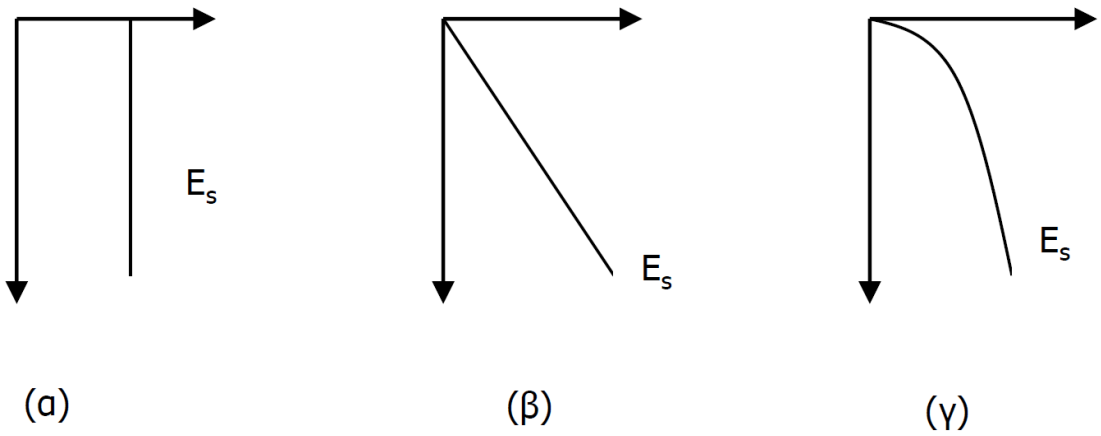

Figure 1.2. *Different distributions of the Elastic Modulus with the depth.*

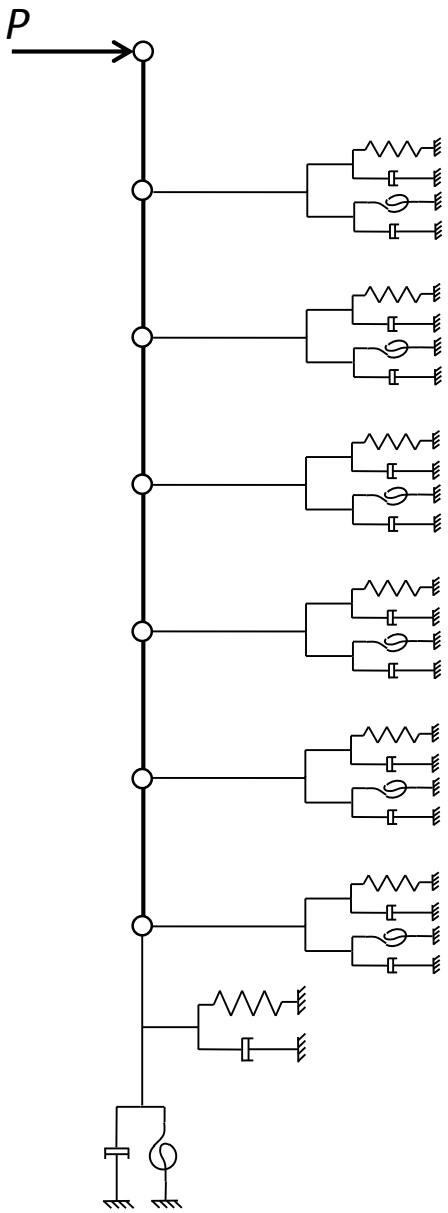

Figure 1.3. *Beam on Winkler foundation*

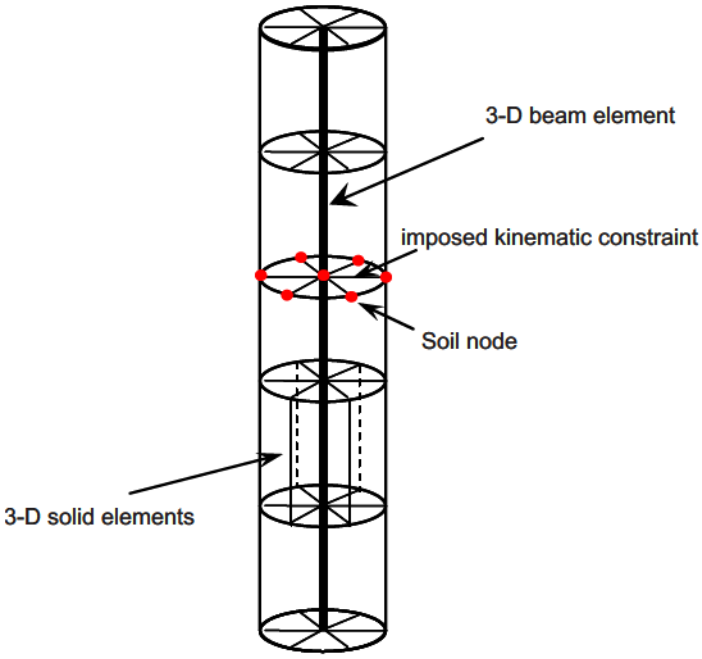

Figure 1.4. *Beam – Plate hybrid in 3-D soil elements.*

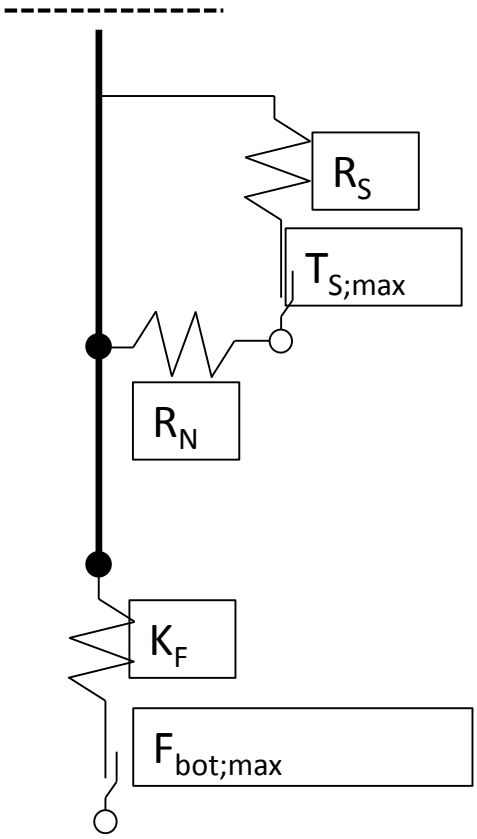

Figure 1.5. *Embedded pile.*

Chapter 2

Macroscopic Mohr-Coulomb based approach of the behaviour of circular piles

2 Macroscopic Mohr-Coulomb based approach of the behaviour of circular piles

2.1 Introduction

The macroelement can be thought of as an advanced finite element, and more precisely a generalized "spring", in which the response of the foundation is described in terms of generalized force versus generalized displacement. This element is placed at the base of the superstructure and aims at reproducing nonlinear interaction phenomena arising at soil – foundation interface. Evidently, the translational and rotational degrees of freedom of a macro-element are all fully coupled. The concept of macroelement is not new in geotechnical engineering. It was originally introduced by Roscoe and Schofield (1956) for shallow foundations. To the best of authors' knowledge, only recently the idea has been extended to pile foundations (Correia et al., 2012). In this paper a mathematical framework for macroelement modeling of single piles is briefly presented, emphasizing the nonlinear behaviour of both the soil and the pile. The calibration of the model parameters is achieved through comparisons with 3D finite element analyses with the use of code PLAXIS. Given that the ultimate lateral capacity of a pile is directly related to its diameter and bending moment resistance, which in turn is a function of the axial force imposed (or developed) on the pile, a simple uniaxial stress-strain model based on the Mohr - Coulomb yield criterion is also developed capable of reproducing the cross-sectional behaviour of circular reinforced concrete piles in terms of bending moment – curvature relationship and bending moment – axial force failure envelopes.

2.2 Elements of Macroelement Modeling

Recent research has shown that the use of laws and equations provided by the theory of elastoplasticity can be directly applicable to the analysis of foundations in cohesive soil under undrained loading conditions (Martin and Houlsby, 2000). It has been demonstrated that this approach provides better results in comparison to Winkler based model, as it is capable of realistically representing the coupling between the various degrees of freedom. Within the framework of elastoplasticity, the "global" response of the pile-soil system is treated in a manner similar to that for the "local" response of an infinitesimally small soil element. The stresses and strains for the soil element are substituted by the generalized forces (in 3-dimensional M-Q-N space) and the corresponding displacements (θ–u–v) respectively. As with the theory of elasto-plasticity, there are 5 main components in a macroelement "assembly", associated with: (a) the foundation response at very small deformations

(elastic response). The elastic stiffness matrix has thus to be determined. (b) The response of the foundation at very large deformations and at failure conditions. The determination of the failure envelope in the generalized 3- dimensional M-Q-N space is thus required. (c) The plastic flow rule that relates the incremental plastic displacements of the foundation to its loading state at near failure conditions, (d) the hardening rule that defines the transition from the elastic to the ultimate limit state, and (e) the unloading-reloading rule in the case of cyclic loading.

2.3 Simplified Constitutive Model for RC Pile Section Behaviour

A Mohr-Coulomb based uniaxial stress-strain constitutive law is developed for modeling the macroscopic behaviour of a RC circular pile section subjected to a combined bending moment and axial force loading. Considering force equilibrium at failure in the axial direction, one obtains:

$$\left(\sigma_c - \frac{4\,N}{\pi\,D^2}\right)A_c = \left(\sigma_t + \frac{4\,N}{\pi\,D^2}\right)A_t \qquad \textbf{(1)}$$

in which σ_c and σ_t are the compressive and tensile strength of the composite (reinforced concrete) section, respectively:

$$\sigma_c = \frac{2\,c\,\cos\varphi}{1-\,\sin\varphi} \qquad \textbf{(2)}$$

$$\sigma_t = \frac{2\,c\,\cos\varphi}{1+\,\sin\varphi}$$

where *c*, *φ* are the strength parameters of the Mohr-Coulomb model, namely the cohesion and the internal friction angle. In Eq (1), A_c and A_t are the pile section areas under compression and tension, respectively, defined as:

$$A_c = \int_0^{x_0} 2\sqrt{x\,(D-x)}\;dx \qquad \textbf{(3)}$$

(3)

$$A_t = \int_{x_0}^{D} 2\sqrt{x\,(D-x)}\;dx$$

in which D is the pile diameter, and x_0 is the abscissa (in a Cartesian coordinate system) that defines the boundary between the zones of the section under compression and tension, respectively. By applying moment limit equilibrium with respect to the center of the pile section, the following equation is derived:

$$M = \sigma_c \int_0^{x_0} 2\sqrt{x\,(D-x)}\,(x_0-x)\,dx + \sigma_t \int_{x_0}^{D} 2\sqrt{x\,(D-x)}\,(x_0-x)\,dx + \left(\frac{D}{2}-x_0\right) N \quad \textbf{(4)}$$

Eqs (1) and (4) form a nonlinear algebraic system. For a given pile diameter and a known combination of bending moment–axial force at structural failure conditions, there are three unknown variables: *c*, *φ* and x_0 . The aforementioned system is solved with the use of a genetic algorithm–based optimization procedure, implemented in MATLAB. The performed
optimization targets to a best fit on a predefined M–N failure envelope by minimizing the relative root mean squared error (rRMSE) of the bending moment at failure (the fitness function):

$$\text{rRMSE}\,(M) = \sqrt{\frac{1}{n}\sum_{i=1}^{n}\left(\frac{M_i - M_{T,i}}{M_{T,i}}\right)^2} \quad \textbf{(5)}$$

in which M_i is the bending moment computed by Eq (4), $M_{T,i}$ is the target bending moment, and n, the number of $M_{T,i} - N_i$ pairs that define the failure envelope. It is interesting to observe that the proposed simplified Mohr-Coulomb–based constitutive model can be easily reduced to a Tresca with tension cutoff– based one, by equating the compressive strength in Eq (2) with $\sigma_c = 2c$ and setting the tensile strength equal to the tension cut-off.

Fig 2.1 shows the M-N failure envelopes for a pile cross-section with a longitudinal reinforcement ratio of *As* = 1.5% and for three different diameters (*D* = 0.8 m, 1 m and 1.5 m). Comparison is given between the predictions of: (a) the proposed optimization procedure, (b) the 3D FE analysis with PLAXIS, and (c) the fiber analysis with the computer code USCRC (Esmaeily 2001). Fig 2.2 shows a 3D visualization of the FE pile model. Observe the formation of a plastic hinge at the bottom of the pile in terms of the incremental plastic shear strain.

2.4 Failure Envelope and Plastic Flow Rule for Piles

Problem Definition

The problem under consideration is that of a pile or a group of piles embedded in a homogeneous cohesive soil of undrained shear strength Su. The pile / pilegroup is subjected to a combined load of overturning moment, horizontal force and axial force at the head / cap until complete failure.

Single Piles

2.4.1 Limit Equilibrium Analysis

Invoking Brom's limit equilibrium theory (1964) for the ultimate lateral capacity of a horizontally loaded free head pile (Fig 2.3), and assuming that the ultimate lateral soil reaction per unit depth is approximated by the expression suggested by Randolph and Houlsby (1984) and Broms (1964):

$$p_y = \begin{cases} \left(2 + \dfrac{\sigma'_v}{S_u} + J\dfrac{z}{D}\right) S_u\, D, & z \le \dfrac{7\,D}{\dfrac{\gamma'\,D}{S_u} + J} \\ 9\,S_u\,D, & otherwise \end{cases} \qquad \textbf{(6)}$$

the following analytical expression for the failure envelope is derived:

$$\frac{M}{M_p} + \left(\frac{Q}{\sqrt{2\,\lambda\,S_u\,D\,M_p}}\right)^2 = 1 \qquad \textbf{(7)}$$

In Eq (6), σ'_v is the vertical effective stress and γ' the effective specific unit weight of the soil. Matlock (1970) stated that the value of J was determined experimentally to be 0.5 for a soft clay and about 0.25 for a medium clay. In Eq (7), M_p is the bending moment capacity of the pile which is a function of the axial load. The bending moment capacity is fully mobilized at a certain depth through the formation of a "plastic" hinge. λ, is a constant accounting for the distribution of the ultimate lateral soil reaction along the pile. By taking into consideration all possible N-Q-M combinations at the pile head and setting $M_y = M_p$ and $Q_y = \sqrt{2\,\lambda\,S_u\,D\,M_p}$, Eq (7) is rewritten in the following general form:

$$f = \begin{cases} \left| sign(Q) \left(\frac{Q}{Q_y}\right)^2 + sign(M) \left|\frac{M}{M_y}\right| \right| - 1 = 0, & \left|\frac{M}{M_y}\right| < 1 \\ \left|\frac{M}{M_y}\right| - 1 = 0 & \left|\frac{M}{M_y}\right| = 1 \\ \left|\frac{N}{N_y}\right| - 1 = 0 & \end{cases} \quad \textbf{(8)}$$

in which N_y is the axial bearing capacity of the pile subjected to tension or compression:

$$N_y = N_t + \left(\frac{N_c}{2} - \frac{N_t}{2}\right) (sign(N) + 1) \quad \textbf{(9)}$$

where N_t is the capacity in tension (without the contribution of the pile tip) and N_c the compressive capacity (with due consideration to the pile tip).

2.4.2 Plastic Flow Rule

According to Brom's theory the post-failure response of the pile is characterized by the formation of a plastic hinge at a certain depth that acts as a rotation pole for the above hinge rigidly deformed portion. With reference to Fig 2.3, the displacement to rotation ratio can be approximated by:

$$\frac{u}{\theta} \approx \frac{u_p}{\theta_p} = \frac{du_p}{d\theta_p} = h_p \quad \textbf{(10)}$$

in which u_p , θ_p and du_p , $d\theta_p$ are the absolute and incremental plastic horizontal displacements and rotations, respectively. Finally, h_p is the depth to the plastic hinge.

By differentiating Eq (7) with respect to the shear force Q and bending moment M, respectively, and assuming an associative plastic flow rule, one obtains after some algebra:

$$\frac{du_p}{d\theta_p} = \frac{Q_f}{\lambda\, S_u\, D} = h_p \quad \textbf{(11)}$$

in which Q_f is the value of Q at failure conditions. Thus, in the framework of a limit equilibrium analysis of the lateral capacity of a single pile, the plastic flow rule is by definition of the associative type!

The undoubtedly very interesting findings about the plastic flow rule and failure criterion are about to be verified in the following section by 3D finite element analysis.

2.4.3 Finite Element Analysis with PLAXIS

A 16 m long pile with a diameter of 1 m embedded in a homogeneous cohesive soil, is analysed. Both the pile and the soil are modeled with 10-node tetrahedral elements. The size of the finite element model is 1.3L x 1.3L in plan view with a depth of 1.5 L (where L is the length of the pile), carefully weighting the effect of the boundaries on the response of the pile and the computational time. Zero-displacement boundary conditions prevent the out of plane deformation at the vertical sides of the model, while the base is fixed in all three directions. Special interface elements are placed between the pile and the soil, thus allowing slippage and gapping to occur. For the total stress analysis under undrained conditions, soil behaviour is described by the Mohr- Coulomb model with $c = S_u = 50$ kPa, $\phi = \psi$ (the dilation angle) = 0°, specific weight of $\gamma = 18$ kN/m3, elasticity modulus of $E_s = 25000$ kPa and Poisson's ratio of $v = 0.45$. Based on the macroscopic constitutive law for reinforced concrete circular pile sections (in section 3), the behaviour of the pile was modeled via a Mohr-Coulomb failure criterion with $c = 15262$ kPa, $\phi = 0o$, tension cut-off $\sigma_t = 7534$ kPa and Elasticity modulus E = 30 GPa, corresponding to a longitudinal reinforcement ratio of $A_s = 1.5$ %. Fig 2.4 compares the failure envelopes in M-Q-N space as predicted by the analytical expression of Eq (8) and calculated by the FE models. The hypothesis of plastic flow rule implied by the limit equilibrium analysis is verified in Fig 2.5 through comparison with finite element analysis results. The discontinuity in plastic hinge position observed at a load angle of $|\omega| \approx 50°$, where the failure envelope reduces to a straight line of constant bending moment, is consistent with associative plastic flow rule. Indeed, for $|\omega| \geq 50°$, perpendicularity of the incremental plastic pile deflection at this point implies failure under pure rotation and zero lateral displacement. The only possible failure mechanism that satisfies this geometrical constraint is the formation of a plastic hinge at the head of the pile.

2.5 Macroelement Modeling

The model is formulated in the framework of classical elastoplasticity, and combines features of: (a) the bounding surface plasticity, (b) the critical state concept, and (c) a hardening evolution law and unloading-reloading rule of the modified Bouc-Wen type. According to this formulation the tangent elastoplastic stiffness matrix that relates the incremental force vector to the incremental displacement vector, is given by:

$$\boldsymbol{K^{ep} = K^e \left[I - \Phi_g \left(\Phi_f^T K^e \Phi_g \right)^{-1} \Phi_f^T K^e H_1 H_2 \right]} \quad \textbf{(12)}$$

in which $\boldsymbol{K^e}$ is the elastic stiffness matrix of the pile, $\boldsymbol{\Phi_f}$ and $\boldsymbol{\Phi_g}$ account for the failure surface and plastic flow rule, respectively, and $\boldsymbol{H_1}$ and $\boldsymbol{H_2}$ describe the hardening law and unloading-reloading rule. The terms in matrices $\boldsymbol{H_1}$ and $\boldsymbol{H_2}$ are functions of the dimensionless hardening parameter ζ, which is of the Bouc-Wen type (Gerolymos and Gazetas, 2005). Figs 2.6 and 2.7 presents numerical examples of the macroelement model for a pile subjected to combined loading of axial force, horizontal force and overturning moment at its head. Comparison is given with results from finite element analysis with code PLAXIS. The properties of the pile and its supporting soil are provided in section 2.4.3.

Figures

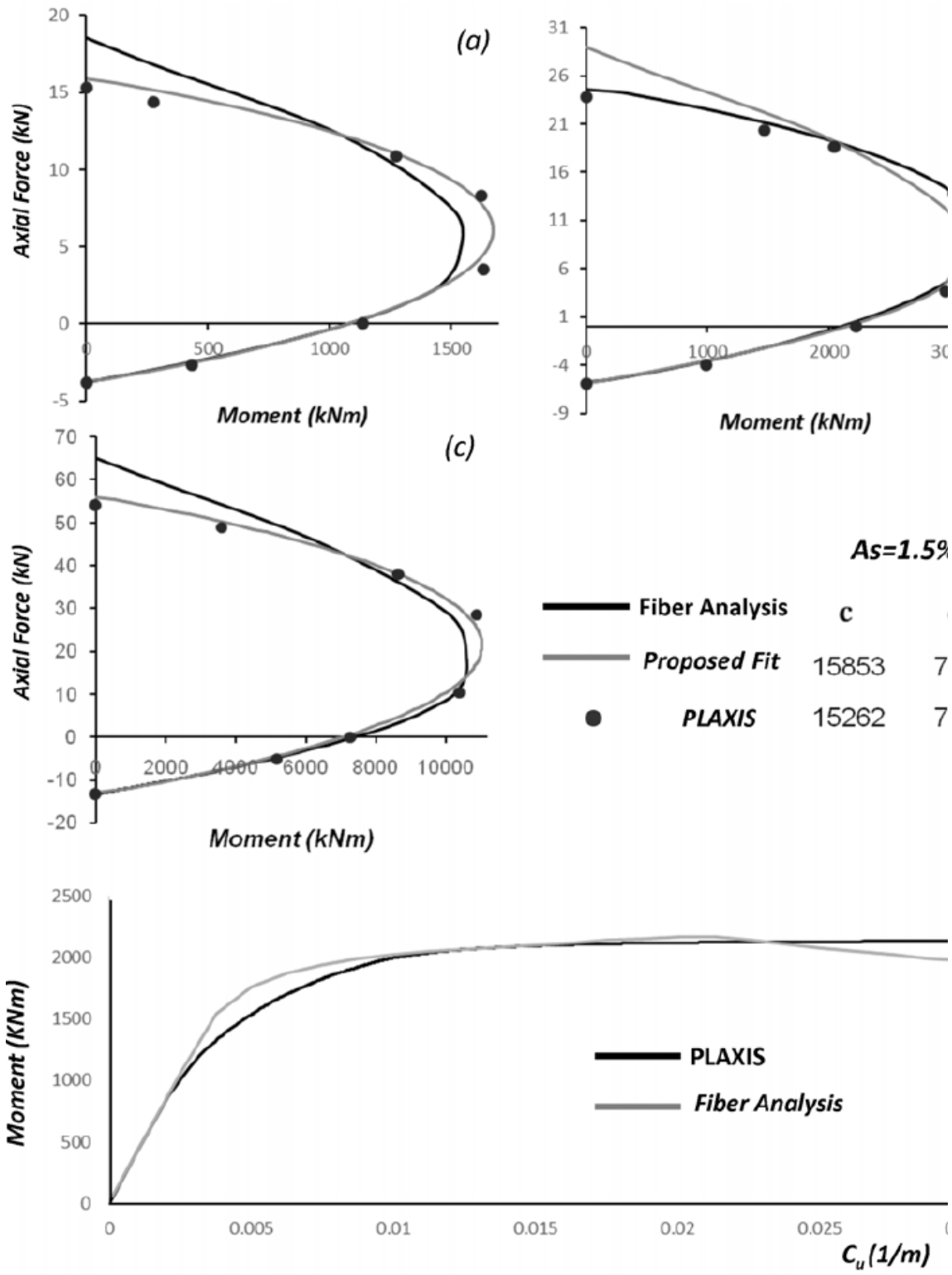

Figure 2.1. *Comparison of M-N failure envelopes for RC pile sections, computed from the Fiber analysis and from PLAXIS and predicted by the proposed optimization procedure for three pile diameters: (a) D = 0.8 m, (b) D = 1 m, (c) D = 1.5 m. (d) Comparison of the bending moment-curvature curve calculated from the fiber analysis and the FE models (PLAXIS) for D = 1 m.*

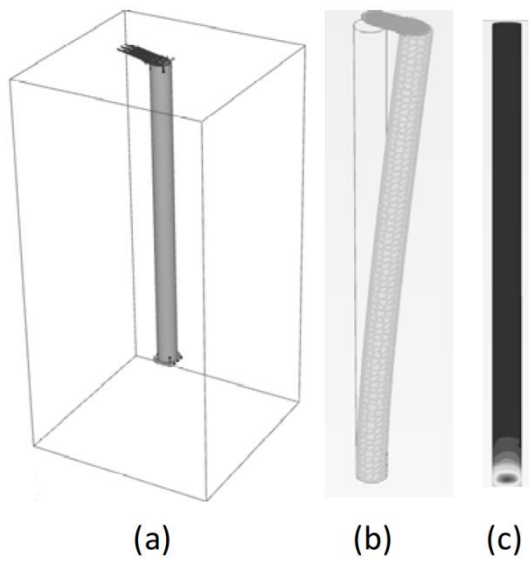

Figure 2.2. *(a) The FE model (PLAXIS) for RC pile section analysis, (b) the deformed FE mesh at failure, (c) contours of the incremental plastic shear strains at failure denoting the formation of a plastic hinge at the bottom of the pile.*

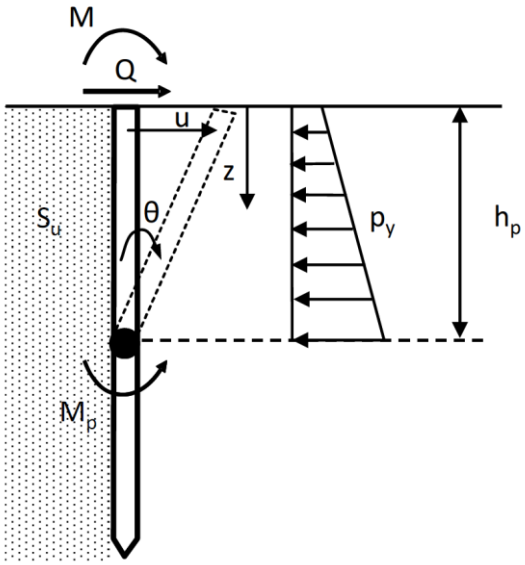

Figure 2.3. *Failure mode of a laterally loaded free-head pile embedded in cohesive soil according to Brom's theory.*

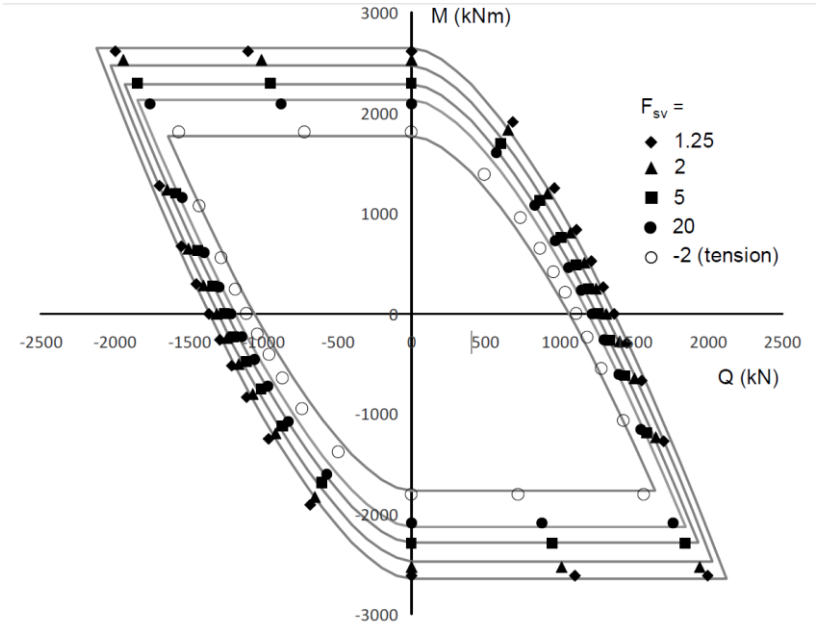

Figure 2.4. *Comparison of the failure envelopes for a pile in cohesive soil, calculated by PLAXIS and predicted by the analytical expression [Eq (8)] for 5 different factors of safety to vertical loading Fsv. The pile has a diameter of D = 1 m and a longitudinal reinforcement ratio of A_s = 1.5 %. Tension (extraction of the pile) is denoted with negative values.*

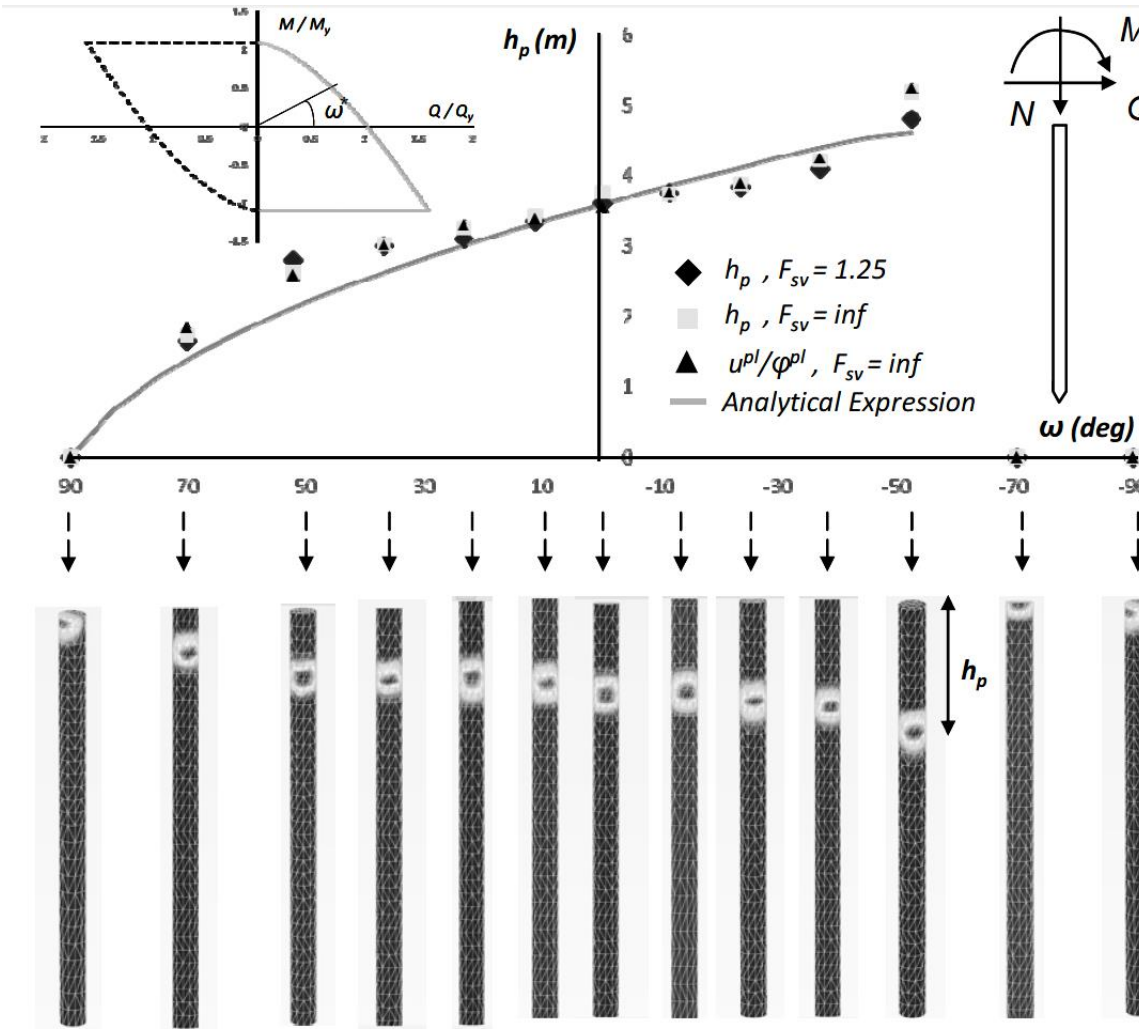

Figure 2.5. *Finite element verification of the associative plastic flow rule for a wide range of load combinations. Observe that the depth to the plastic hinge h_p increases for increasing negative load angles [M / Q = ω, ω* = (Q_y / M_y) ω] reaching a maximum value at the vertex of the failure envelope (at approximately ω = -50°). For load angles greater than |ω| > 50° , the plastic hinge moves violently from its deepest location to the head of the pile.*

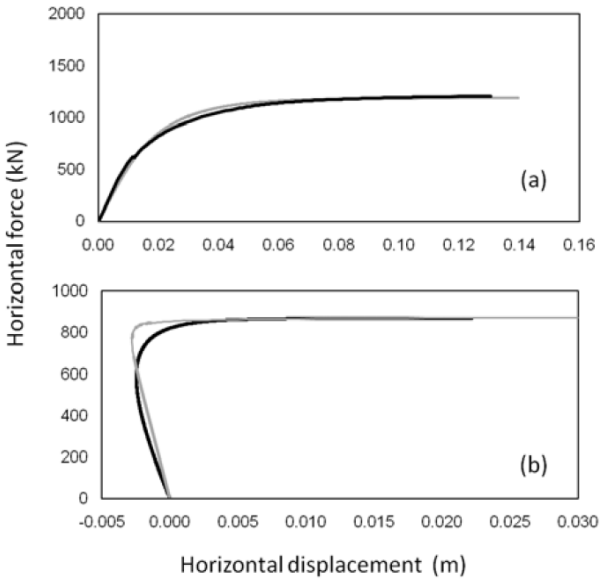

Figure 2.6. *Comparison of horizontal force versus horizontal displacement curves at the head of the pile, predicted by the macroelement and calculated from the finite element analysis (PLAXIS) for the following load combinations: (a) Pure shear loading and F_{sv} = inf, (b) combined shear force-overturning moment for a load angle of ω = - 70° and F_{sv} = inf*

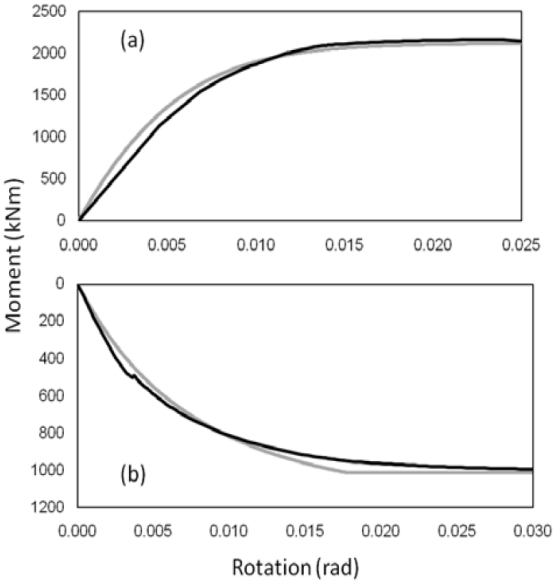

Figure 2.7. *Comparison of overturning moment versus rotation curves at the head of the pile, predicted by the macroelement and calculated from the finite element analysis (PLAXIS) for the following load combinations: (a) Pure moment loading and F_{sv} = 5, (b) combined shear force-overturning moment for a load angle of ω= -36° and F_{sv} = -2 (tension)*

Chapter 3

Internal Force Diagrams Computation

3 Internal Force Diagrams Computation

3.1 PLAXIS approach

Although PLAXIS can calculate internal force diagrams of elastic piles, this is not the case with non-linear piles. In elasticity, the internal forces can be calculated by putting a slender beam along the shaft of the pile with a Young modulus (E) approximately 10.000 times smaller of the stiffness of the pile, so as not to affect the pile response in loading. By completing the calculations, the beam returns the force components in relation with the strain / curvature components. This relation is defined according to Bernoulli beam theory:

$$N = EA\varepsilon \qquad M_2 = EI_2k_2$$

$$Q_{12} = kGA\gamma_{12} \qquad M_3 = EI_3k_3$$

$$Q_{13} = kGA\gamma_{13}$$

where A: Beam cross section area
E: Young's Modulus in axial direction
I_2: Moment of inertia against bending around the second axis
I_3: Moment of inertia against bending around the third axis
and k is the shear correction factor. The shear modulus G is taken as G= ½E.

The above-mentioned force components are multiplied by the factor m= $\frac{E_{pile}}{E_{beam}}$ so as to get the real diagrams of axial force, shear force and bending moment. However, the linearity does not apply for loads near the failure of pile, because in this case emerges severe plasticity which leads to a reduction of the elastic modulus and the above-mentioned equations cannot explain the actual pile response. As a result, emerges the need of a tool to compute these forces, analyze them and propose ways of better pile design.
In this thesis a model of numerical integration through MATLAB programming language is proposed. The procedure that is followed takes as input data the stresses which are derived from the experiment simulation results and through a series of commands, the structural force diagrams are extracted.
The concept is to use the stresses of the Gauss points and by interpolating them in a circular area of same depth, define an area of influence of each interpolated point, in addition integrate them numerically and extract the results at each pile depth.

3.2 Voronoi decomposition

The region of influence of each interpolated Gauss point is defined by the Voronoi tessellation method. The finite set of points are given in the cyclic plane and each site p_k is simply a unique point and its corresponding Voronoi cell

P_k consisting of every point whose distance to p_k is less than or equal to its distance to any other site. Each such cell is obtained from the intersection of half-spaces, and hence it is a convex polygon. The segments of the Voronoi diagram are all the points in the plane that are equidistant to the two nearest sites. The Voronoi vertices (nodes) are the points equidistant to three (or more) sites. However, a problem arises due to the fact that the region of influence of the points across the circumference extends to infinity. The proposed solution to this problem is to regard pseudo-points adjacent to the points of the circumference, along the radius of circle and on the outer side. These points are neglected afterwards in the calculations.

```
X=CO(:,1);
Y=CO(:,2);
[v,c]=voronoin([X(:) Y(:)]);
```

3.3 Numerical Integration

In addition to Voronoi decomposition, the area of the unique regions is acquired so as to proceed to the numerical integration. For the case where only symmetric loading x-wise is applied to the head of the pile, internal forces are calculated according to the expressions:

$$\mathrm{N} = \sum_{k=0}^{n} \sigma_{zz}(k) dA(k) \quad \textbf{(1)}$$

$$M_y = \sum_{k=0}^{n} \sigma_{zz}(k) dA(k) (X_c - X(k)) \quad \textbf{(2)}$$

$$\mathrm{Q}_x = \sum_{k=0}^{n} \sigma_{zx}(k) dA(k) \quad \textbf{(3)}$$

Where: N is the axial force, M is the bending moment, Q is the shear force and n is the number of total Voronoi regions. σ_{zz} and σ_{zx} are the stresses of the elements of the pile, the sign of which is conventionally defined as in figure 3.3. X_c is the x-component of the center of a pile intersection. The reference point according to which moments are determined is the X_c, so as to avoid measuring any additional moment that may be caused due to the eccentricity of the normal stresses distribution. Two approaches were made to estimate the force values of the pile. One in 2-Dimensional area and one in 3-Dimensional space.

3.4 Slice Method

This approach attempted to take advantage of the automatic interpolation PLAXIS made in every required depth section. The interpolation to the specific depth is obtained in the finite element formulation from the interpolation of the nodal normals with the shape functions. The command script reads a five-column matrix, every row of which is representing the X position, Y position, Z position, the σ_{zz} stress and σ_{zx} stress. This can be easily modified in order to take into account moment and shear forces in the perpendicular direction. However, this procedure produces different stress values to same points due to the fact that two or more adjacent Gaussian points are interpolated to the same intersection point. These interpolated values are averaged in order to have unique points and their values, and then sorted to abbreviate the calculation time.

```
P=xlsread('Plaxis_Mat.xlsx','Plaxis_Mat','A3:E362');
P(:,3)=[];
CO_plaxis=unique(P(:,1:2),'rows','sorted');
last_plaxis = length(CO_plaxis);
X_plaxis=CO_plaxis(:,1);
Y_plaxis=CO_plaxis(:,2);
sigma_plaxis=zeros(size(X_plaxis));
shear_plaxis=zeros(size(X_plaxis));
for i=1:last_plaxis
    k=0;
    sum1=0;
    sum2=0;
    for j=1:length(P)
        if and(P(j,1)==CO_plaxis(i,1),P(j,2)==CO_plaxis(i,2))
            k=k+1;
            sum1=sum1+P(j,3);
            sum2=sum2+P(j,4);
        end
    end
    sigma_plaxis(i,1)=sum1/k;
    shear_plaxis(i,1)=sum2/k;
end
```

3.5 Interpolation

The automatically produced section-points of PLAXIS, may not be well-handled, because, for instance, of the bad combination of the circumferential points with the respective outer Voronoi pseudo-points, or because of probable inadequate distribution of stresses throughout the pile intersection. What is proposed is to perform interpolation on the 2-D scattered data set, in order to pass the values of stresses from the sample values (sigma_plaxis) at the given point locations (X_plaxis,Y_plaxis) to any query point (x,y) and produce a linearly interpolated

value of stress (sigma). To achieve the interpolation, it must be defined a grid corresponding to the polar coordinates of the query points. This grid is afterwards converted to a Cartesian-coordinate set of points, for better handling. Regarding the points very close to the circumference or on it, which are not enclosed to the area defined by the Gauss points and cannot be interpolated, it is chosen an extrapolation method according to which, these points acquire the stress value of their nearest Gauss point. Although this procedure may sound approximative or inaccurate, extrapolation is applied only to a minor set of points with only slightly different stress value of their adjacent integration points, that no significant change of the structural forces is detected.

```
r=linspace(0,(Xmax-Xmin)/2,20);
theta=linspace(0,2*pi,40);
[r,theta]=meshgrid(r,theta);
x=(Xmax+Xmin)/2+r.*cos(theta);
y=(Ymax+Ymin)/2+r.*sin(theta);
F_sigma=scatteredInterpolant(X_plaxis,Y_plaxis,sigma_plaxis, ...
'linear','nearest');
sigma=F_sigma(x,y);
F_shear=scatteredInterpolant(X_plaxis,Y_plaxis,shear_plaxis, ...
'linear','nearest');
shear=F_shear(x,y);
```

However, the grid of the interpolated points is not well-handled; hence the coordinates and their respective values are reshaped into the more convenient form of vectors. In addition, the double coordinate values are deleted and the remaining are sorted in increasing order, in respect to the X coordinate. Subsequently, the external boundary coordinates are added to the Nx2 coordinate matrix and then, the area of the polygon specified by the vertices in the vectors X and Y of each Voronoi polygon is created. The forces can be calculated according to the (1) - (3) equations.

```
x=reshape(x,[],1);
y=reshape(y,[],1);
sigma=reshape(sigma,[],1);
shear=reshape(shear,[],1);
Ptemp=[x,y];
[COtemp,ia,ic]=unique(Ptemp,'rows','sorted');
sigmatemp=zeros(size(ia));
for i=1:length(ia)
    sigmatemp(i)=sigma(ia(i));
end
sigma=[zeros(extsize,1); sigmatemp];
sheartemp=zeros(size(ia));
for i=1:length(ia)
    sheartemp(i)=shear(ia(i));
end
shear=[zeros(extsize,1); sheartemp];
CO=[bounds;COtemp];
last = length(CO);
X=CO(:,1);
Y=CO(:,2);
[v,c]=voronoin([X(:) Y(:)]);
figure;
voronoi(X,Y)
 plabels = arrayfun(@(n) {sprintf('P%d', n)}, (1:last)');
 Hpl = text(X, Y, plabels, 'FontWeight', ...
       'bold', 'HorizontalAlignment','center', ...
       'BackgroundColor', 'none');
 dA=zeros(last-extsize,1);
for i=(extsize+1):last
    dA(i)=polyarea(v(c{i},1),v(c{i},2));
end
A=sum(dA);
title(['Area = ' num2str(A)]);
dN=zeros(last-extsize,1);
for i=(extsize+1):last
    dN(i)=dA(i)*sigma(i);
end
N=sum(dN);
coeff=polyfit(X((extsize+1):last),sigma((extsize+1):last),1);
x0=coeff(1,2)/(-coeff(1,1));
dM=zeros(last-extsize,1);
for i=(extsize+1):last
    dM(i)=dA(i)*sigma(i)*((Xmax+Xmin)/2-X(i));
end
M=sum(dM);

dQ=zeros(size(X_plaxis));
dQ((extsize+1):last)=dA((extsize+1):last).*shear((extsize+1):last);
Q=sum(dQ);
NMQ=[N;M;Q]
```

3.6 Volume method

There are two main disadvantages of using separate intersections in two dimensional space. First, the multiple interpolations that have to be done both manually by the commands and automatically with PLAXIS, return results with low accuracy and considerable divergence. In addition, the internal force values have to be calculated in each depth separately and then the diagrams be formed.
Regarding this issue, there is proposed a different approach which takes into account the stresses of the whole pile, directly from the Gauss points. These stresses are interpolated at each depth that is queried and subsequently, the former procedure of the separate intersection approach is followed. In this case, the Voronoi decomposition is also made after the interpolation in the plain.
The Coordinate matrix is now Nx3 and the third column is related with the depth Z. The procedure is similar to the one in 2-D approach, but in this case the grid is a three dimensional matrix and the interpolation is done in space.

```
r=linspace(0,(Xmax-Xmin)/2,25);
theta=linspace(0,2*pi,80);
zeta=linspace(Zmax,Zmin,abs(Zmin-Zmax)+1)';
zeta1=zeta;
[r,theta,zeta]=meshgrid(r,theta,zeta);
xgrid=(Xmax+Xmin)/2+r.*cos(theta);
ygrid=(Ymax+Ymin)/2+r.*sin(theta);

F_sigma = scatteredInterpolant(CO_plaxis,sigma_plaxis, ...
'linear','nearest');
sigmagrid = F_sigma(xgrid,ygrid,zeta);
F_shear = scatteredInterpolant(CO_plaxis,shear_plaxis, ...
'linear','nearest');
sheargrid = F_shear(xgrid,ygrid,zeta);
```

Regarding the internal forces generation, it is done at each predefined depth of pile, inside a for-loop. In each loop, the forces are calculated according to the procedure defined in 2-D approach.

```
NMQ=zeros(3,size(zeta,3));
for I=1:size(zeta,3)
    xloop=reshape(xgrid(:,:,I),[],1);
    yloop=reshape(ygrid(:,:,I),[],1);
    sigmaloop=reshape(sigmagrid(:,:,I),[],1);
    shearloop=reshape(sheargrid(:,:,I),[],1);
    Ploop=[xloop,yloop];
    [COloop,ia,ic]=unique(Ploop,'rows','sorted');
    sigmalooptemp=zeros(size(ia));
    shearlooptemp=zeros(size(ia));
    for i=1:length(ia)
        sigmalooptemp(i)=sigmaloop(ia(i));
        shearlooptemp(i)=shearloop(ia(i));
    end
    sigma=[zeros(extsize,1); sigmalooptemp];
    shear=[zeros(extsize,1); shearlooptemp];
    CO=[bounds;COloop];
    last = length(CO);
    X=CO(:,1);
    Y=CO(:,2);
    [v,c]=voronoin([X(:) Y(:)]);
    plabels = arrayfun(@(n) {sprintf('P%d', n)}, (1:last)');
    Hpl = text(X, Y, plabels, 'FontWeight', ...
        'bold', 'HorizontalAlignment','center', ...
        'BackgroundColor', 'none');
    dA=zeros(last-extsize,1);
    for i=(extsize+1):last
        dA(i)=polyarea(v(c{i},1),v(c{i},2));
    end
    A=sum(dA);
    title(['Area = ' num2str(A)]);
    dN=zeros(last-extsize,1);
    for i=(extsize+1):last
        dN(i)=dA(i)*sigma(i);
    end
    N=sum(dN);
    coeff=polyfit(X(extsize+1:last),sigma(extsize+1:last),1);
    x0=coeff(1,2)/(-coeff(1,1));
    dM=zeros(last-extsize,1);
    for i=(extsize+1):last
        dM(i)=dA(i)*sigma(i)*((Xmax+Xmin)/2-X(i));
    end
    M=sum(dM);
    dQ=zeros(last-extsize,1);
    dQ((extsize+1):last)=dA((extsize+1):last).*shear ...
    ((extsize+1): last);
    Q=sum(dQ);
    NMQ(:,I)=[N;M;Q];
end
```

3.7 Validation

The validity of the results of the above-mentioned calculations is examined by comparing the internal force diagrams of beam element in elasticity with linear behavior of soil and pile and the respective diagrams that are extracted from the matlab code. The results are also validated by semi-analytical expressions that give the moment of a pile on a given depth according to the distribution of the normal stresses. For the simulation, is used a monopile which is subjected exclusively to lateral loading in x direction.

Semi - analytical expression

We assume a circular pile intersection in depth z with polar coordinates (r,θ), as in figure 3.2.

$$M_y(z) = \int \sigma_{zz}\, x\, dA$$

$$x = \mathrm{r}\,\cos\theta \qquad \text{and} \qquad A = \mathrm{r}\,\mathrm{dr}\,\mathrm{d}\theta$$

$$M_y(z) = 2 * \int_{-\frac{\pi}{2}}^{\frac{\pi}{2}} \int_{0}^{R} \sigma_{zz}\, r\, \cos\theta\, r\, dr d\theta$$

Because of the elastic behavior and the absence of axial loading, it is fair to assume linear stress distribution with zero value at the pile center.

$$\sigma_{zz} = \frac{\sigma_{max}(z)}{R}\, x = \frac{\sigma_{max}(z)}{R}\, r\, \cos\theta$$

Thus,

$$M_y(z) = 2 * \int_{-\frac{\pi}{2}}^{\frac{\pi}{2}} \int_{0}^{R} \frac{\sigma_{max}(z)}{R}\, r^3\, \cos^2\theta\, dr d\theta$$

$$M_y(z) = \frac{2\,\sigma_{max}(z)}{R} * \int_{-\frac{\pi}{2}}^{\frac{\pi}{2}} \int_{0}^{R} r^3\, cos^2\theta\, dr d\theta$$

$$\Rightarrow \qquad M_y(z) = \frac{\pi}{4}\, R^3\, \sigma_{max}(z)$$

Where $\sigma_{max} \approx |\sigma_{min}|$

The results of the validation are shown in figures 3.25 – 3.27.

3.8 Result visualization

N-M-Q diagrams

The aforementioned results are eventually visualized to get also a qualitative indication of their validity and a general perspective of the pile response under static loading. Thus, it is possible a practical comparison of the structural forces that are extracted from the proposed method with the respective ones from alternative methods. These diagrams are handled for constructional purposes regarding the design of the pile and the pile enforcement. The presentation of the diagrams is chosen to form an area of three diagrams in a row.

```
%Visualizations
subplot(1,3,1);
plot(NMQ(1,:),zeta1,'-b*','LineWidth',2,'MarkerSize',8);
hold on
plot([0 0],[Zmax Zmin], 'k:');
title('Axial Force (N)', 'FontSize', 20);
xlabel('(kN)');
ylabel('Depth (m)');
set(gca,'XAxisLocation','top');
set(gca,'YAxisLocation','right');
hold off
subplot(1,3,2);
plot(NMQ(2,:),zeta1,'-r*','LineWidth',2,'MarkerSize',8);
hold on
plot([0 0],[Zmax Zmin], 'k:');
title('Bending Moment (M)', 'FontSize', 20);
xlabel('(kNm)');
ylabel('Depth (m)');
set(gca,'XAxisLocation','top');
set(gca,'YAxisLocation','right');
hold off
subplot(1,3,3);
plot(NMQ(3,:),zeta1,'-g*','LineWidth',2,'MarkerSize',8);
hold on
plot([0 0],[Zmax Zmin], 'k:');
title('Shear Force (Q)', 'FontSize', 20);
xlabel('(kN)');
ylabel('Depth (m)');
set(gca,'XAxisLocation','top');
set(gca,'YAxisLocation','right');
set(gcf,'Color',[0.4,0.4,0.4],'Toolbar','none')
set(gcf, 'Position', get(0,'Screensize'));
hold off
```

3.9 Stress distribution

In conjunction with the internal force diagrams, the normal and shear stress distribution in each depth are visualized. Matlab has not the option to plot stress distribution in a cyclic area. Thus, the proposed solution is to create a squared intersection with edge length equal to the pile diameter and grid density unvarying to the Voronoi grid density. The stress value of each grid on the square is acquired by bilinear, 2-D interpolation of the p_k sites of the Voronoi grid. For presenting reasons, the intersections shown on the 3-D figures 3.22 and 3.23 are at **two meter distance.**

```
[x_rec, y_rec, z_rec] =
meshgrid(linspace(Xmin,Xmax,100),linspace(Ymin,Ymax,100)…
   ,linspace(Zmax,Zmin,abs(Zmin-Zmax)/2+1));
sigma_rec = griddata(xgrid,ygrid,zeta,sigmagrid,x_rec,y_rec,z_rec);
shear_rec = griddata(xgrid,ygrid,zeta,sheargrid,x_rec,y_rec,z_rec);

figure;
slice(x_rec,y_rec,z_rec,sigma_rec,[],[],[Zmax:-2:Zmin]);
axis ([10 11 10 11 -6 0]);
title('Normal Stress (kPa)');
set(gcf,'Color',[0.4,0.4,0.4])
colorbar
zoom (3)
pan on
set(gcf, 'Position', get(0,'Screensize'));
figure;
slice(x_rec,y_rec,z_rec,shear_rec,[],[],[Zmax:-2:Zmin]);
axis equal;
title('Shear Stress (kPa)');
set(gcf,'Color',[0.4,0.4,0.4])
colorbar
zoom (18)
pan on
set(gcf, 'Position', get(0,'Screensize'));
```

Figures

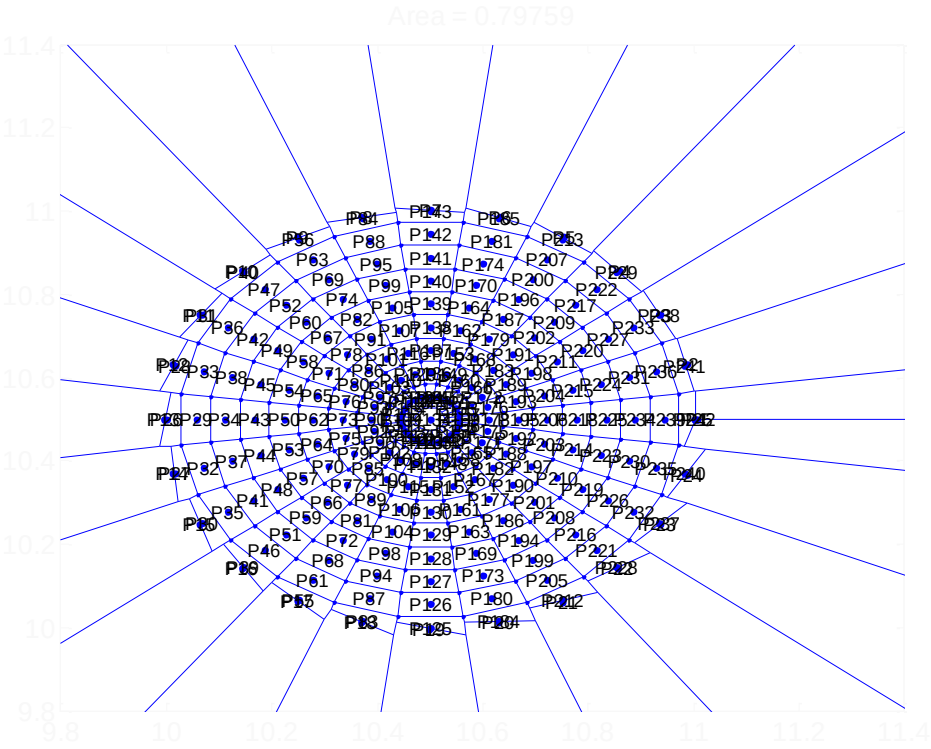

Figure 3.1. *Intersection of a pile at specific depth. Pk are the Voronoi regions to which the pile is intersected.*

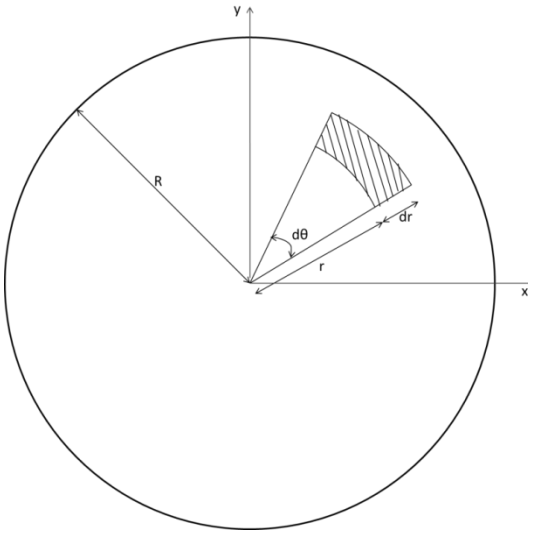

Figure 3.2. *Polar coordinates of pile intersection stress points*

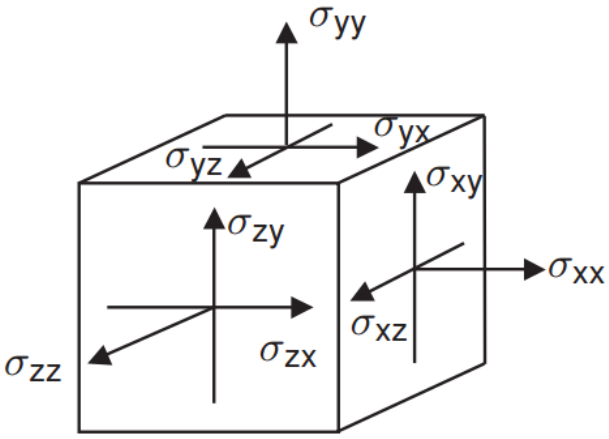

Figure 3.3. *General three dimensional coordinate system and sign convention for stresses*

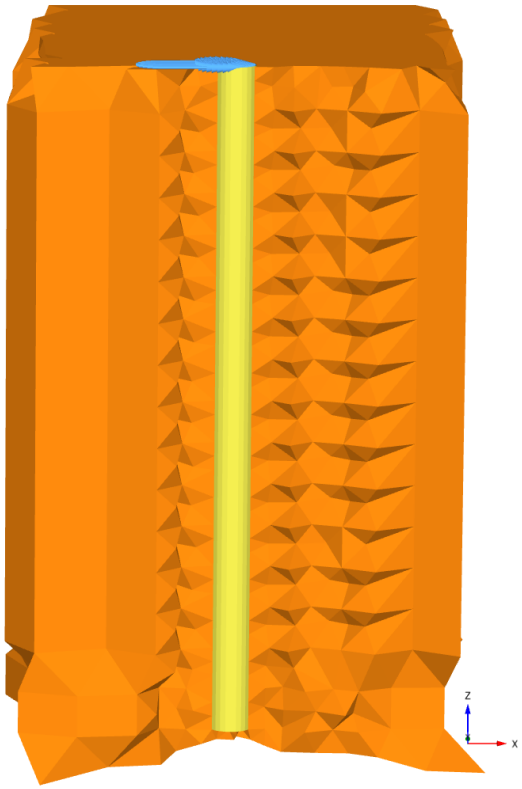

Figure 3.4. Instance of lateral loading of the monopile. This type of loading is examined below

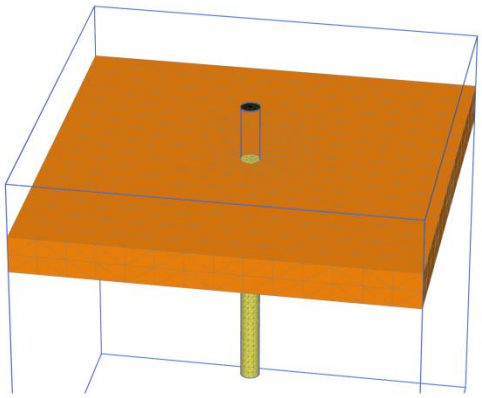

Figure 3.5. *Pile intersection along the depth in Slice Method. The element nodes must coincide with the pile depth at the specific intersection*

Soil element	Stress point	Local number	X [m]	Y [m]	Z [m]	σ_{nn} [10^3 kN/m^2]	σ_{ns} [kN/m^2]
Clus. 2 - El. 4067 ElastoplasticPile-As1.SSoft	16265	1	10.505	10.497	0.003	-2.835	2095.867
	16266	2	10.505	10.498	0.016	-2.825	2096.670
	16267	3	10.508	10.488	0.010	-2.847	2084.891
	16268	4	10.513	10.496	0.010	-2.911	2120.696
Clus. 2 - El. 4068 ElastoplasticPile-As1.SSoft	16269	1	10.507	10.506	0.003	-2.821	2102.847
	16270	2	10.505	10.506	0.016	-2.839	2087.438
	16271	3	10.513	10.508	0.010	-2.904	2073.788
	16272	4	10.510	10.519	0.010	-2.879	2058.598
Clus. 2 - El. 4069 ElastoplasticPile-As1.SSoft	16273	1	10.500	10.505	0.003	-2.783	2093.384
	16274	2	10.498	10.506	0.016	-2.778	2092.964
	16275	3	10.500	10.519	0.009	-2.802	2095.159
	16276	4	10.491	10.506	0.009	-2.720	2113.358
Clus. 2 - El. 4070 ElastoplasticPile-As1.SSoft	16277	1	10.498	10.497	0.003	-2.788	2089.091
	16278	2	10.497	10.498	0.016	-2.772	2088.298
	16279	3	10.489	10.496	0.010	-2.722	2109.201
	16280	4	10.497	10.489	0.009	-2.812	2078.809
Clus. 2 - El. 4071 ElastoplasticPile-As1.SSoft	16281	1	10.034	10.418	0.018	-5.160	2165.853
	16282	2	10.127	10.391	0.019	-2.542	1471.680
	16283	3	10.068	10.308	0.018	-5.855	2424.803
	16284	4	10.068	10.308	0.010	-5.583	2347.775
Clus. 2 - El. 4072 ElastoplasticPile-As1.SSoft	16285	1	10.137	10.193	0.017	-6.017	2528.277
	16286	2	10.232	10.203	0.018	-1.853	1729.098
	16287	3	10.221	10.114	0.017	-5.060	2478.386
	16288	4	10.221	10.114	0.009	-4.897	2365.635
Clus. 2 - El. 4073 ElastoplasticPile-As1.SSoft	16289	1	10.356	10.055	0.018	-4.450	2485.208
	16290	2	10.484	10.123	0.019	-2.904	2087.897
	16291	3	10.468	10.030	0.018	-4.174	2297.793
	16292	4	10.479	10.030	0.010	-3.943	2268.835
Clus. 2 - El. 4074 ElastoplasticPile-As1.SSoft	16293	1	10.385	10.173	0.009	-2.559	2099.548
	16294	2	10.319	10.211	0.016	-2.380	2052.398
	16295	3	10.308	10.130	0.016	-2.454	2072.184
	16296	4	10.428	10.180	0.020	-1.886	2079.595
Clus. 2 - El. 4075 ElastoplasticPile-As1.SSoft	16297	1	10.801	10.292	0.020	-4.402	1687.219
	16298	2	10.887	10.236	0.018	-1.948	841.811
	16299	3	10.809	10.151	0.018	-2.643	1093.550
	16300	4	10.888	10.238	0.011	-2.022	890.028

Figure 3.6. *PLAXIS table, from which, the normal and shear stresses at each specific point are extracted*

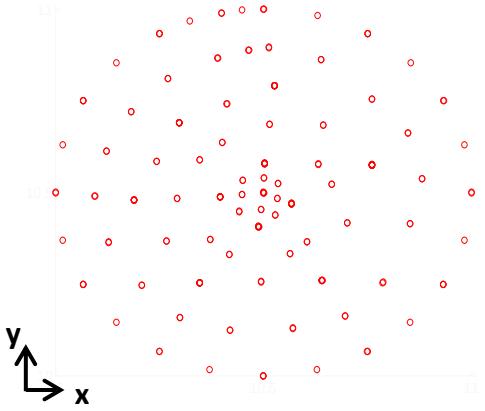

Figure 3.7. *Node distribution at the pile intersection of the non-elaborated data. Many nodes have varied values of stresses due to the interpolation of different Gauss points*

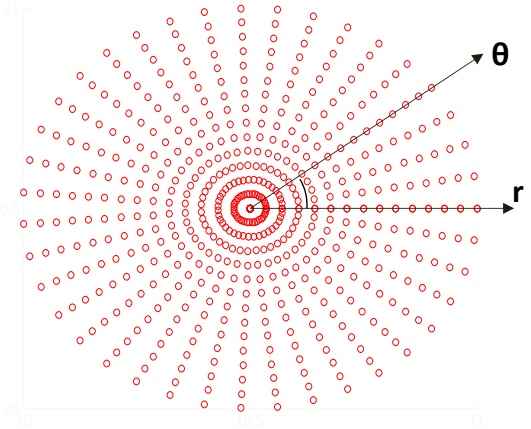

Figure 3.8. *Node distribution at the pile intersection after the implementation of specific grid pattern to the stress points*

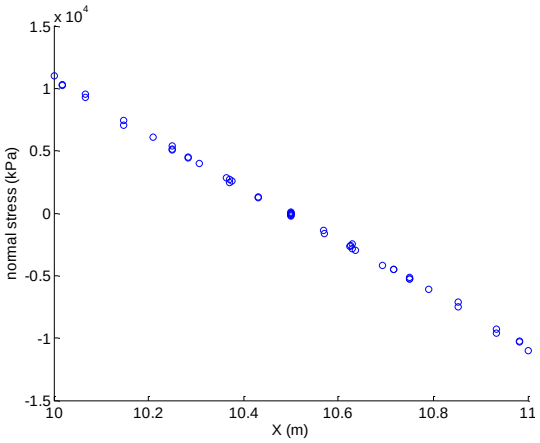

Figure 3.9. *Normal stress distribution, in elasticity, of the non-elaborated data*

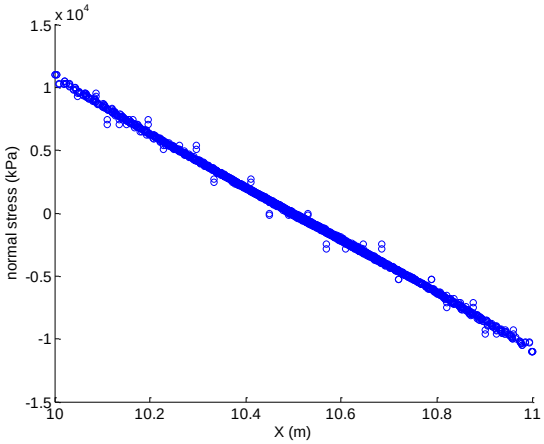

Figure 3.10. *Normal stress distribution, in elasticity, of the interpolated data*

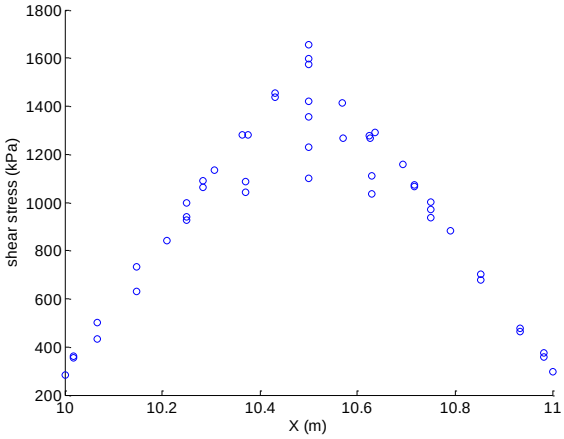

Figure 3.11. *Shear stress distribution, in elasticity, of the non-elaborated data*

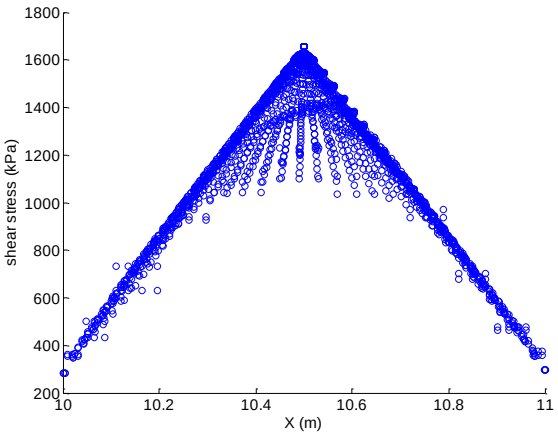

Figure 3.12. *Shear stress distribution, in elasticity, of the interpolated data*

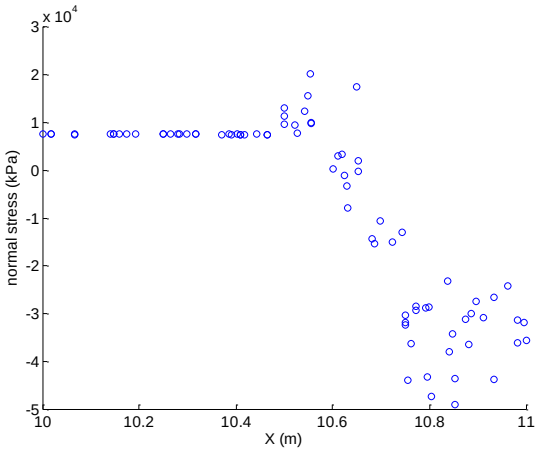

Figure 3.13. *Non-linear stress distribution of normal stresses, of the non-elaborated data*

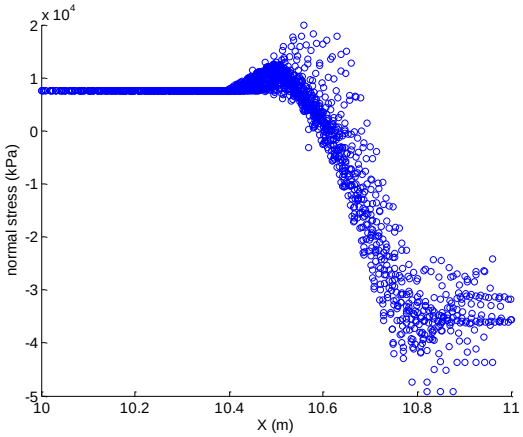

Figure 3.14. *Non-linear stress distribution of normal stresses, of the interpolated data*

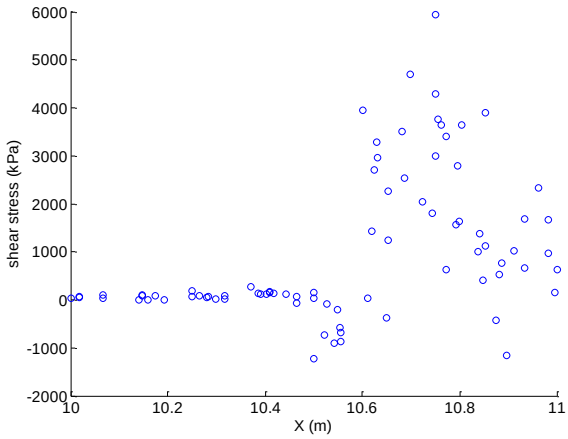

Figure 3.15. *Non-linear stress distribution of shear stresses, of the non-elaborated data*

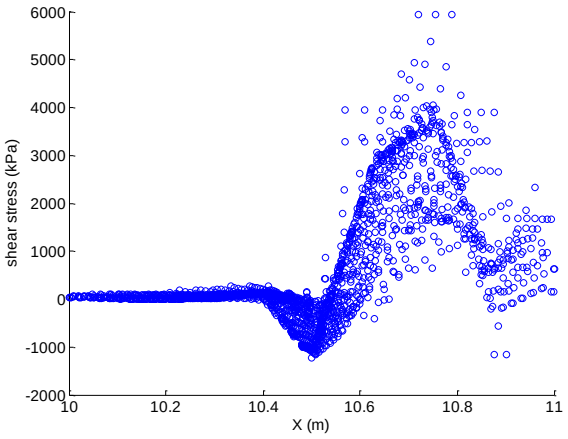

Figure 3.16. *Non-linear stress distribution of normal stresses, of the interpolated data*

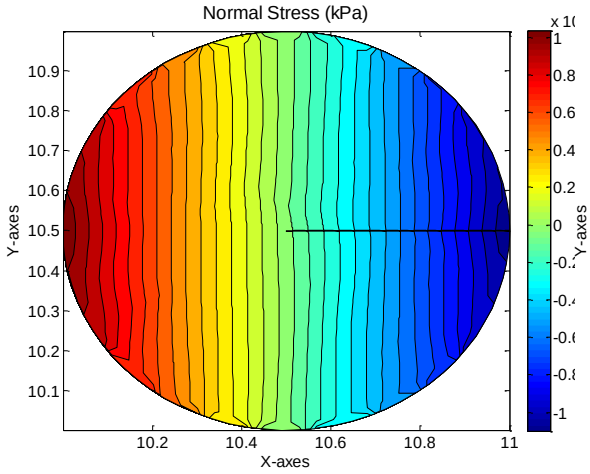

Figure 3.17. *Contour of normal stress distribution of the interpolated data, in elasticity*

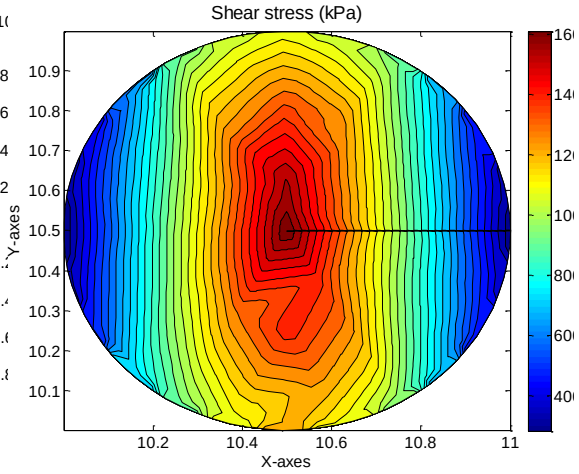

Figure 3.18. *Contour of shear stress distribution of the interpolated data, in elasticity*

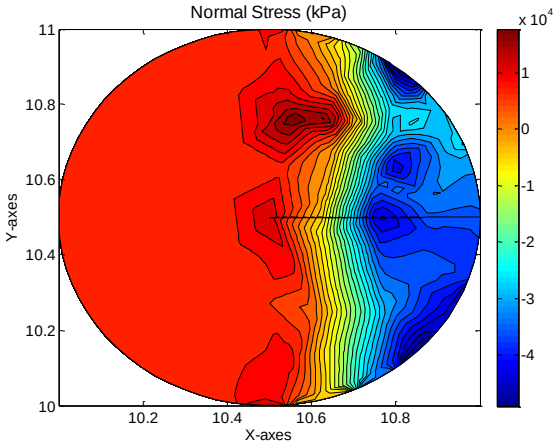

Figure 3.19. *Contour of non-linear normal stress distribution of the interpolated data*

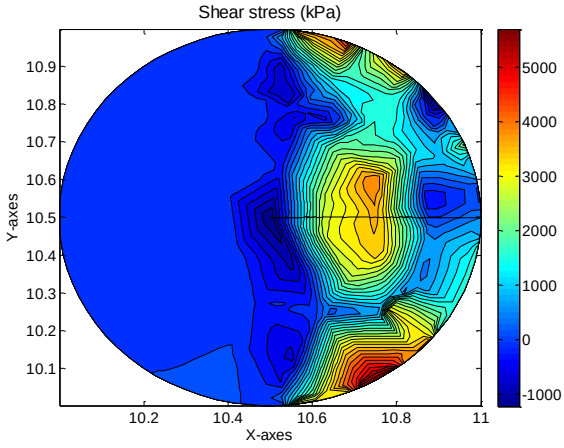

Figure 3.20. *Contour of non-linear shear stress distribution of the interpolated data*

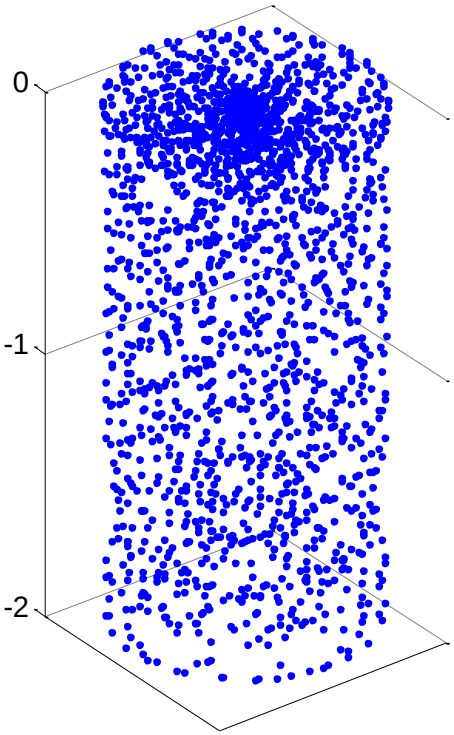

Figure 3.21. *Distribution of the non-elaborated stress points (Gauss points) in the pile volume (only the first 2 meters of the pile are shown)*

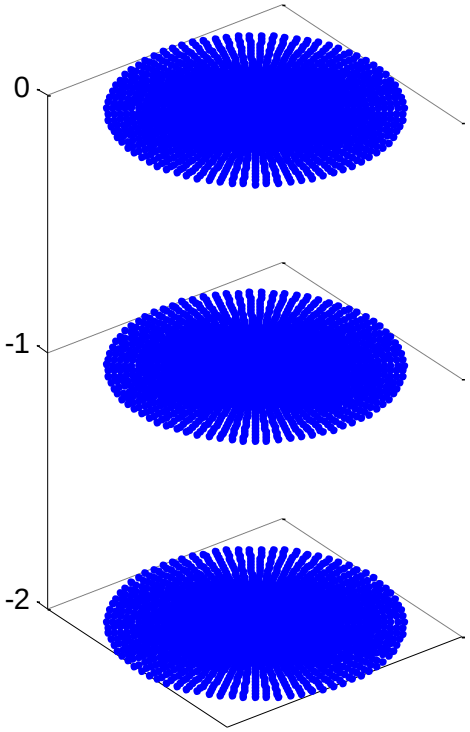

Figure 3.22. *Distribution of the stress points (Gauss points) in the pile volume after the spatial interpolation to specific depths (only the first 2 meters of the pile are shown)*

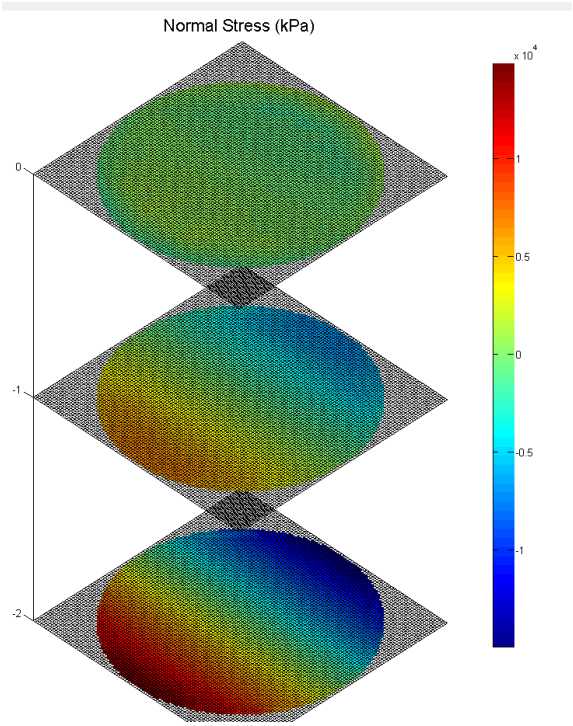

Figure 3.23. *Normal stress distribution at each pile depth(only the first 2 meters of the pile are shown)*

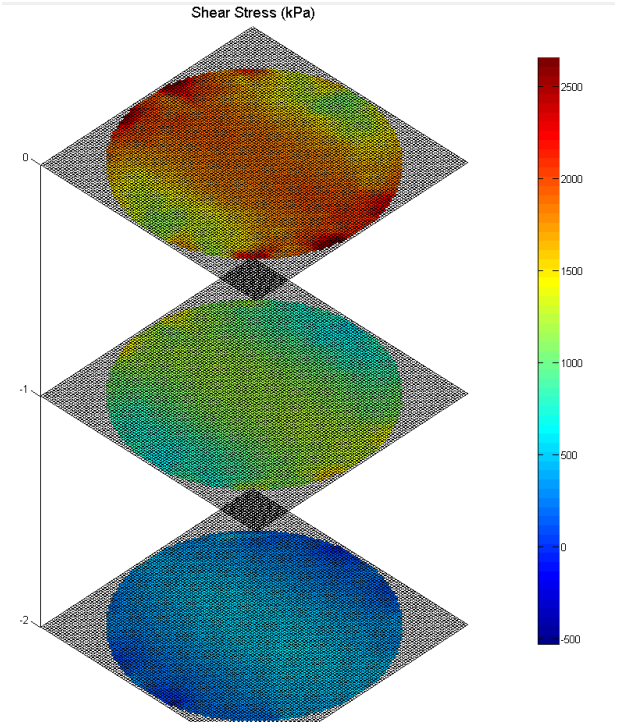

Figure 3.24. *Shear stress distribution at each pile depth(only the first 2 meters of the pile are shown)*

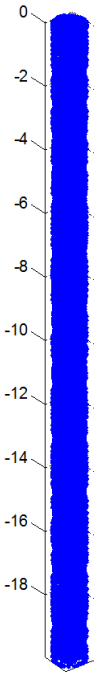

Figure 3.25. *Total Gauss points along the pile as extracted from PLAXIS*

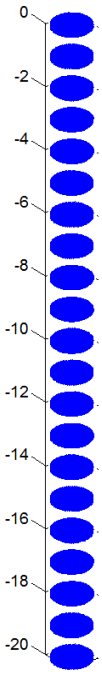

Figure 3.26. *Stress points after elaboration. Internal Forces are computed at each depth according to the interpolated data*

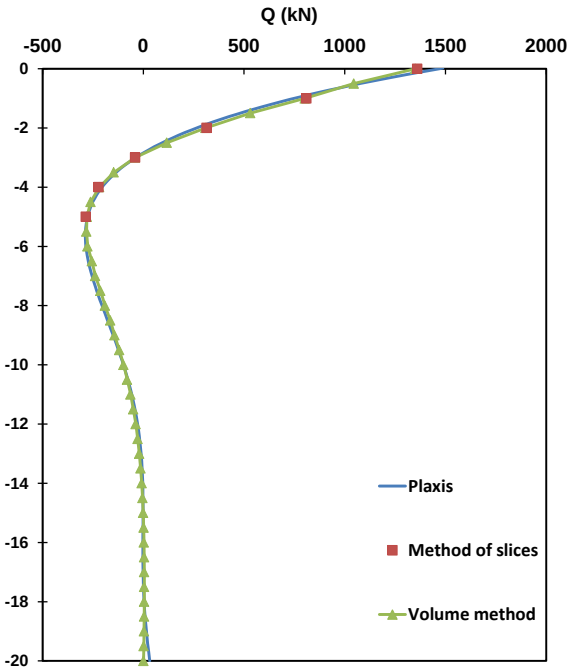

Figure 3.27. *Shear Force. Comparison of the two methods with the results derived from PLAXIS, in elasticity*

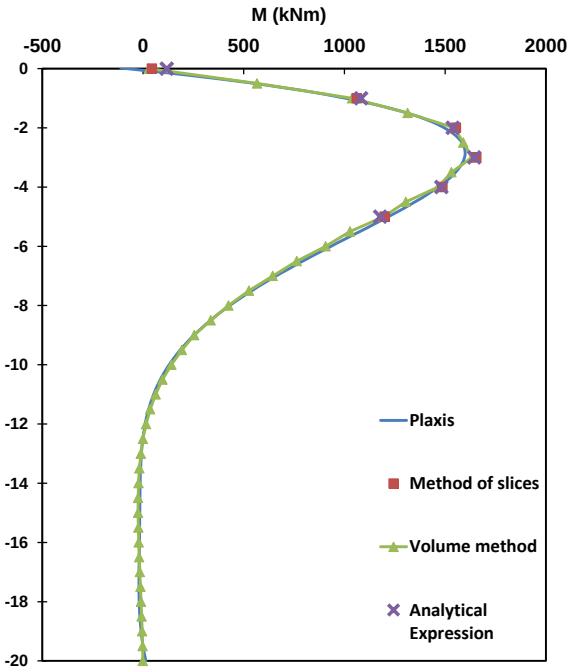

Figure 3.28. *Bending moment. Comparison of the two methods with the results derived from PLAXIS, in elasticity and the semi-analytical expression*

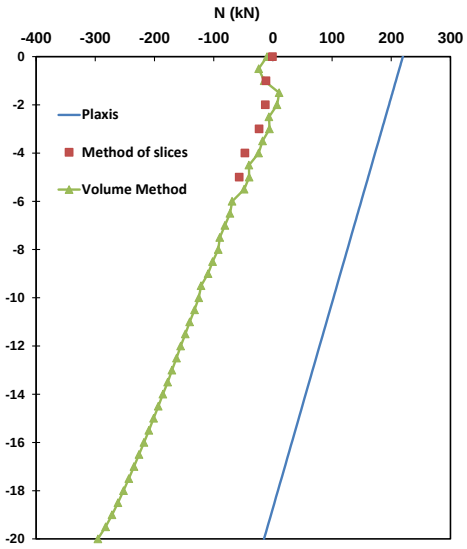

Figure 3.29. *Axial Force. Comparison of the two methods with the PLAXIS results, in elasticity. The difference between the proposed methods and the PLAXIS results may be attributed to the assumption PLAXIS makes which regards the pile as beam. Thus, in order to define border conditions for the pile, considers the pile footing as free edge with zero axial force. In reality, the pile footing commits axial force due to the difference between the specific weight of the reinforced concrete of the pile and that of the soil.*

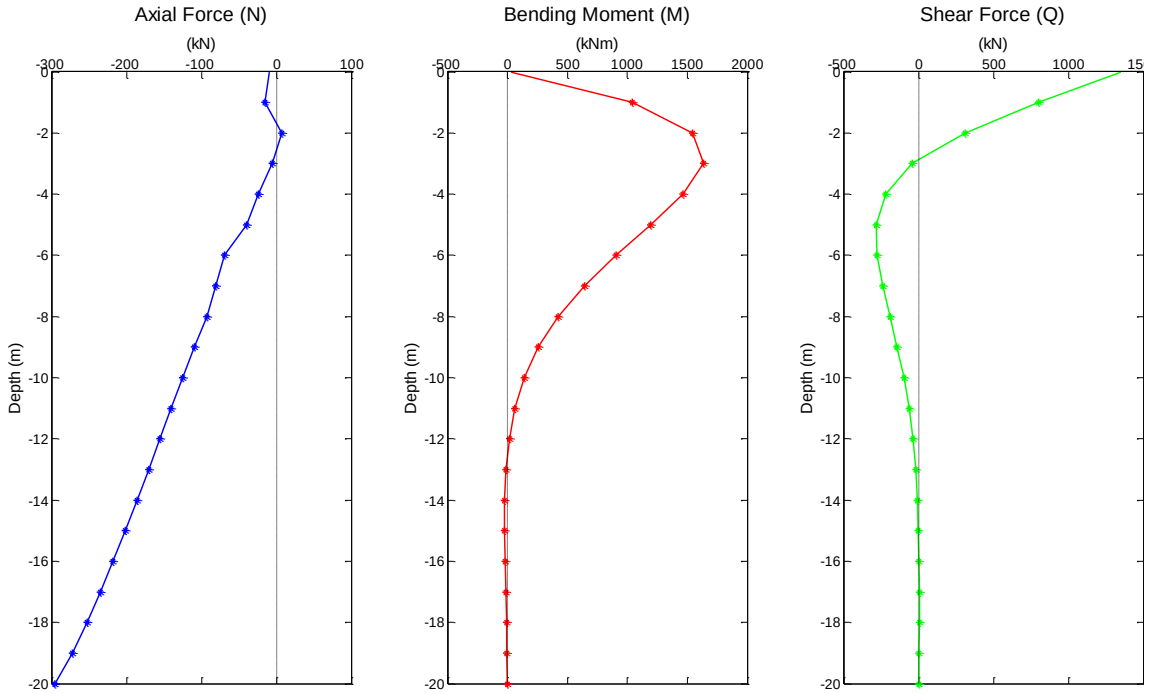

Figure 3.30. *Internal Force diagrams (N,M,Q) as extracted at each pile depth according to the Volume Method*

Chapter 4

Application to Single Pile

4 Application to Single Pile

4.1 Limit Equilibrium Approach

The case of a free-head flexible pile embedded in clay with constant undrained shear strength Su is studied. In this case the soil resistance is

$$P_y = A\, S_u\, D, \qquad \textbf{4.1}$$

where, as mentioned before:

$$A = \lambda_2 + \frac{\sigma'_v}{S_u} + J\,\frac{z}{D} \qquad \text{(Matlock 1970)} \qquad \textbf{4.2}$$

$$\text{for } z \le \frac{7\,D}{\frac{\gamma'\,D}{S_u} + J}$$

And $A = \lambda_2$, otherwise

From static equilibrium:

$$P_y\, f = Q \qquad \textbf{4.3}$$

$$P_y\, f\, \frac{f}{2} = Q\, f + M - M_{pl} \qquad \textbf{4.4}$$

From 3.3:

$$f = \frac{Q}{P_y} \qquad \textbf{4.5}$$

And by applying (4.5) in (4.4):

$$M_{pl} + P_y \left(\frac{Q}{P_y}\right)^2 \frac{1}{2} = Q\,\frac{Q}{P_y} + M \;\Rightarrow$$

$$\frac{M}{M_{pl}} + \left(\frac{Q}{\sqrt{2\,P_y\,M_{pl}}}\right)^2 = 1 \qquad \textbf{4.6}$$

By setting:

$$M_y = M_{pl}$$

$$Q_y = \sqrt{2\,P_y\,M_{pl}}$$

equation (3.6) becomes

$$\frac{M}{M_y} + \left(\frac{Q}{Q_y}\right)^2 = 1 \qquad \textbf{4.7}$$

By taking into consideration all possible N-Q-M combinations at the pile head the failure envelope for a flexible pile embedded in clay with constant undrained shear strength (**4.8**-**4.10**):

$$f = \begin{cases} \left| sign(Q)\left(\frac{Q}{Q_y}\right)^2 + sign(M)\left|\frac{M}{M_y}\right| \right| - 1 = 0, & \left|\frac{M}{M_y}\right| < 1 \\ \left|\frac{M}{M_y}\right| - 1 = 0 & \left|\frac{M}{M_y}\right| = 1 \\ \left|\frac{N}{N_y}\right| - 1 = 0 & \end{cases}$$

where,

$$N_y = N_t + \left(\frac{N_c}{2} - \frac{N_t}{2}\right)(sign(N) + 1) \qquad \textbf{4.11}$$

N_c , N_t the ultimate compressive and tensile capacity respectively.

Assuming an associated flow rule (in which the plastic potential function g coincides with the yield function f) the plastic displacement u^{pl} and the plastic rotation ϕ^{pl} give:

$$\frac{u^{pl}}{\varphi^{pl}} = \frac{2\,Q\,M_y}{{Q_y}^2} = f \qquad \textbf{4.12}$$

confirming that the incremental plastic displacement vectors at the point of failure are normal to the yield locus.

4.2 Finite Element Verification

The proposed failure envelopes and the new method for the calculation of the structural forces are checked against three-dimensional numerical analysis for flexible pile and pile-groups embedded by using the finite element code Plaxis 3D.

4.2.1 Static pushover tests

Considering that the foundation supports a 1-DoF oscillator, one expects that radial loading paths on the M-Q plane are applied in the system. Through a series of force-controlled analyses the failure envelope is ultimately determined. Prior to that, the foundation has undergone vertical loading N to a fraction $\chi = N/Nu$ of its ultimate capacity. *[Cremer, Pecker, Davenne 2001; Gouvernec 2004; Gajan, Kutter, Phalen, Hutchinson, Martin 2005]*.

4.2.2 Static pushover tests

The steps followed in our numerical experiments represent the actual conditions in the field. The soil undergoes geostatic loading and then a part of the soil is replaced by the foundation, on which a vertical load N is applied increasingly till a specified value of $\chi = N/Nu$ is reached. Afterwards, the vertical load is kept constant and a combination of horizontal force and moment is applied at the head of the pile till the complete failure of the system. Apparently, this implies the state in which no further lateral loading can be undertaken. The above procedure is repeated for various factors of safety against vertical loading and for various radial loading paths. Our aim is to extract the ultimate capacities under pure moment Mu and pure horizontal force Q_u, and then sweep the M-Q plane so that a cross-section of the failure envelope is revealed. Repeating this procedure from the Ultimate Axial Compression Capacity to the ultimate Axial Tension Capacity the total 3D Failure Envelope in M-QN space is designed.

4.3 Finite Element Modelling

A 16 m long pile with 1 m diameter is embedded in the soil. The distance from the pile tip to the bottom of the model is 6 m. Figure (4.5) depicts the finite element discretization of the problem. Approximately 48000 elements were used for each analysis. The soil is modeled with 10-node tetrahedral elements while the pile is modeled as a soil volume calibrated with the previously macroscopic hardening Soil model approach to simulate the behavior of a circular concrete pile with As=1.5% . A sensitivity analysis for the lateral boundaries is carried out to ensure the accuracy of the model, placing them finally at the distance of 0.6L. The selected Soil is Clay with constant with the depth Undrained Shear Strength Su=50 kPa, specific weight γ=20 kN/m3 and E_s=25000 kN/m and its behavior is described by the Mohr-Coulomb Model. The poisson's ratio is v=0.45 while the angle of friction is ϕ=0° to simulate undrained water conditions. The pile has an elasticity Modulus of Ec=30*10^6 KN/m, a poisson's ratio v=0.2 and a specific weight practically zero (γ=0.01 KN/m2) to ensure that the derived ultimate loads are the total ones, while cohesion is chosen to be c=15262 kPa, the angle of friction ϕ=0° and tension cut-off strength equal to 7534 kPa in order to capture the correct pile behavior. An Interface is used between the pile and the soil enabling gapping and slippage with a friction coefficient R=1.

4.4 Results

Figure 4.1 displays the failure envelope of concrete pile, as defined from the equation 4.7. Figure 4.2 shows the combinations of moment and shear force at failure, which were chosen for the study of the pile forces. The influence of the vertical load can clearly be captivated in Fig. 4.3 where the maximum capacities magnify by the increase of the axial load. Figures 4.8 – 4.25 show the structural forces as extracted from MATLAB code, for combinations at failure and for characteristic failure mechanisms. The effect of axial force to the moment capacity and the moment distribution along the pile is examined afterwards, in figures 4.26 – 4.32. Firstly, the case of single pile embedded in soft clay is studied, subjected to different axial loading, which results to different factors of safety.

Figures

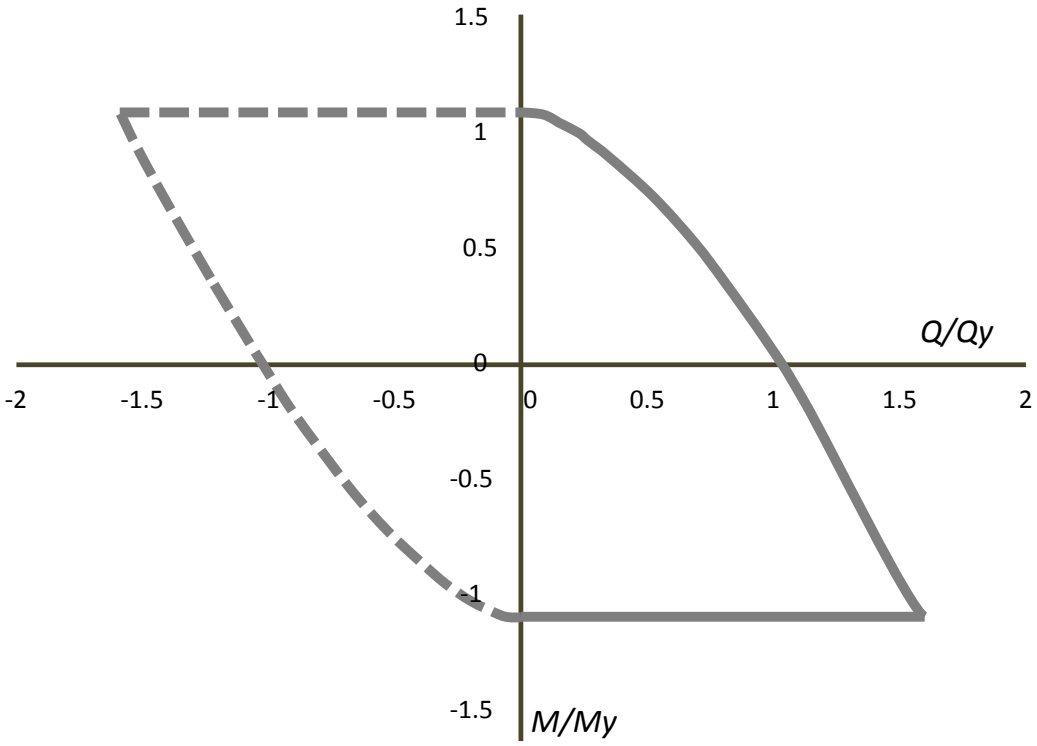

Figure 4.1. *Failure envelope for specific axial force, for a circular concrete pile with As=1.5%*

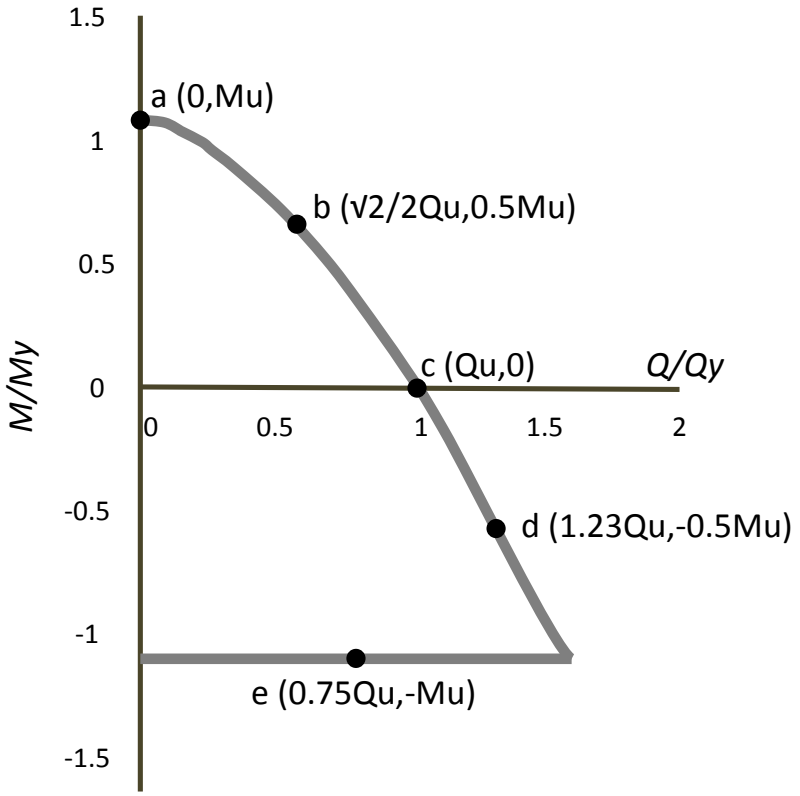

Figure 4.2. *From the y'y symmetric failure envelope, 5 combinations of Moment and Shear force were chosen, that represent characteristic areas of the failure zones*

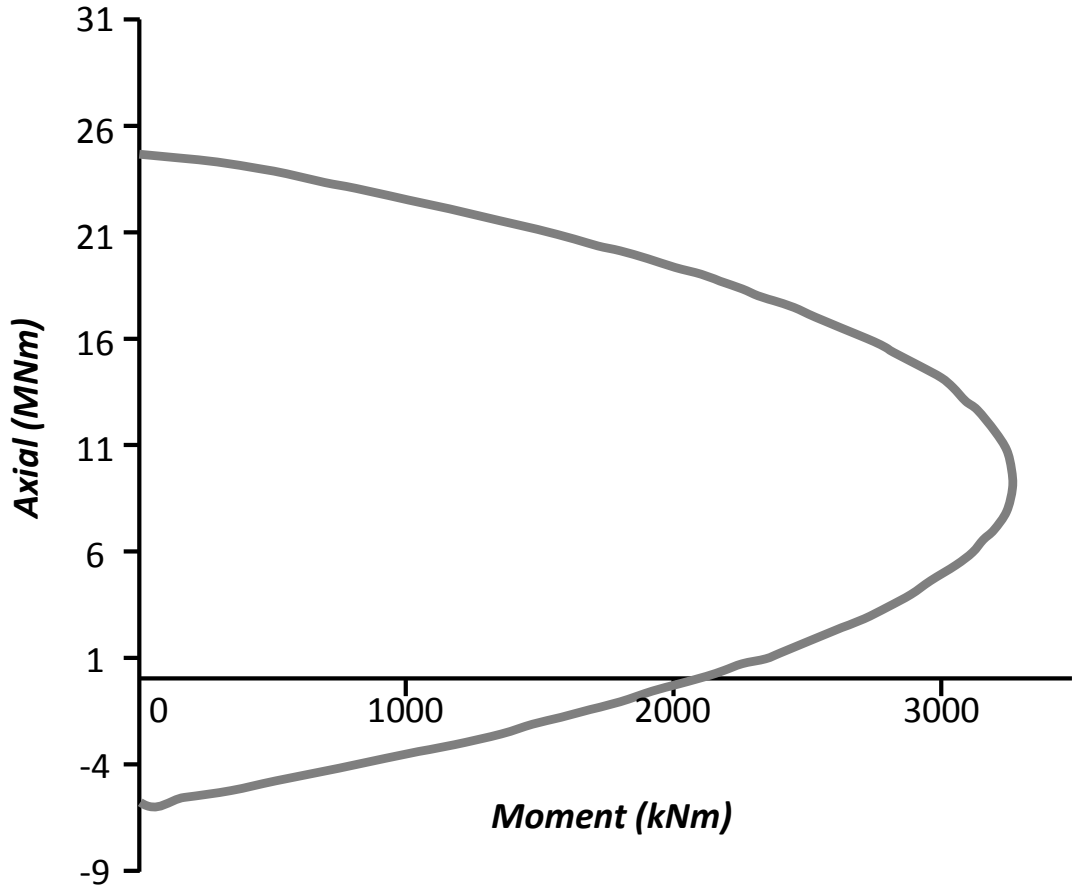

Figure 4.3. *Moment – Axial force interaction diagram, for cylindrical concrete pile with As=1.5%. The dependence of the moment capacity with respect to the pile axial force is represented*

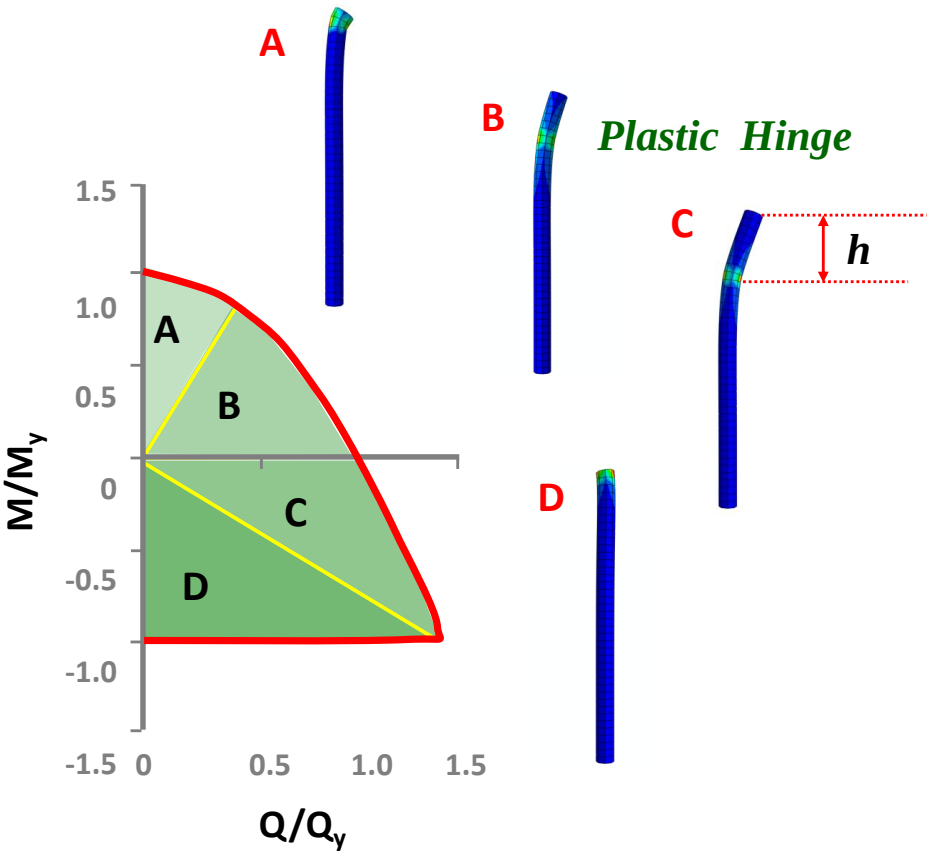

Figure 4.4. *Failure mechanisms of single piles with respect to the different Moment – Shear force combinations*

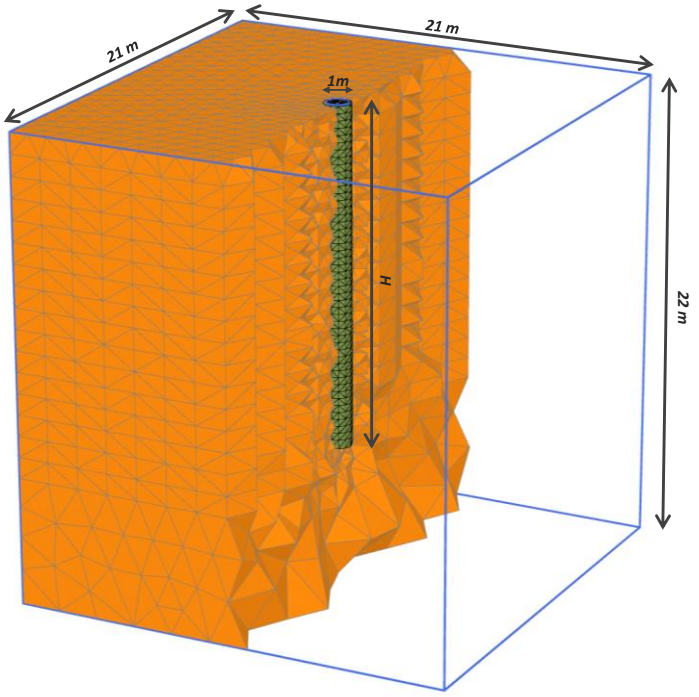

Figure 4.5. *The finite element model of single, flexible pile in clay*

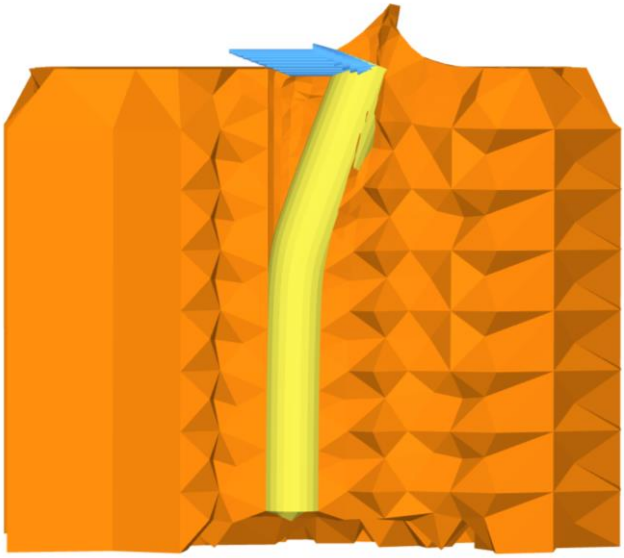

Figure 4.6. *Vertical intersection of pile under horizontal loading. This figure depicts clearly the three types of non-linearity and their interaction as a system: The soil non-linearity, the pile plastification and the geometric non linearities*

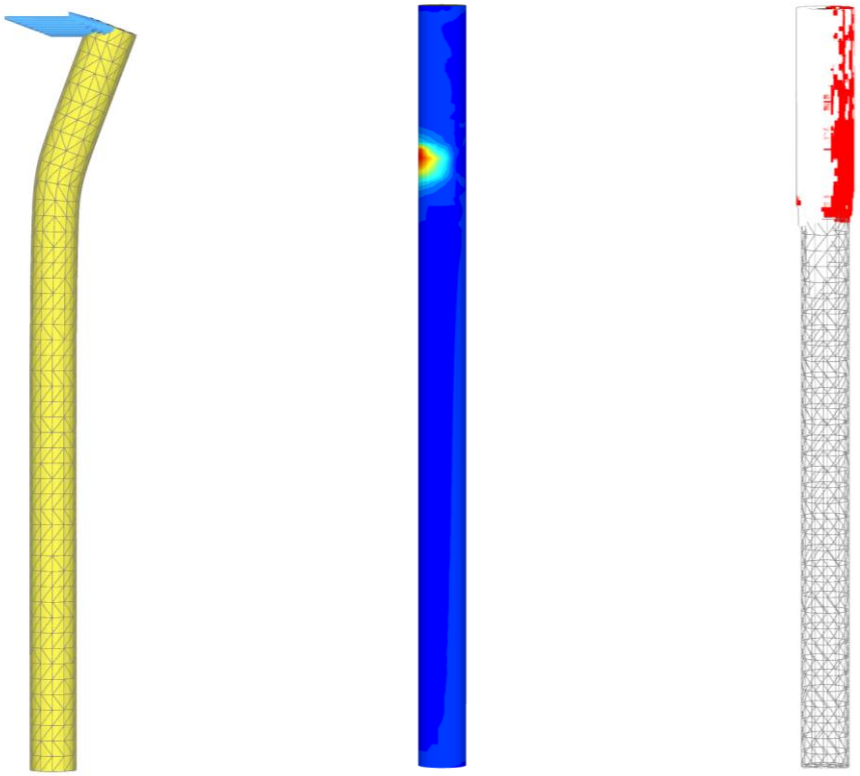

Figure 4.7. *Pile under horizontal loading. The three figures show respectively the deformed mesh of pile in failure, the pile deviatoric strains ($\Delta\gamma_s$) which show the plastic hinge region, and the pile plastic points i.e. the plasticized Mohr – Coulomb points (red) and the tension cut-off points (white)*

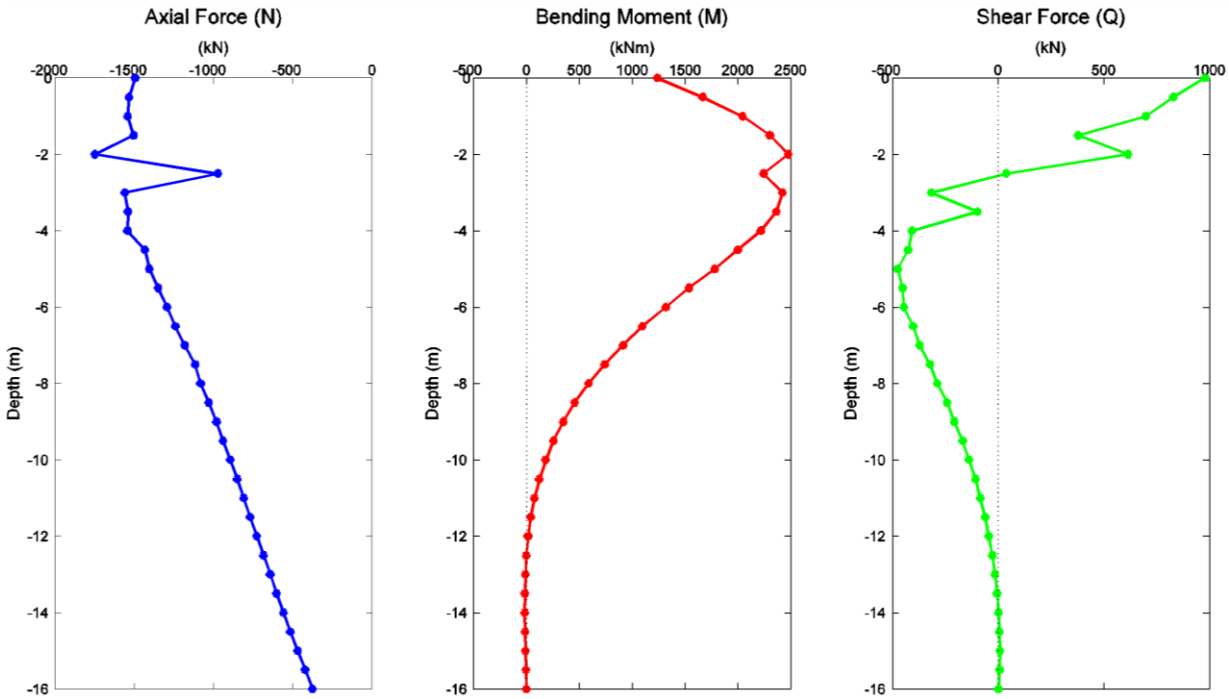

Figure 4.8. *Structural forces of single pile with SF_v=2 at failure combination:* $\left(\sqrt{2}/_2\ Q_u\ , 0.5\ M_u\right)$

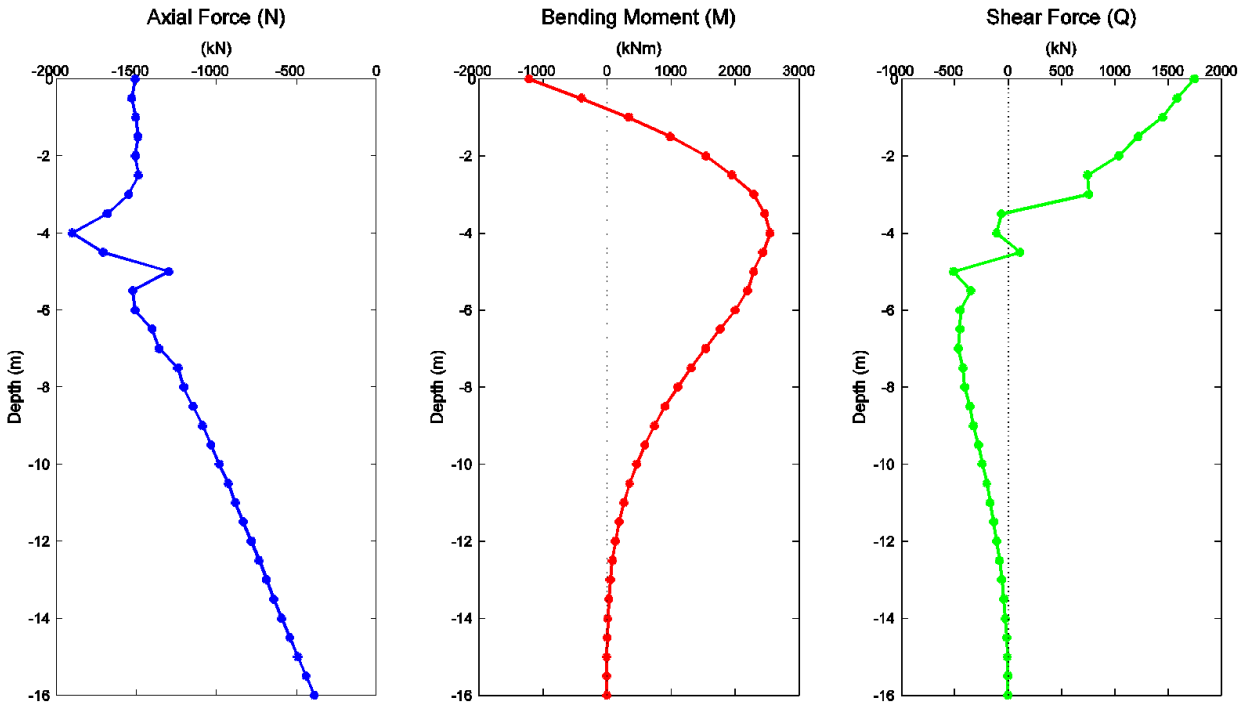

Figure 4.9. *Structural forces of single pile with SF_v=2 at failure combination:* $\left(1.23\ Q_u\ , -0.5\ M_u\right)$

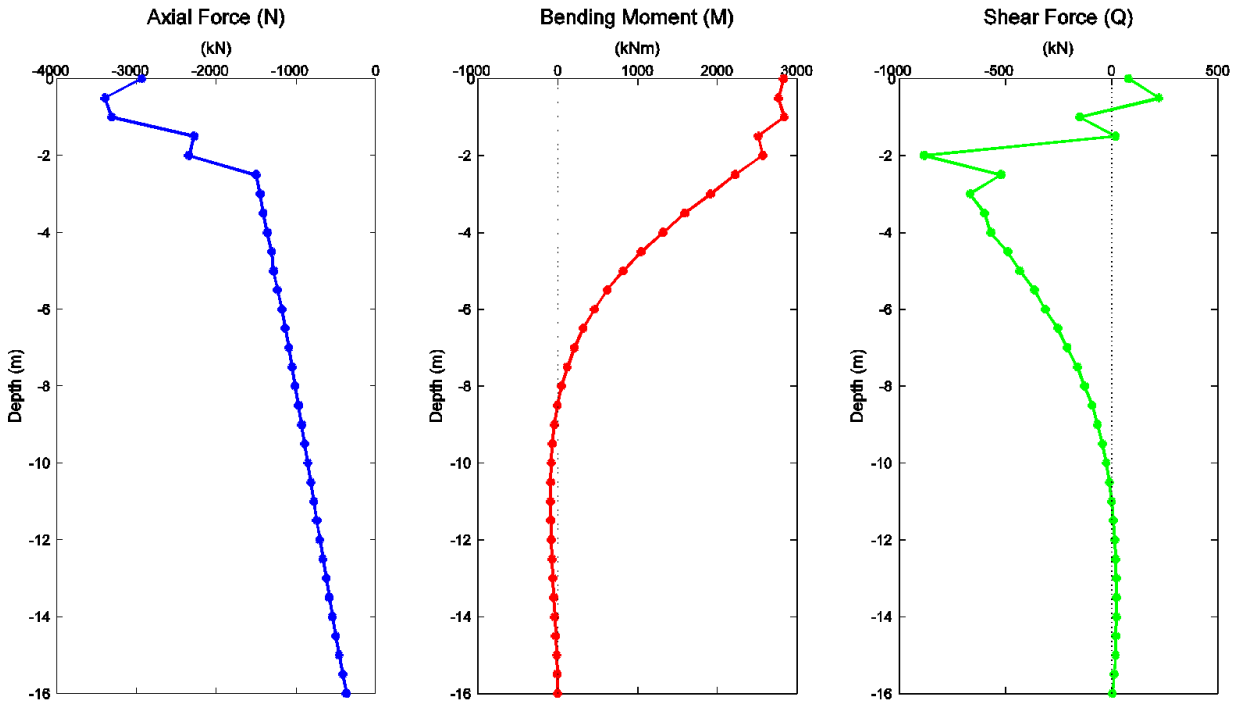

Figure 4.10. *Structural forces of single pile with SF_v=2 at failure combination:* $(0\ ,\ M_u)$

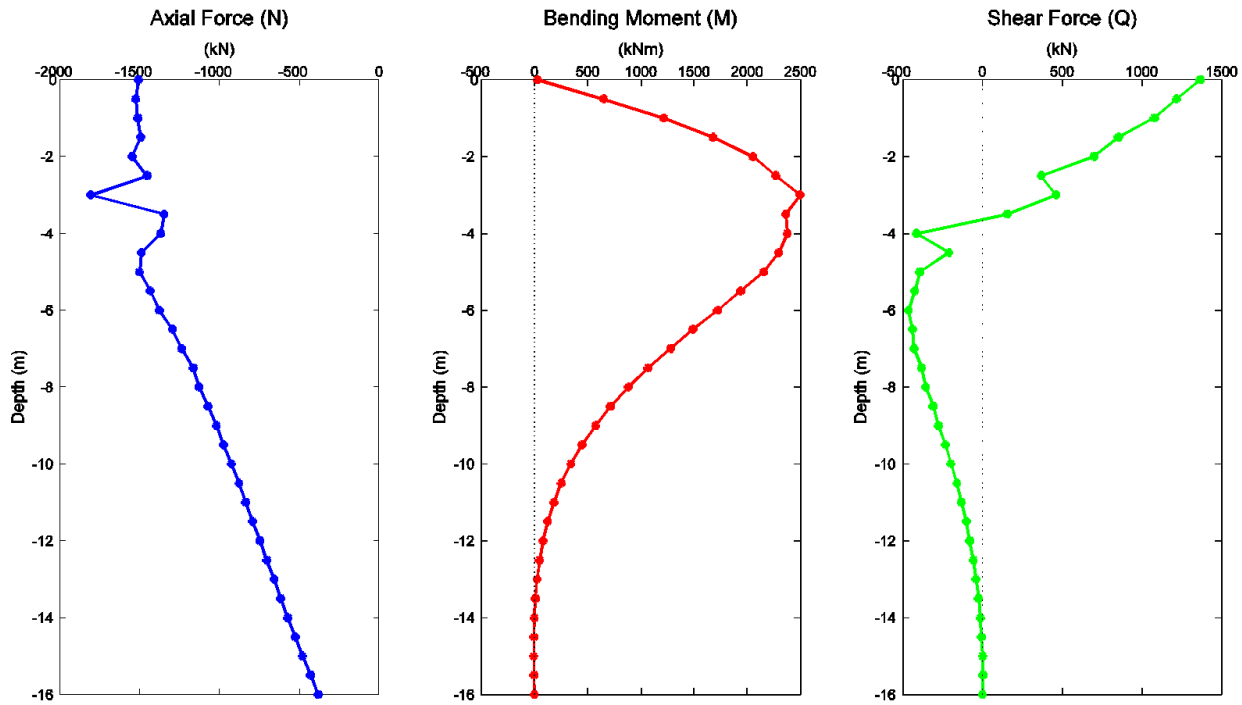

Figure 4.11. *Structural forces of single pile with SF_v=2 at failure combination:* $(\ Q_u\ , 0)$

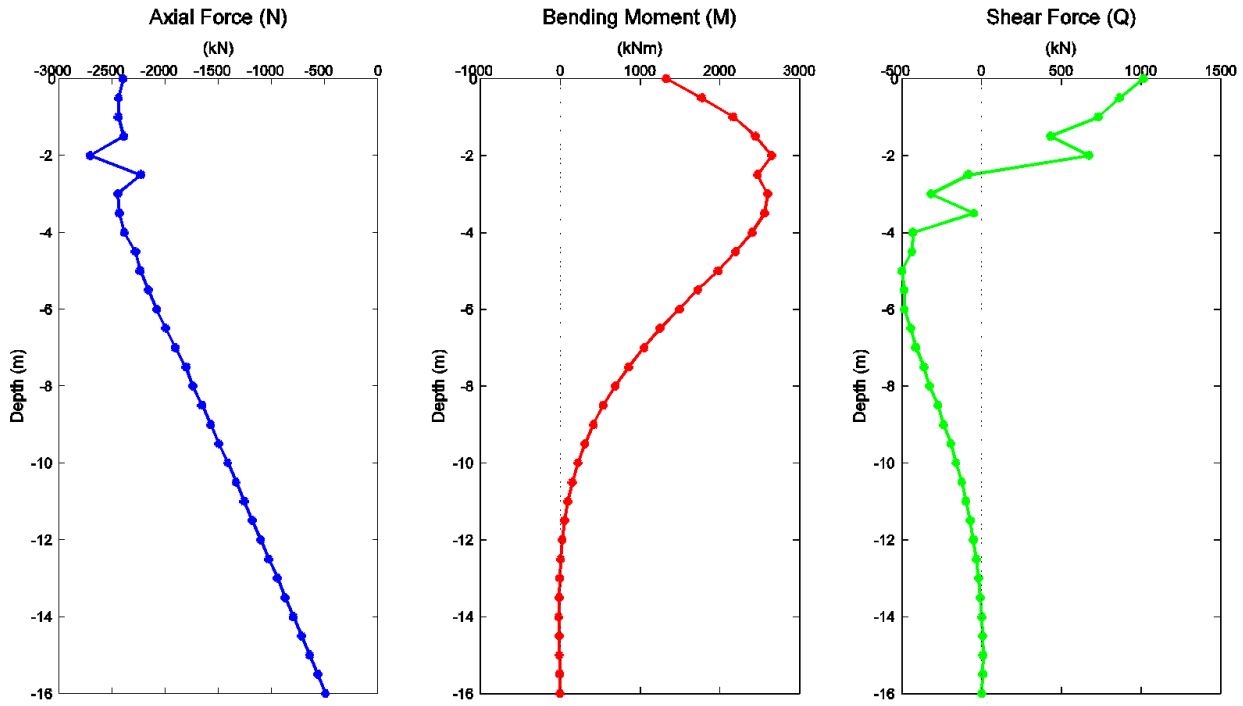

Figure 4.12. *Structural forces of single pile with SF_v=1.25 at failure combination:* $\left(\sqrt{2}/_2\ Q_u\ , 0.5\ M_u\right)$

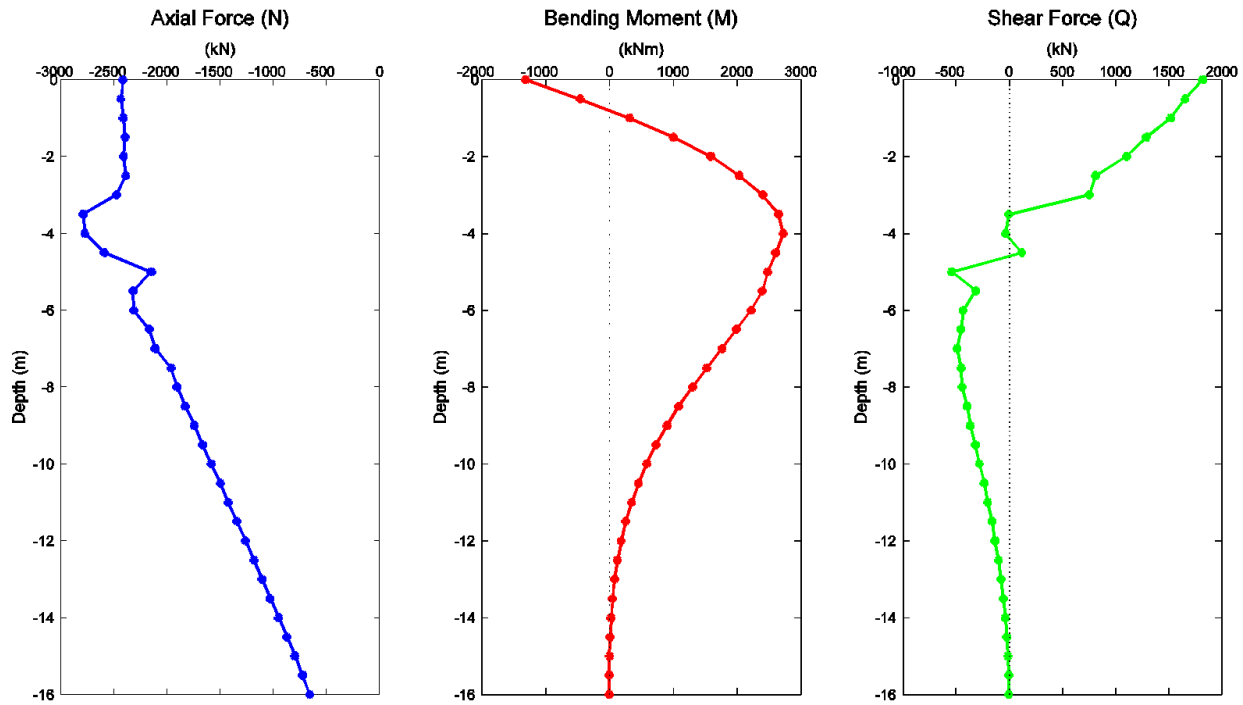

Figure 4.13. *Structural forces of single pile with SF_v=1.25 at failure combination:* $\left(1.23\ Q_u\ , -0.5\ M_u\right)$

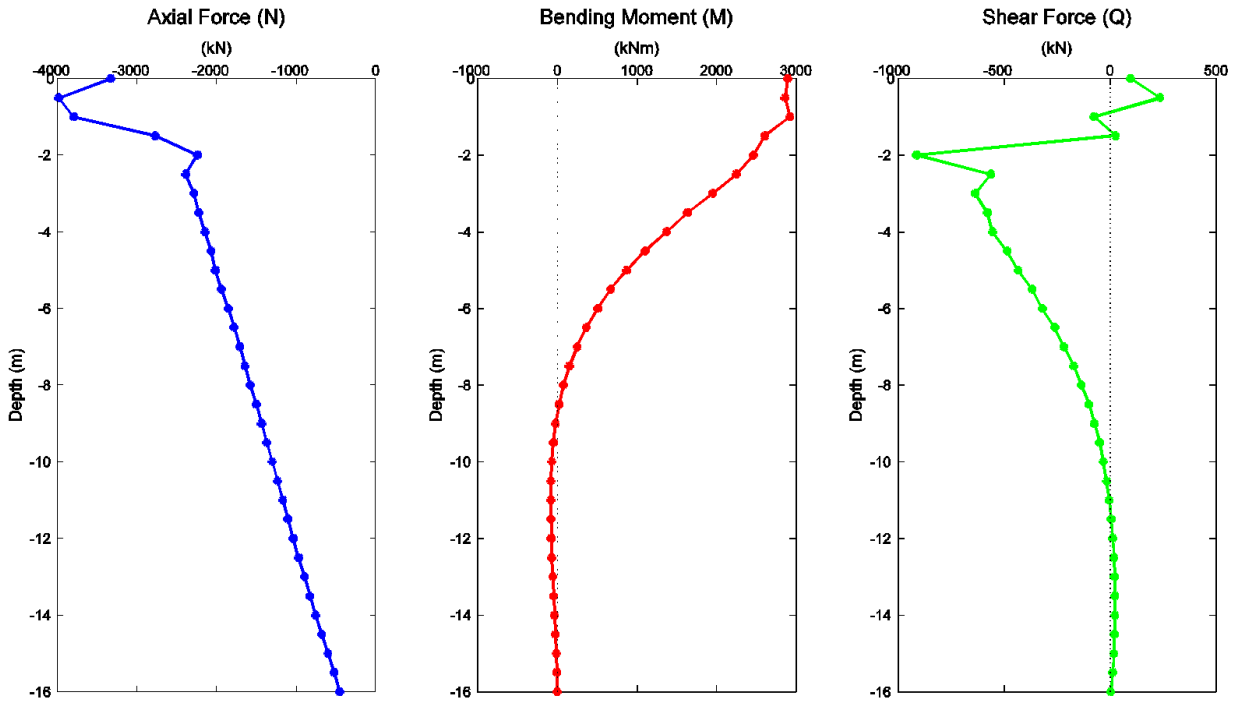

Figure 4.14. *Structural forces of single pile with SF_v=1.25 at failure combination:* $(0\ ,M_u)$

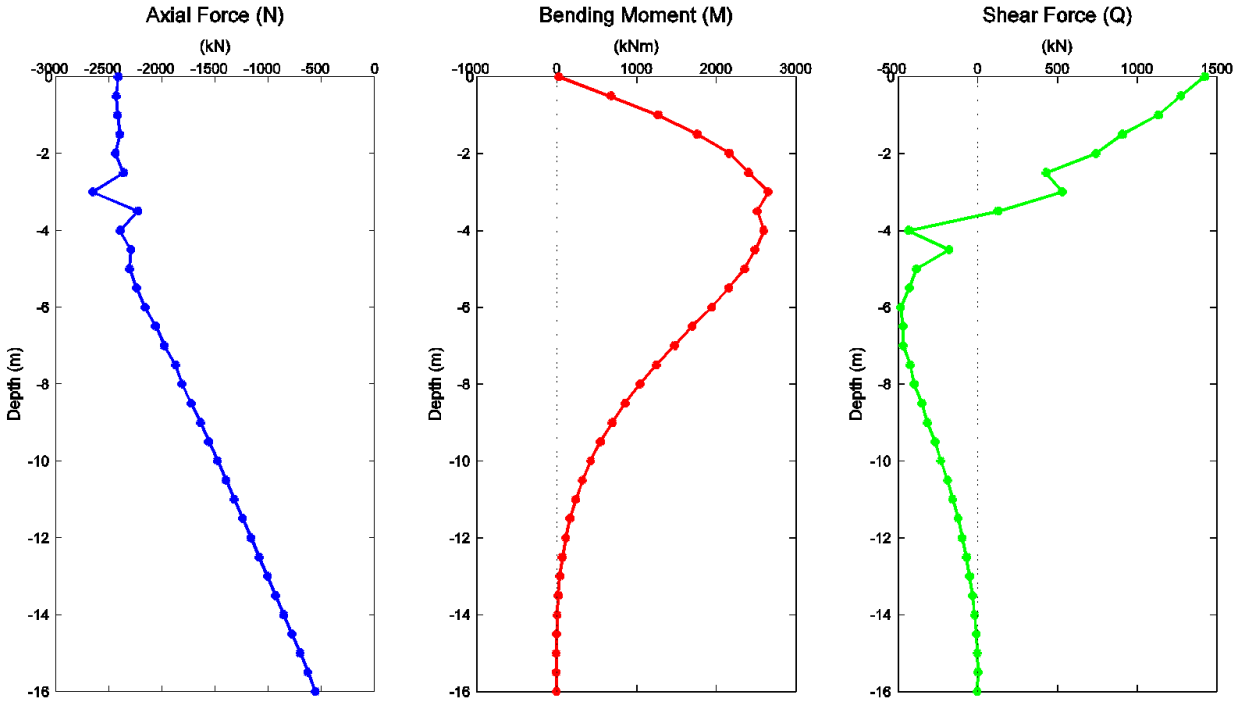

Figure 4.15. *Structural forces of single pile with SF_v=1.25 at failure combination:* $(Q_u\ ,0)$

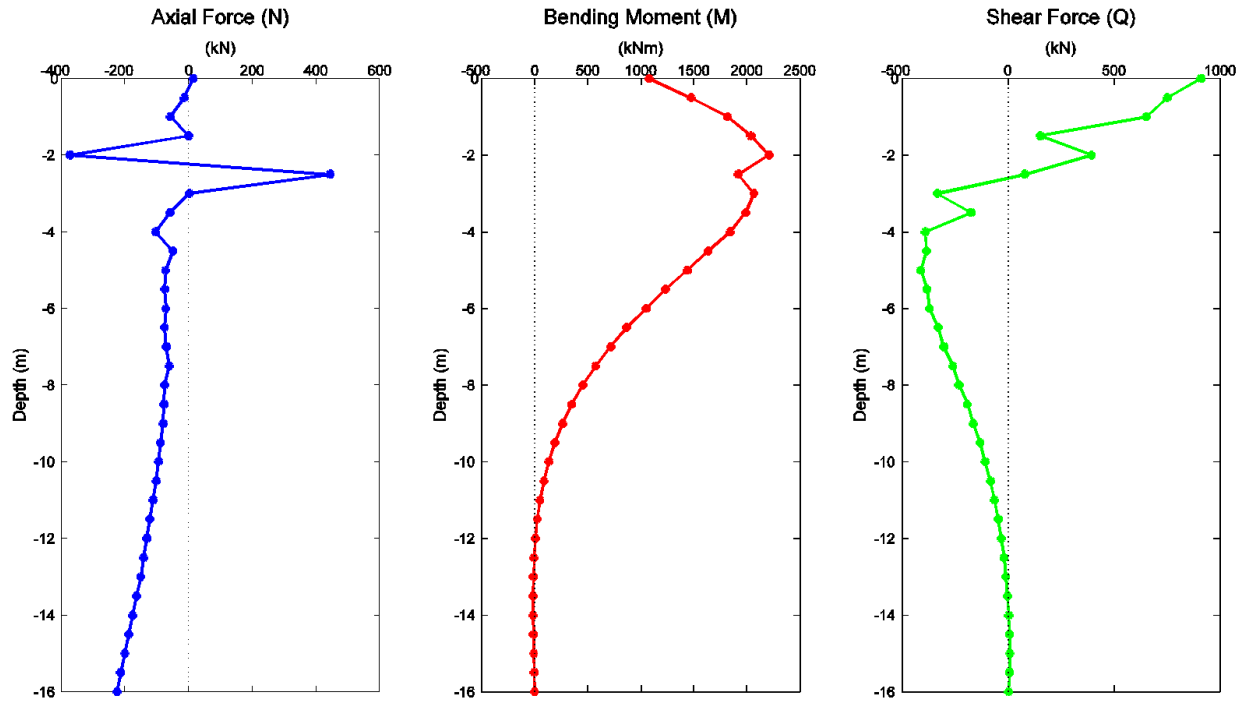

Figure 4.16. *Structural forces of single pile with SF_v=∞ at failure combination:* $\left(\sqrt{2}/_2\ Q_u\ , 0.5\ M_u\right)$

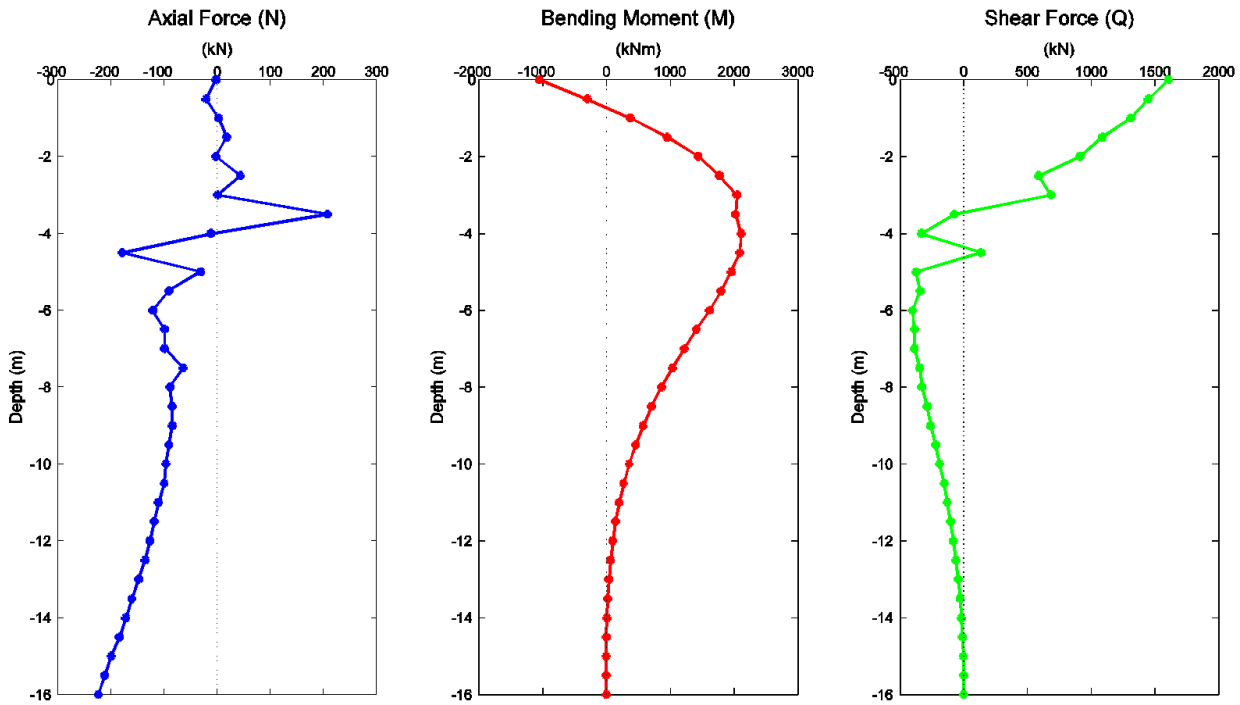

Figure 4.17. *Structural forces of single pile with SF_v=∞ at failure combination:* $\left(1.23\ Q_u\ , -0.5\ M_u\right)$

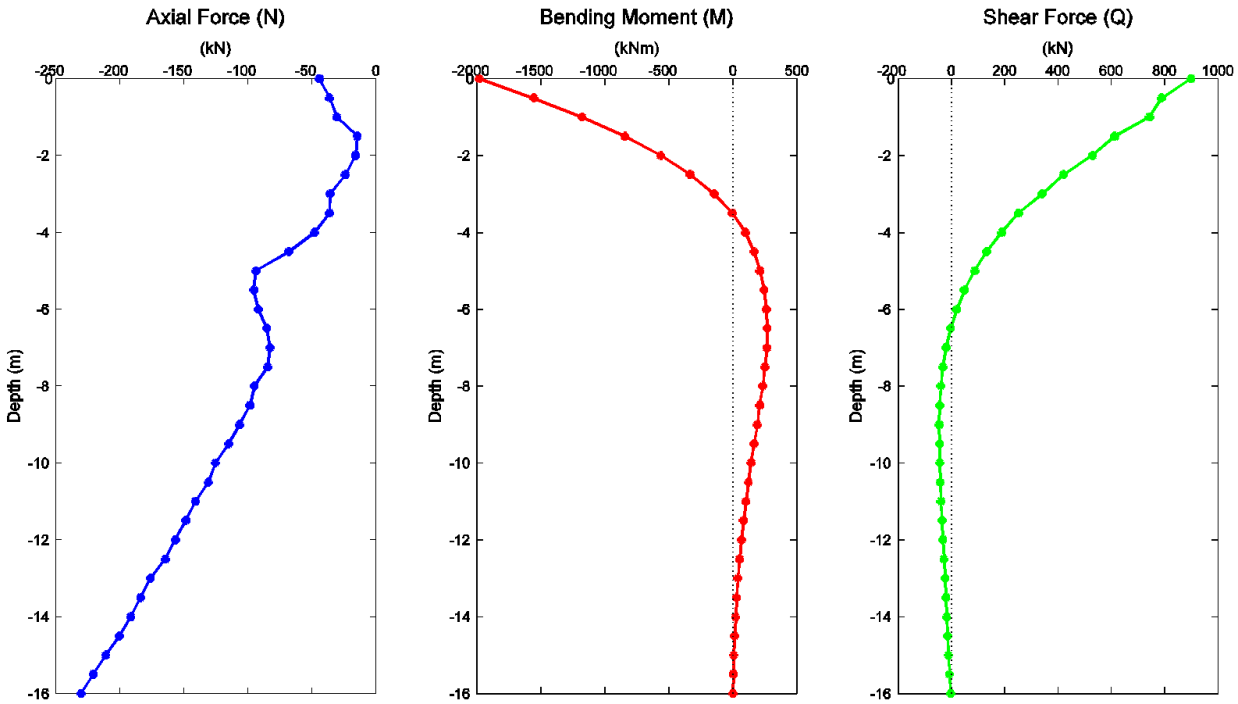

Figure 4.18. *Structural forces of single pile with SF_v=∞ at failure combination:* $(0.75\ Q_u\ , -M_u)$

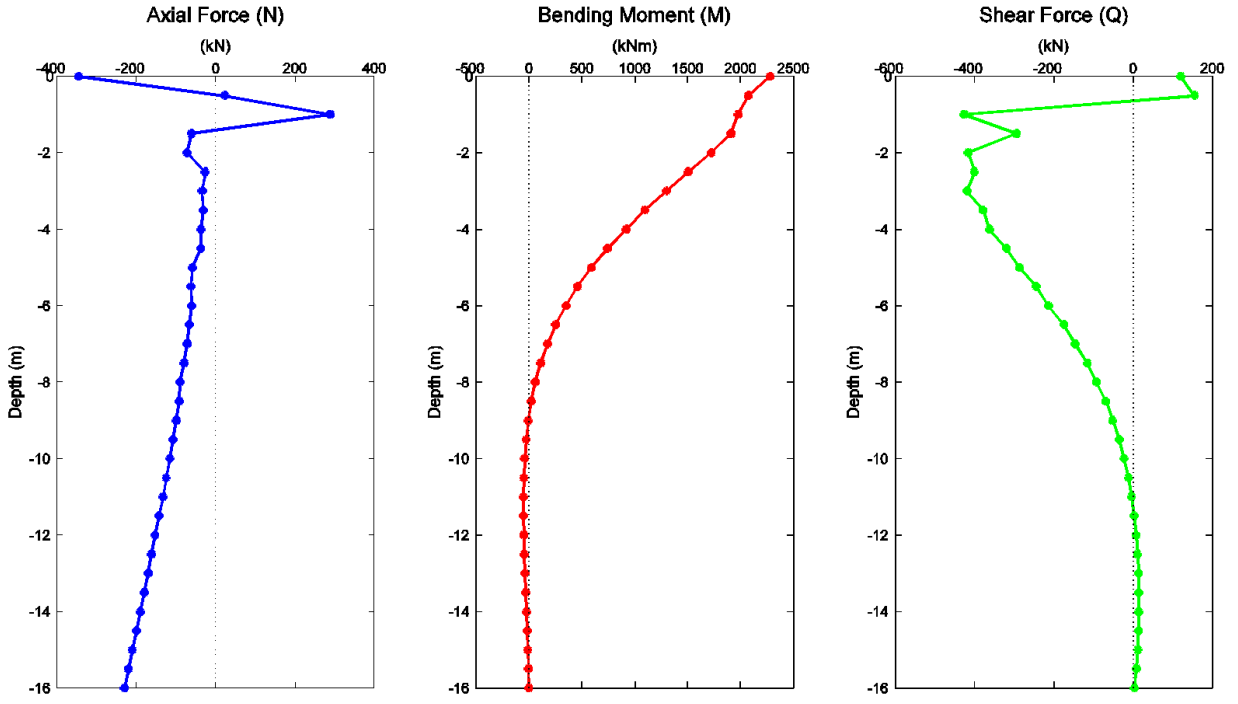

Figure 4.19. *Structural forces of single pile with SF_v=∞ at failure combination:* $(0\ , M_u)$

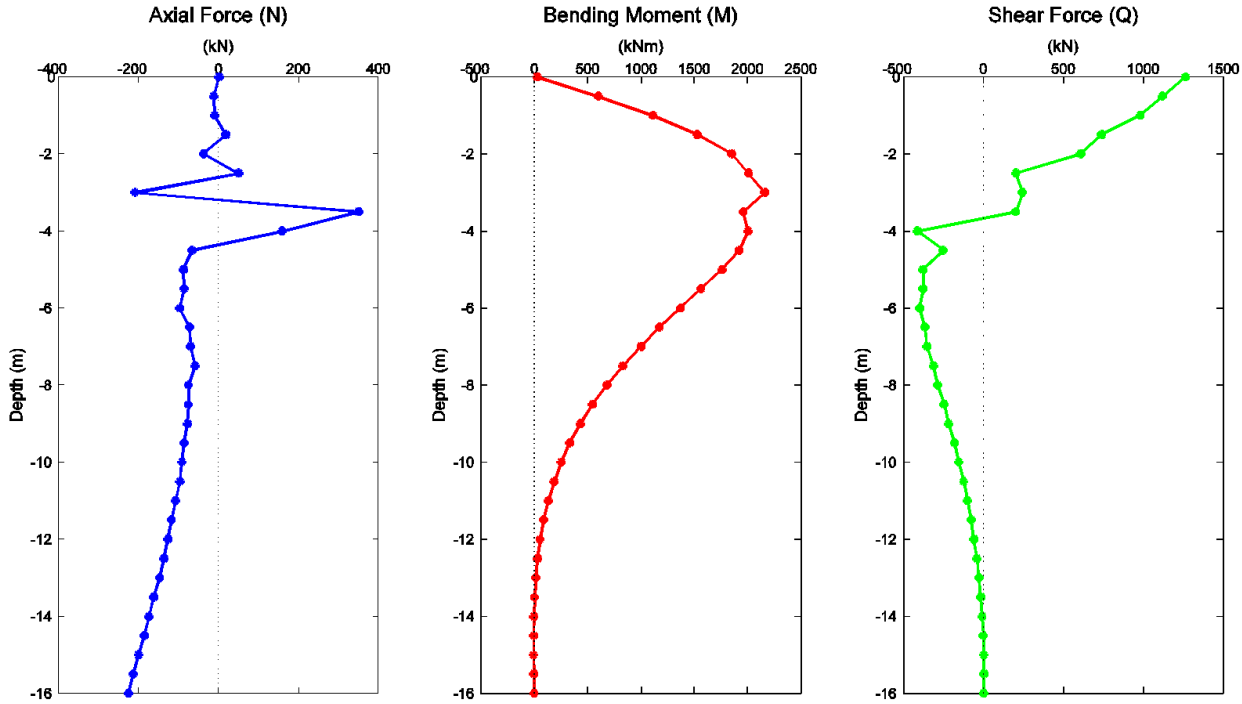

Figure 4.20. *Structural forces of single pile with SF_v=∞ at failure combination:* $(Q_u\ , 0)$

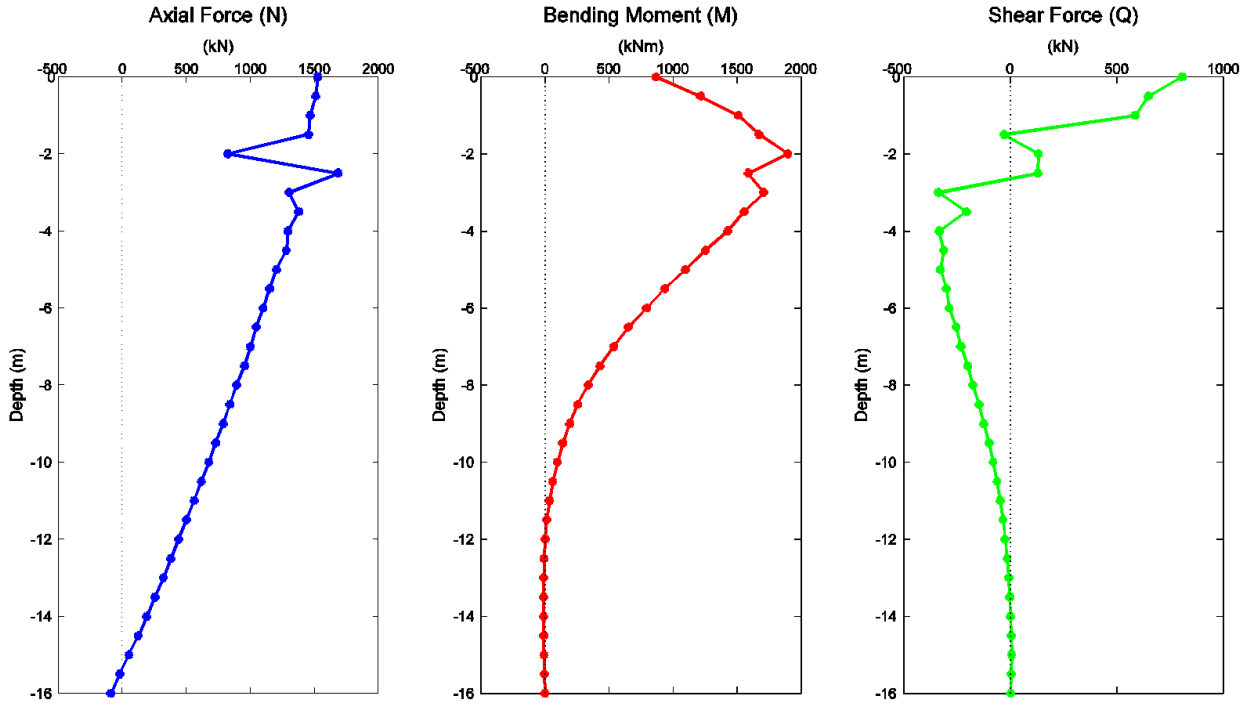

Figure 4.21. *Structural forces of single pile with SF_v= -2 at failure combination:* $\left({}^{\sqrt{2}}/_{2}\ Q_u\ , 0.5\ M_u\right)$

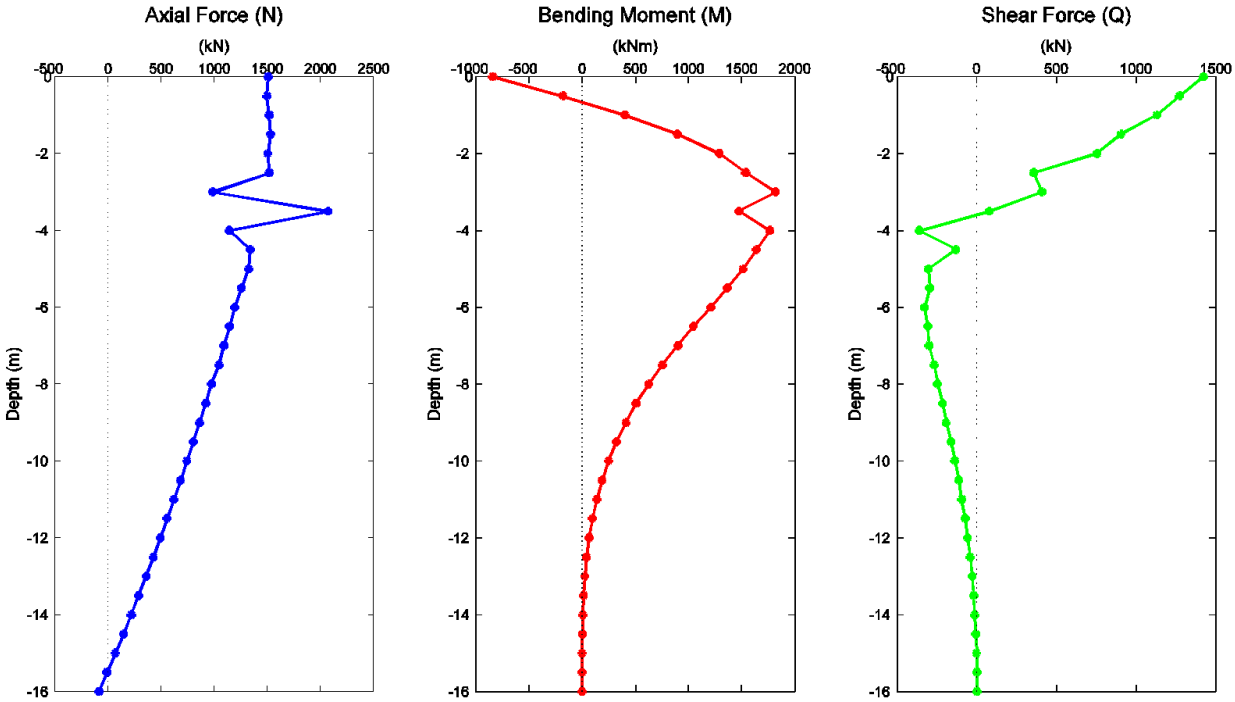

Figure 4.22. *Structural forces of single pile with SF_v= -2 at failure combination:* $\left(1.23\ Q_u\ , -0.5\ M_u\right)$

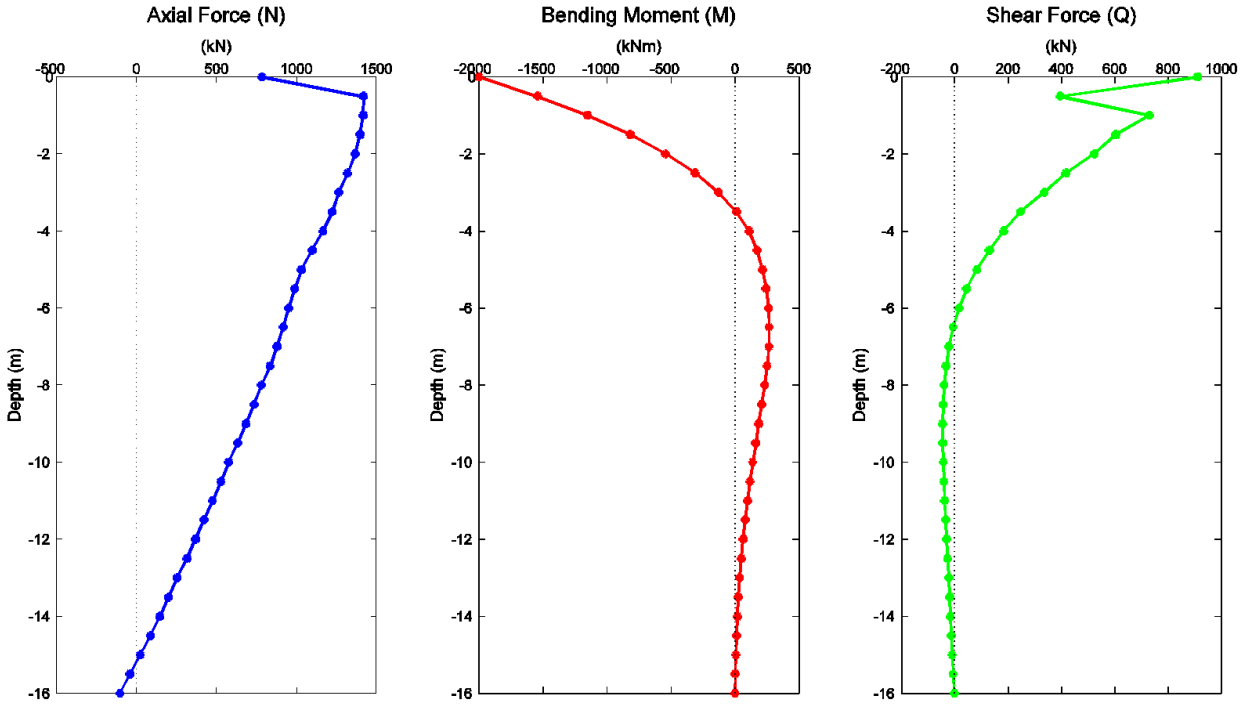

Figure 4.23. *Structural forces of single pile with SF_v= -2 at failure combination:* $\left(0.75\ Q_u\ , -M_u\right)$

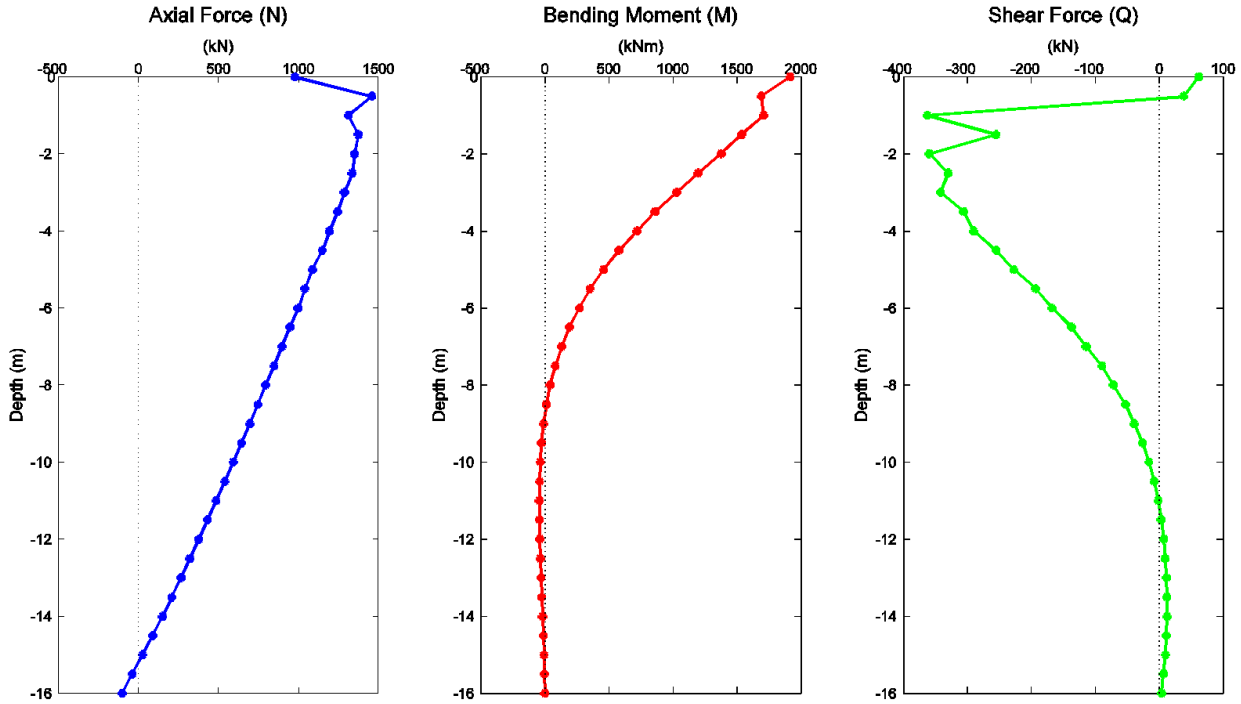

Figure 4.24. *Structural forces of single pile with SF_v= -2 at failure combination:* $(0\ ,M_u)$

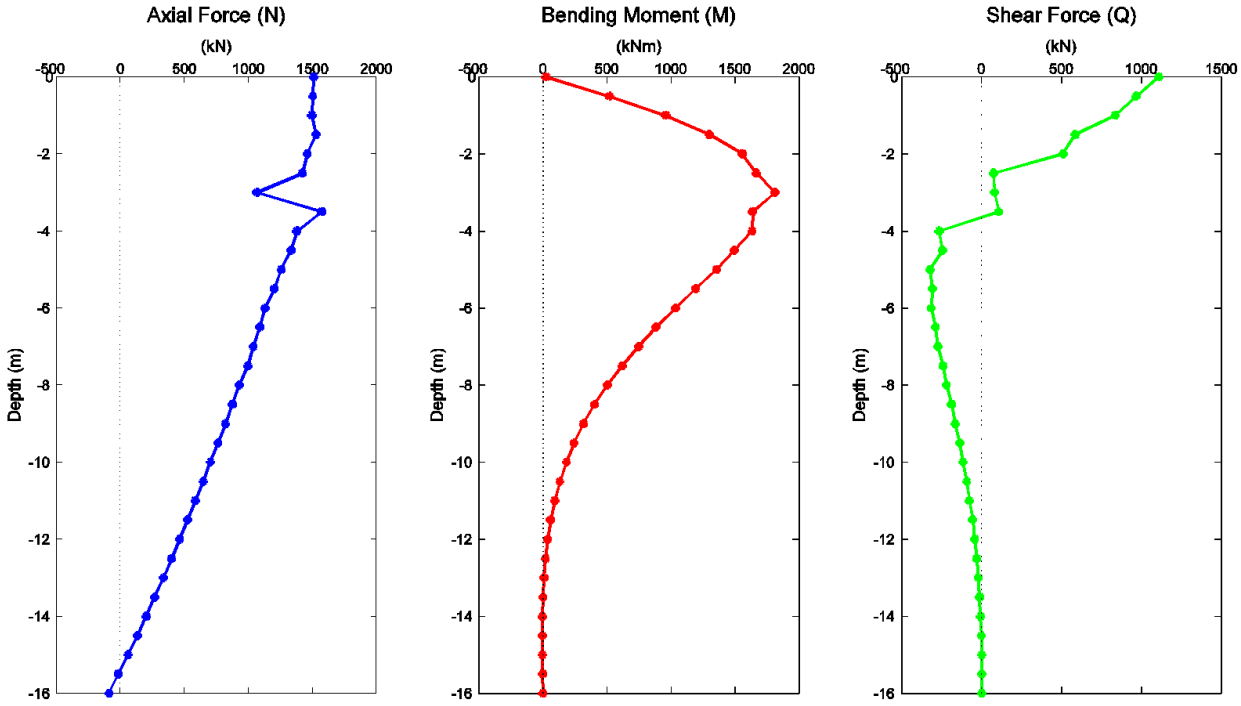

Figure 4.25. *Structural forces of single pile with SF_v= -2 at failure combination:* $(Q_u\ ,0)$

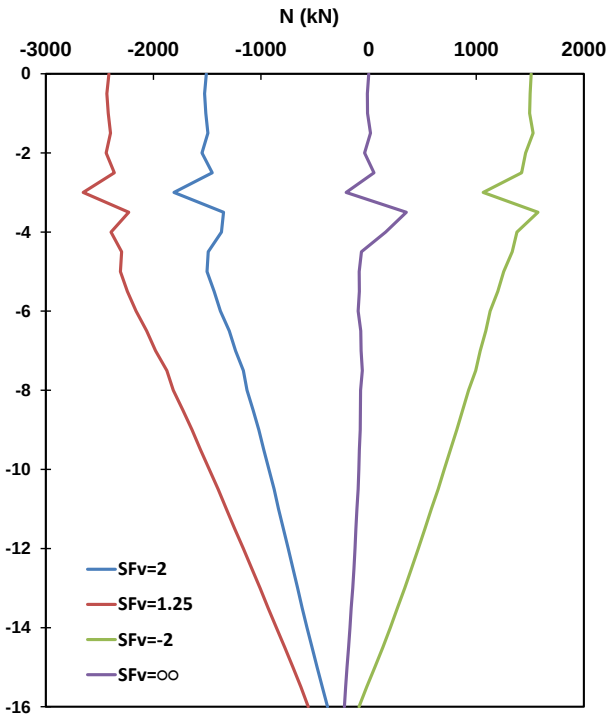

Figure 4.26. *Axial loading, for different safety factors. Pile embedded in clay with Su=50kPa*

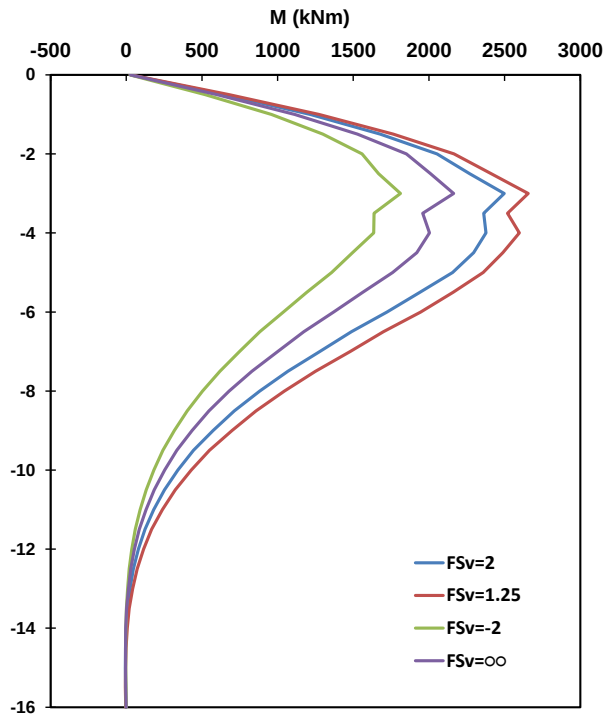

Figure 4.27. *Moment capacity under horizontal loading, for different safety factors*

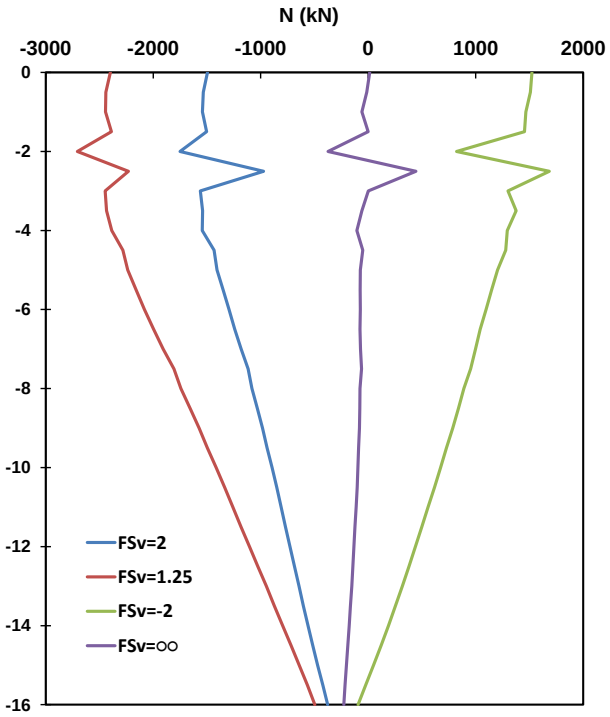

Figure 4.28. *Axial loading, for different safety factors. Pile embedded in clay with Su=50kPa*

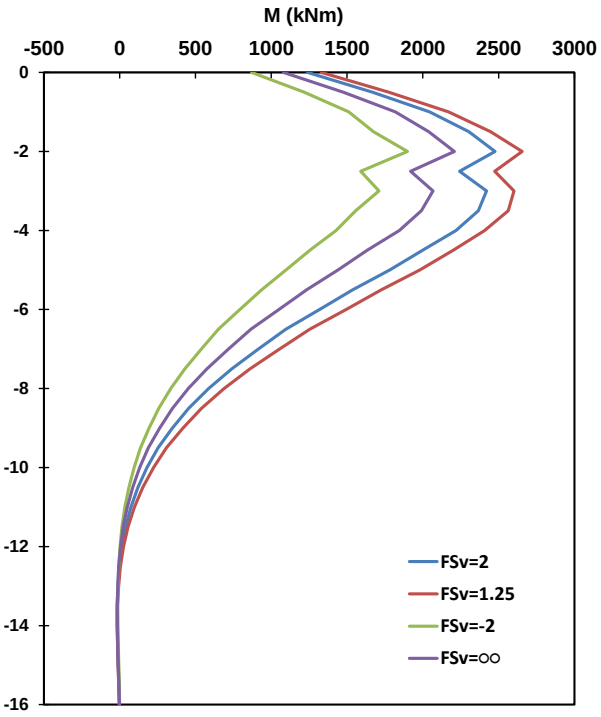

Figure 4.29. *Moment capacity under combination of horizontal loading and bending moment* $\left(\sqrt{2}/_2\ Q_u\ , 0.5\ M_u\right)$*, for different safety factors*

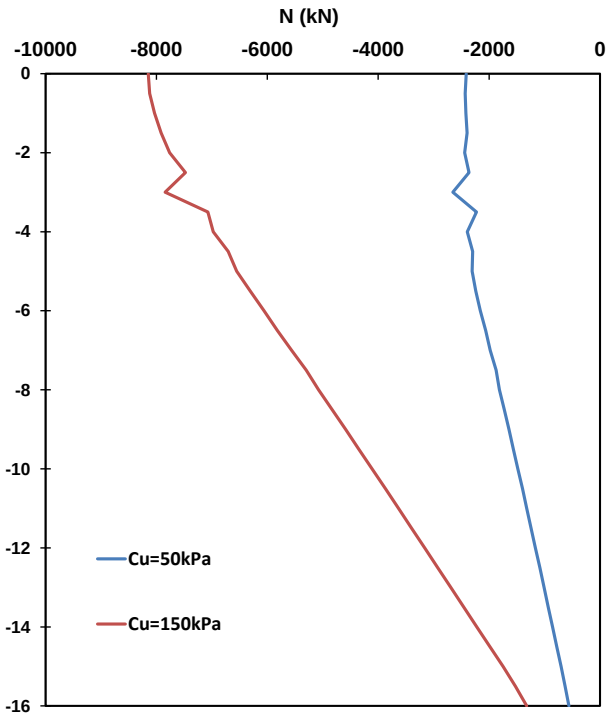

Figure 4.30. *Axial loading, for pile embedded in clay with a)Su=50kPa b)Su=150kPa. The factor of safety is SF_V=1.25*

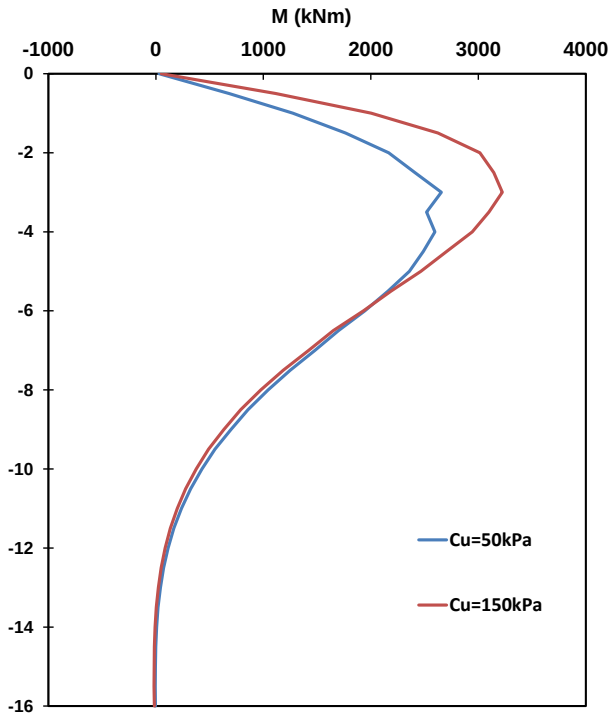

Figure 4.31. *Moment capacity under horizontal loading, for varying undrained shear strength*

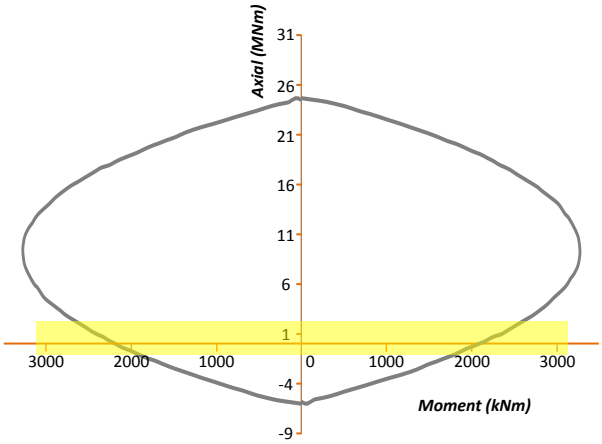

Figure 4.32. *The yellow area illustrates the range of influence of the axial force to the pile moment capacity, for different factors of safety, as shown in figures 4.26 & 4.28. It is shown that for a pile embedded in soft clay (Su=50kPa), no major change in pile bearing capacity is noticed*

Chapter 5

Application to Pile Group

5 Application to Pile Group

5.1 Limit Equilibrium Approach

The case of a fixed-head 3x3 Pile-Group embedded in clay with constant undrained shear strength Su is studied. According to the 2x2 mechanisms of failure, the equations for the 3x3 Pile-group are applied to find the failure load.

$$M_y = 9\,M_{pl_0} + \frac{9}{2}\left(N_{ys} - \frac{N}{9}\right) l$$

where M_{pl_0} is the moment capacity of pile with zero axial loading, N_{ys} is the axial pile capacity to: $\begin{cases}\text{compression } (N_c)\\ \text{tension } (N_t)\end{cases}$ and l is the length of the pile

5.2 Finite Element Verification

The problem studied is a 3x3 Pile-group subjected to combined vertical load N, horizontal load Q and overturning moment. The problem is analyzed as previously with the use of the advanced Finite Element code Plaxis 3D. Figure 5.1 shows the Finite Element Model. The size of the finite element mesh is 29x29x22 taking into consideration the effect of boundaries on the pile-group's ultimate response and the computational time. The piles have a diameter D=1 m and the distance between all the pile centers is 3 meters. A 9x9m plate is chosen as pile-cap, while a sensitivity analysis is performed to ensure the fixed pile/pile-cap connection, setting its elastic modulus equal to E=300*10^6 kPa and its thickness of 10 meter. The piles have the aforementioned properties, i.e. an elastic modulus of E=30*10^6, a specific weight γ=0.1kN/m^3, Poisson's ratio v=0.2 and its behavior is governed by the Mohr-Coulomb model with c = 15262 kPa, ϕ=0 and tension cut-off strength equal with 7534 kPa. Interfaces are placed between the piles and the soil enabling gapping and slippage with a friction coefficient R=1. The soil is Clay with γ=20kN/m^3 constant with the depth Su=50 kPa and Es=25000 kPa, obeying the Mohr-Coulomb model too and the Poisson's ratio is v=0.45 to simulate undrained conditions. The final model consists of 175000 elements with a finer discretization around the pile-group. The steps followed in the numerical experiments are similar to the previous investigation. The total failure Envelopes of the soil-foundation system are extracted by applying various horizontal load – moment combinations in the normal (θ=0°) and diagonal direction (θ=45°) for seven different safety factors from ultimate axial tensile to ultimate compressive capacity

5.3 Results

The application to the 3x3 Pile-group shows major differences depending to the undrained shear strength of the soil. Specifically, for the Pile-group embedded in soft clay with Su=50kPa, no major differences in moment capacity of the piles are observed (Fig. 5.10 and 5.12). However, in stiffer clay with Su=150kPa, where the piles reach close to the failure of their axial force capacity, wide divergence to the moment capacity of the piles in same row are noticed. (Fig. 5.19 and 5.21). Regarding the right pile, it reaches its maximum moment capacity as Fig. 5.22 shows, whereas the left pile, due to its tensile strength, develops almost zero moment.

Figures

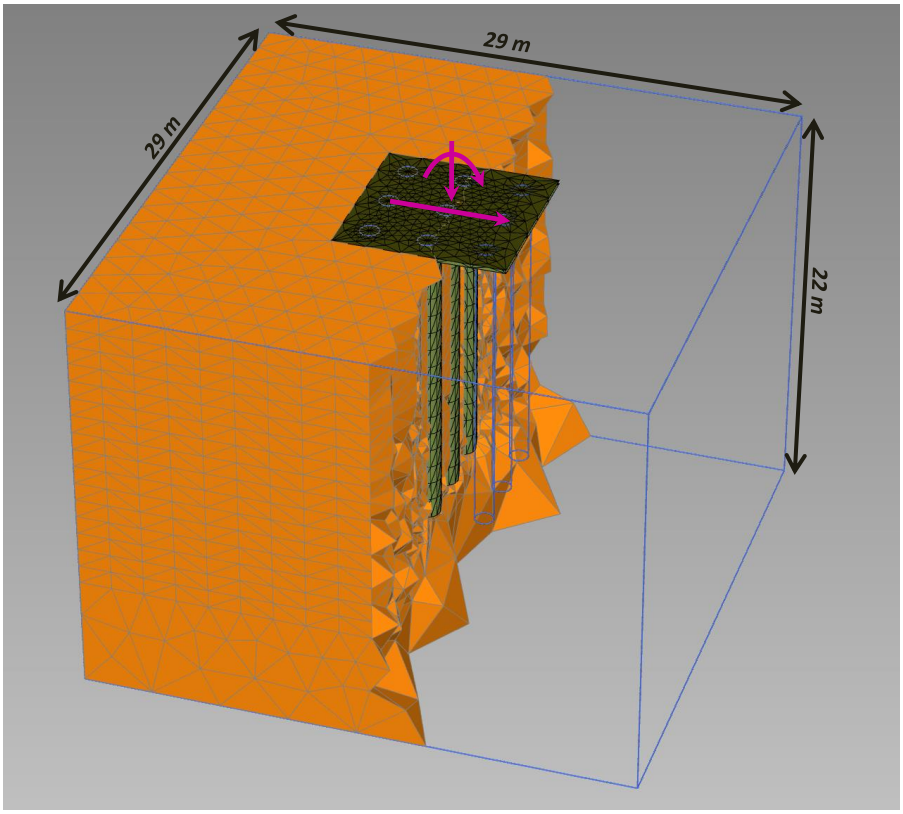

Figure 5.1. *The finite element model of 3x3 Pile-group, in clay*

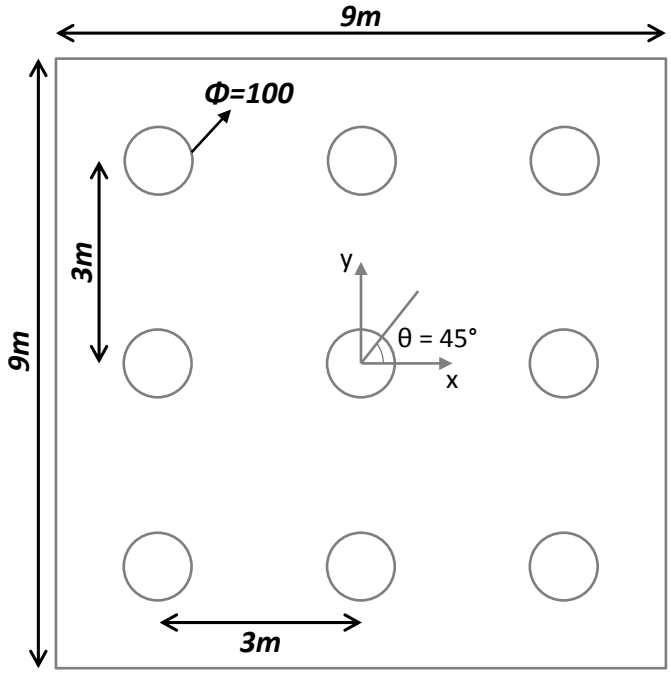

Figure 5.2. *Pile cap dimensions*

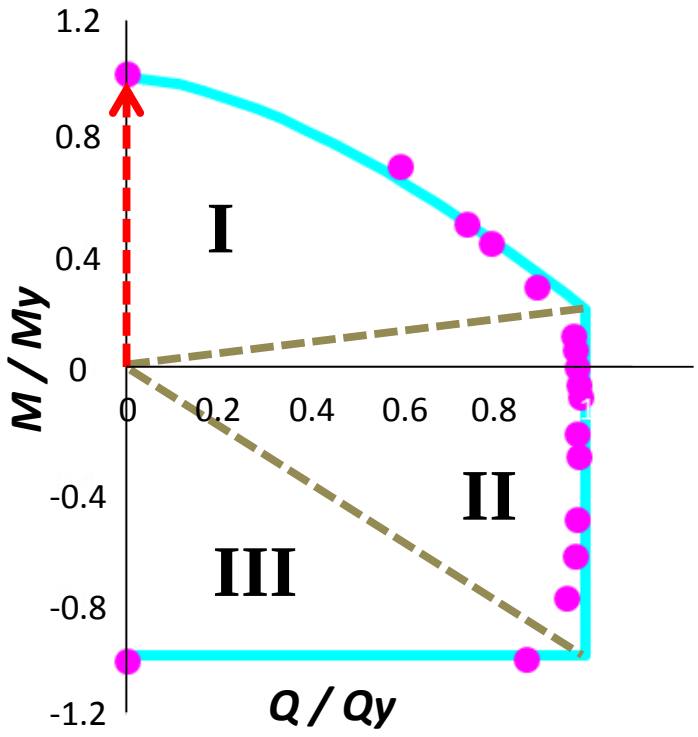

Figure 5.3. *Failure envelope of 2x2 Pile-group. The different regions define different failure mechanisms.*

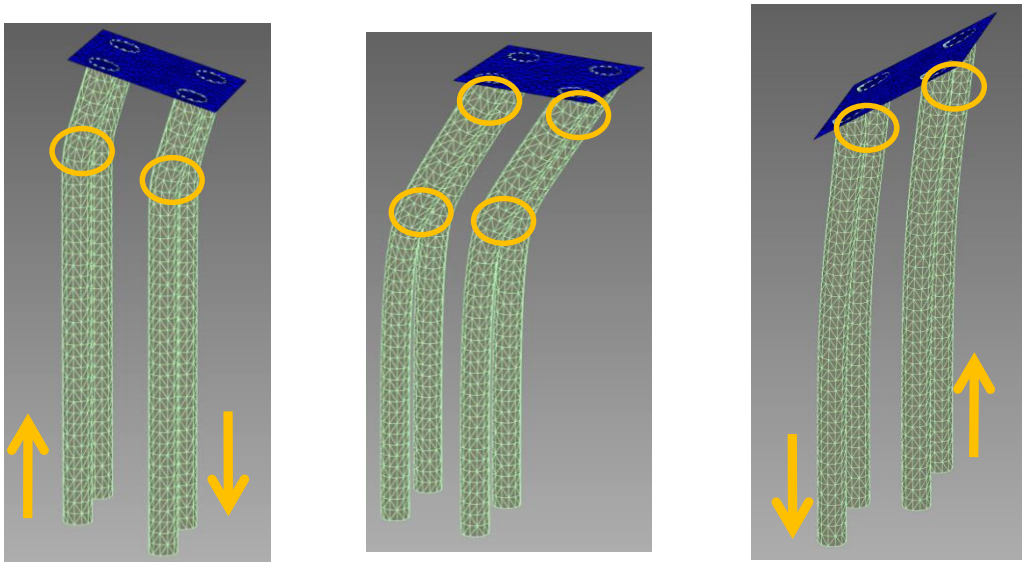

I Two plastic hinges below cap and bearing capacity failure

II Four Plastic Hinges at cap and below

I Two Cap plastic hinges and bearing capacity failure

Figure 5.4. *Illustration of the failure mechanisms for combinations of Q-M magnitudes in separate regions of the failure envelope.*

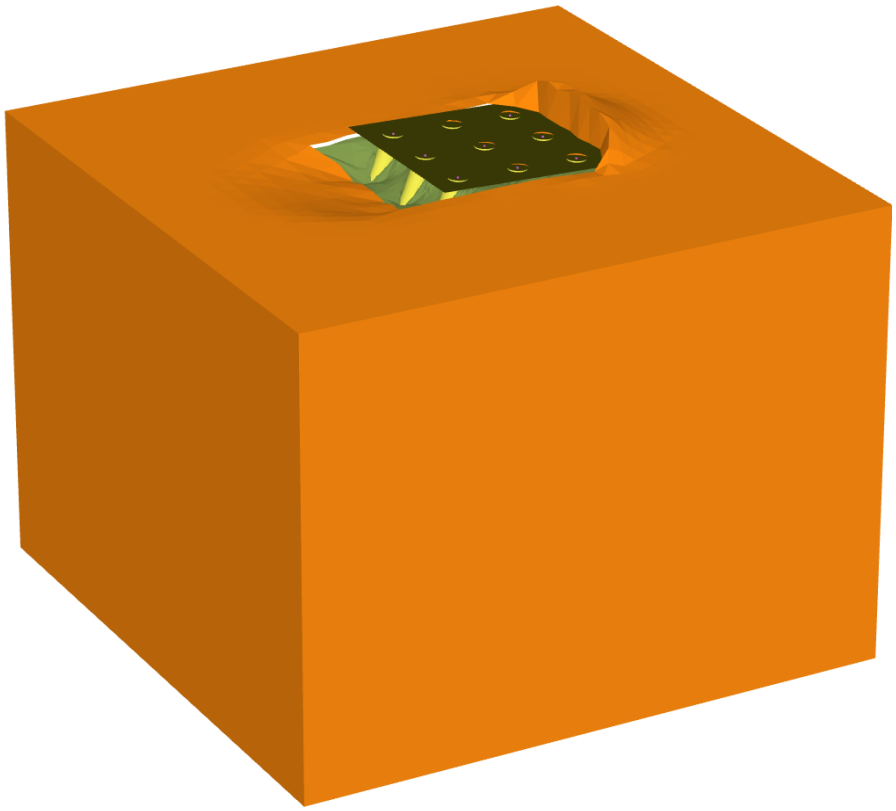

Figure 5.5. *The Pile-group mesh under horizontal loading and SF_v=2*

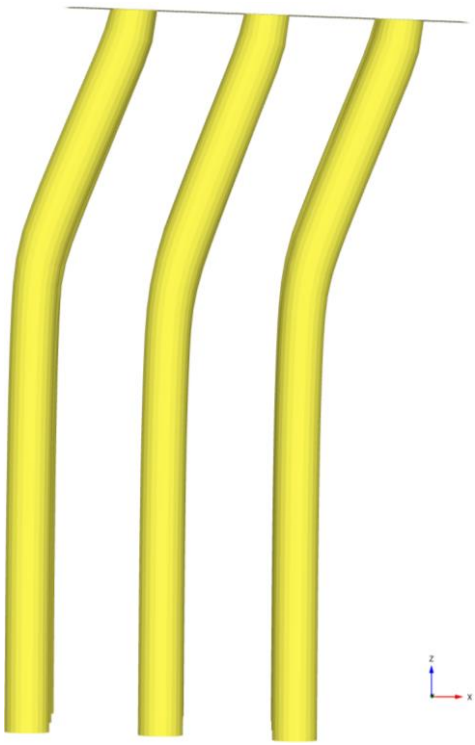

Figure 5.6. *Pile-group deformed mesh*

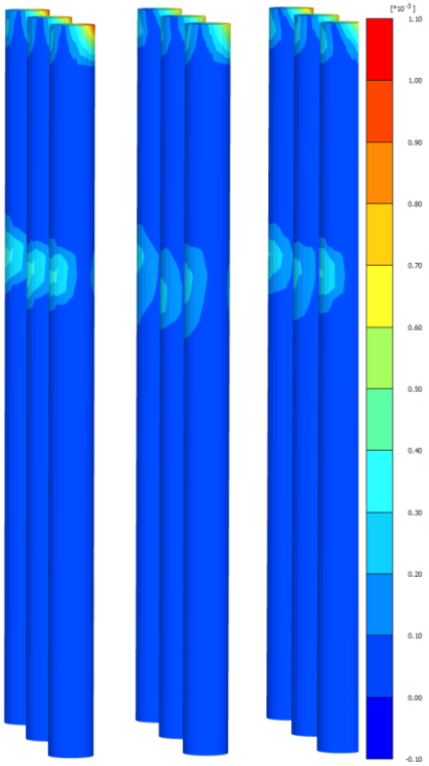

Figure 5.7. *Pile-group deviatoric strains ($\Delta\gamma_s$), which indicate the regions of the plastic hinges (2 in every pile)*

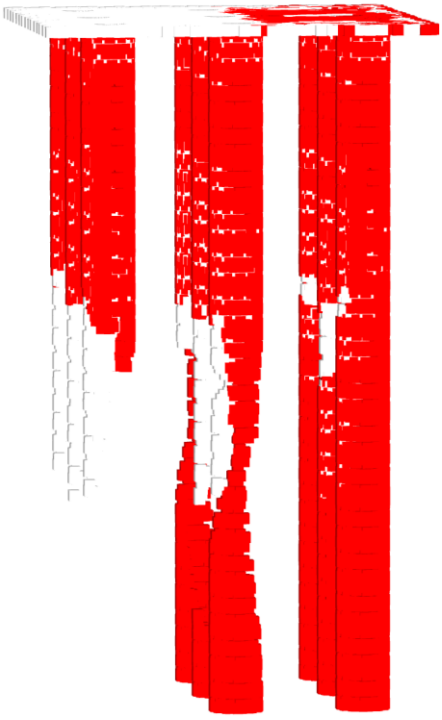

Figure 5.8. *Pile-group plastic points i.e. the plasticized Mohr – Coulomb points (red) and the tension cut-off points (white)*

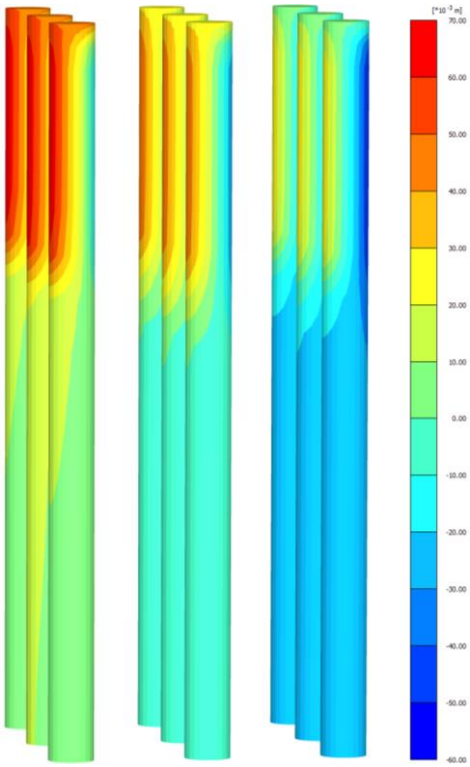

Figure 5.9. *Pile-group vertical deformations (u_z)*

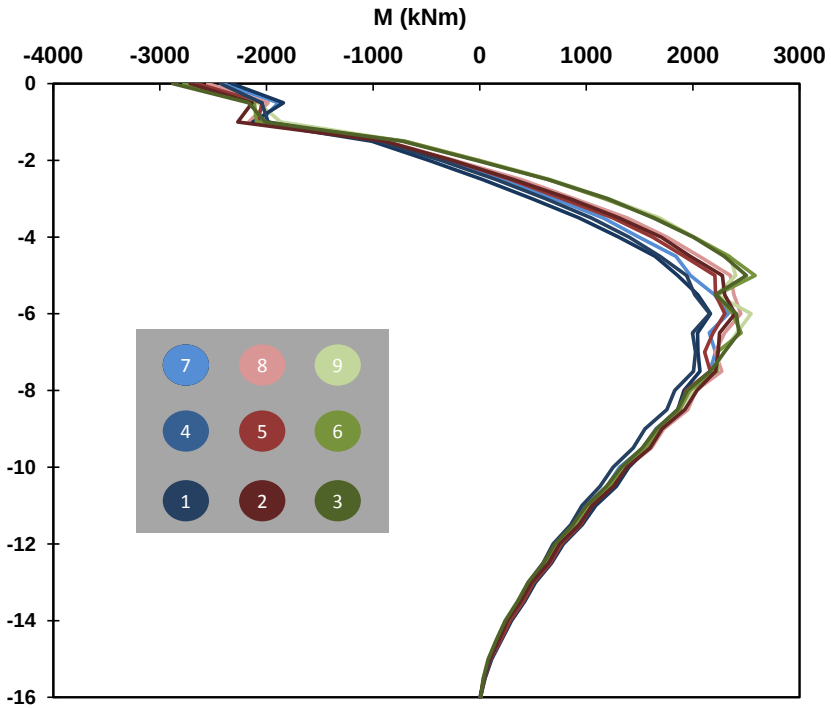

Figure 5.10. *Moment diagram of piles in Pile-group, embedded in clay with Su=50kPa and SF_v=2, under horizontal loading*

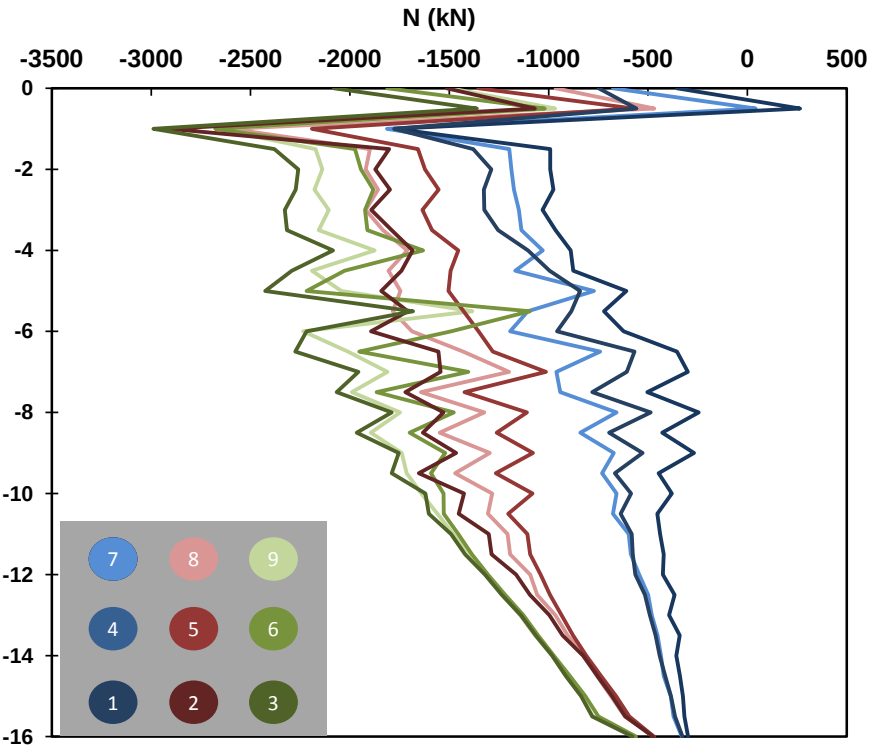

Figure 5.11. *Axial force of every pile. Pile-group embedded in clay with Su=50kPa*

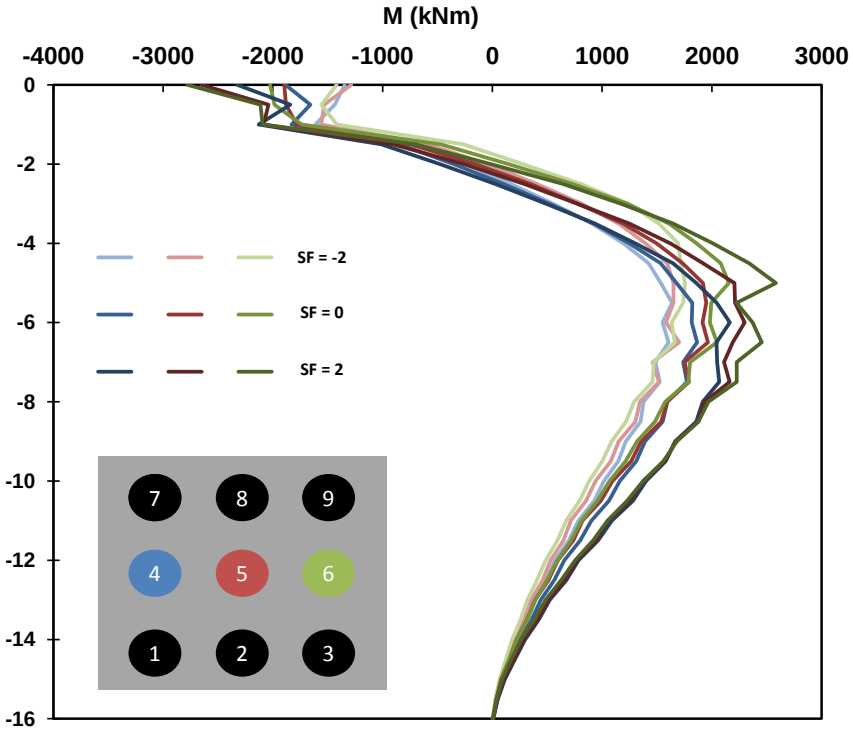

Figure 5.12. *Moment diagram of the three piles in middle row under different vertical loads (vertical factors of safety) of pile group embedded in clay with Su=50kPa*

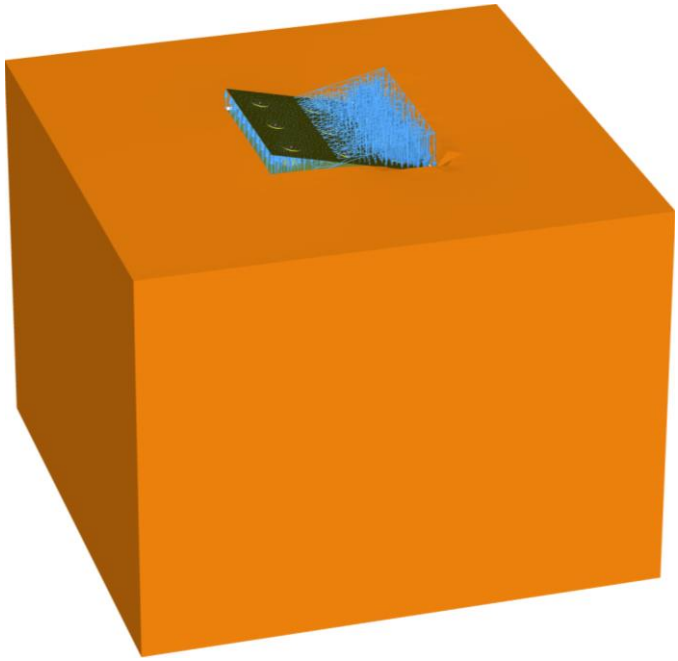

Figure 5.13. *Pile-group cluster with SF_v=5, embedded in stiff clay (Su=150kPa) subjected to bending moment*

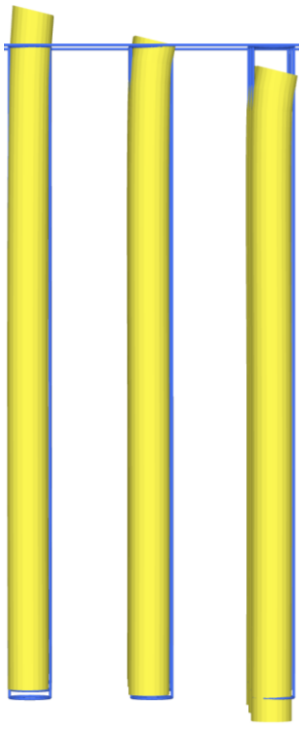

Figure 5.14. *Pile-group deformed mesh*

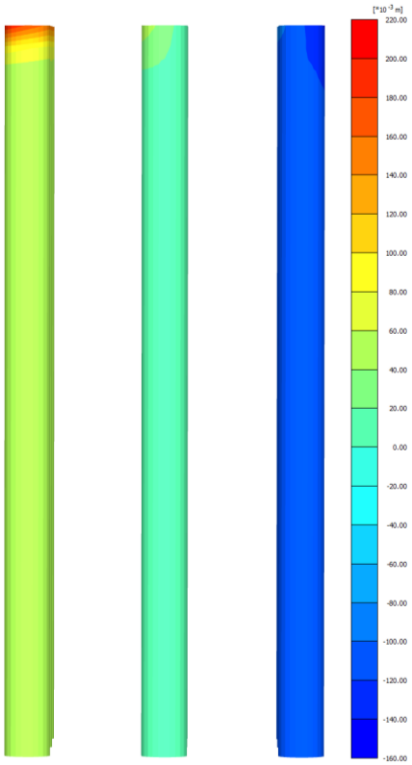

Figure 5.15. *Pile-group vertical deformations (u_z)*

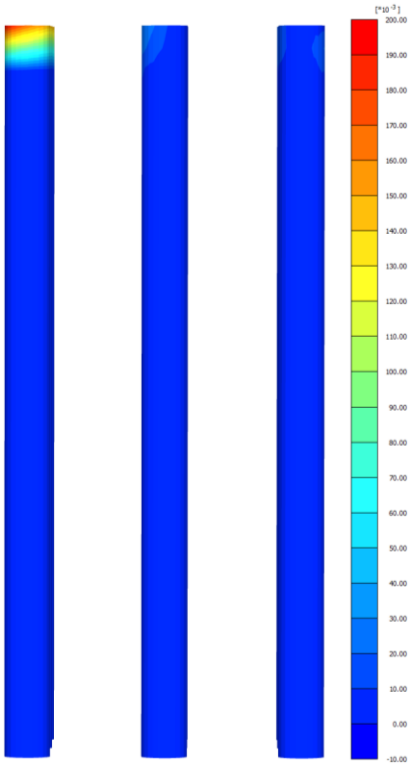

Figure 5.16. *Pile-group deviatoric strains ($\Delta\gamma_s$), which indicate the regions of the plastic hinges (1 at every top of pile)*

Figure 5.17. *Pile-group plastic points i.e. the plasticized Mohr – Coulomb points (red) and the tension cut-off points (white)*

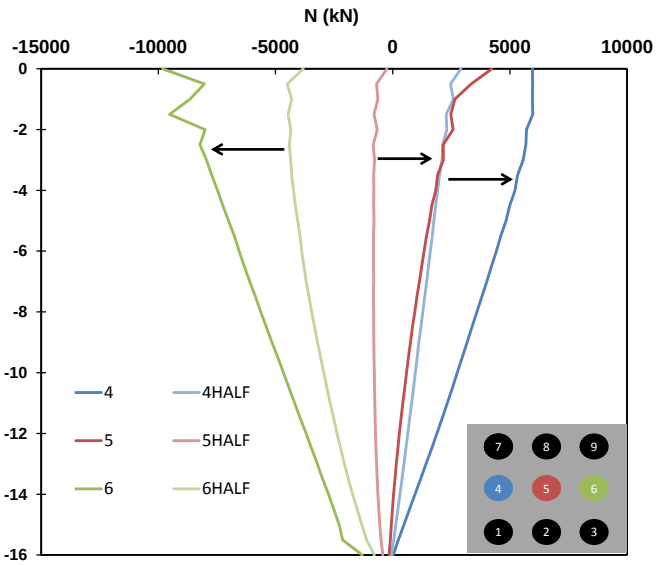

Figure 5.18. *Axial force of the middle row of Pile-group at half of failure loading and at failure*

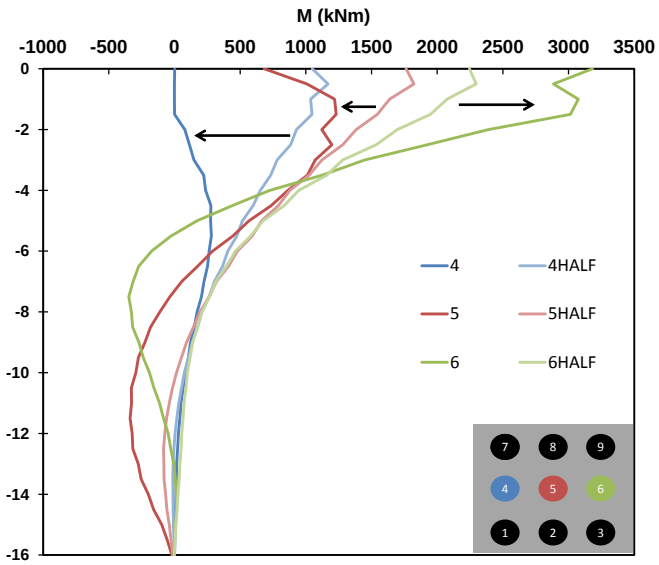

Figure 5.19. *Bending moment of the middle row of Pile-group at half of failure loading and at failure*

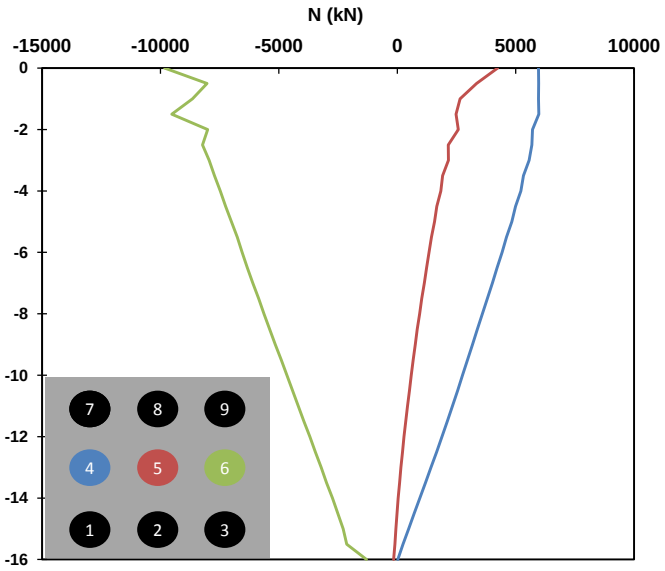

Figure 5.20. *Axial force of Pile-group middle row, embedded in clay with Su=150kPa and with SF_v=5*

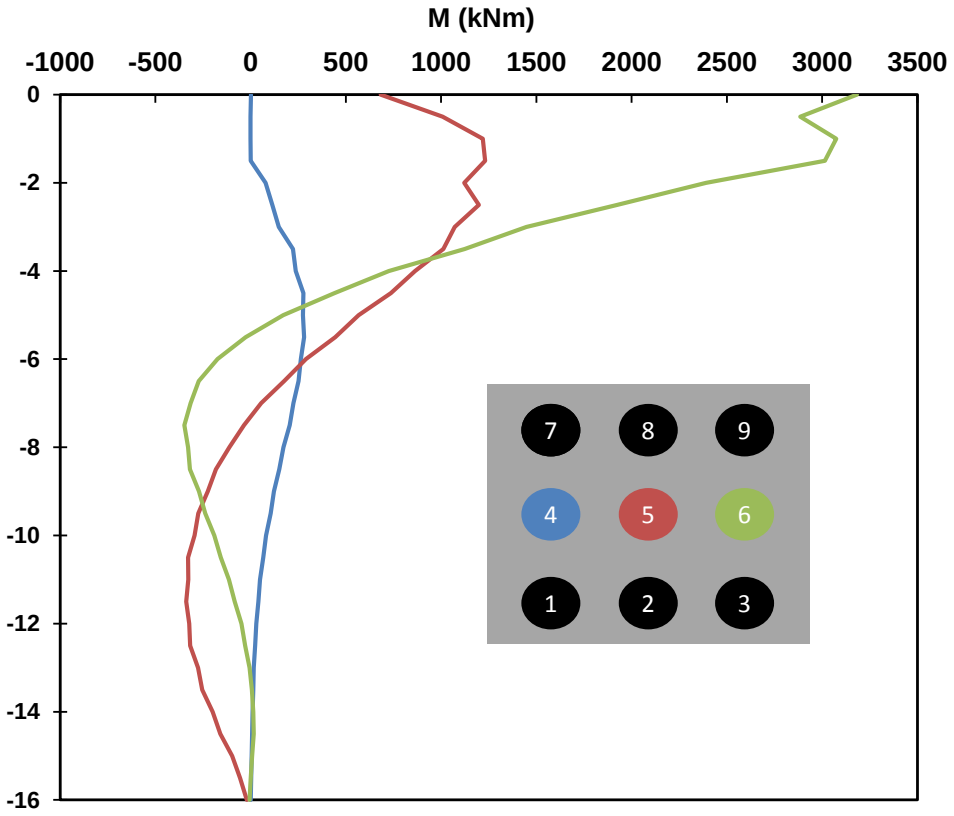

Figure 5.21. *Bending moment of Pile-group middle row embedded in clay with Su=150kPa and with SF_v=5. It is shown clearly the effect the different axial force to every pile has, to the moment distribution of the pile. Regarding the compressed right pile, the axial force reacts beneficial on the moment capacity, whereas, the axial force of the tensioned left pile has detrimental influence to the pile moment capacity*

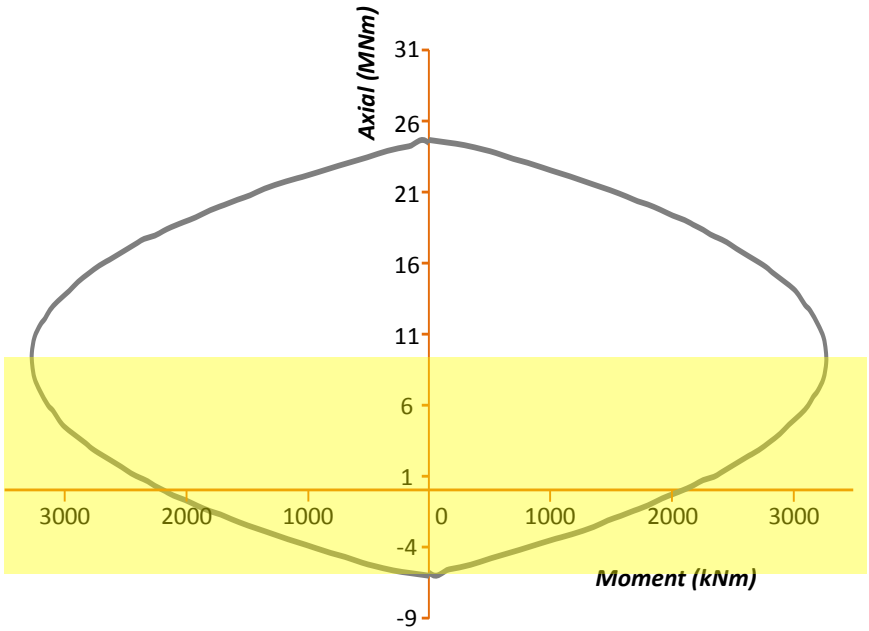

Figure 5.22. *The above-mentioned results of figure 3.21 are validated by this figure, where can be seen clearly the effect of the axial force to the moment capacity. The yellow area illustrates the range of the axial force of the Pile-group middle row, embedded in clay with Su=150kPa. Major changes are observed to the pile moment capacity according to the axial force of the pile.*

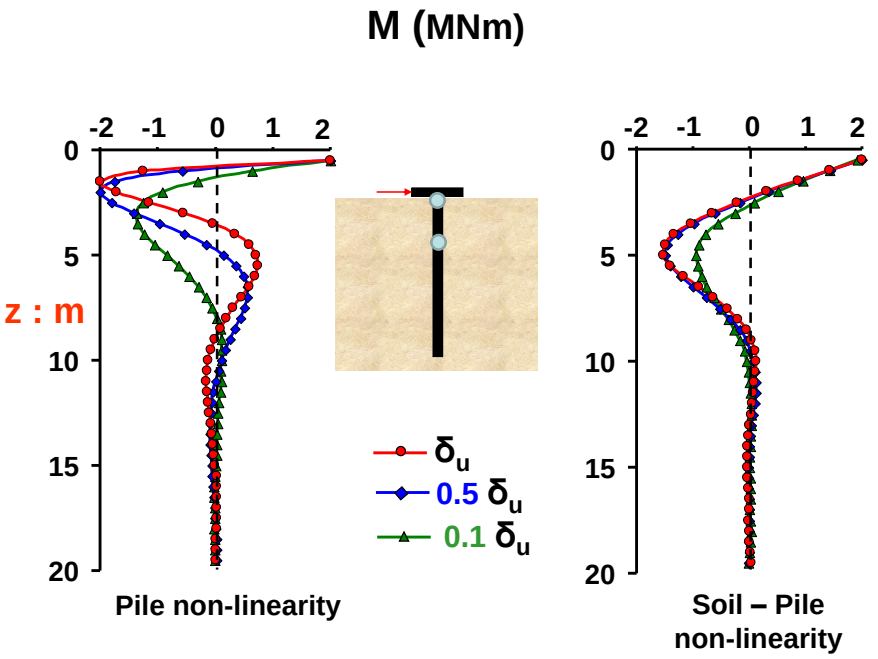

Figure 5.23. *As proposed to N. Gerolymos Ph.D. thesis, the two plastic hinges of fixed-head pile tend to approach one another near failure. This explains why the piles of the Pile-group of Fig. 5.16 have only one plastic hinge. The plastic hinges below cap tend to the pile head and at failure both plastic hinges coincide at pile head*

Chapter 6

Conclusions

5 Conclusions

This thesis dealt with the development of a new algorithm which calculates the pile response in terms of internal forces, under arbitrary loading. The implementation of the method was made to single pile as well as to pile-group loading, of nine piles in rectangular shape joined together with a pile cap. Both of which were subjected to static monotonic loading. The constitutive model of piles that is used is the Macroscopic Mohr-Coulomb based approach and the surrounding soil is undrained clay.

Our first aim was to develop a new approach able to simulate in finite element modeling the pile behavior accurately. Taking into consideration the drawbacks and weaknesses of the existing methods a new tool is designed capable of capturing the pile material properties and response in elasticity, in plasticity and incorporating the effects of random loading.

Our second aim was to develop a new method of extracting the structural forces of the pile that overcomes the drawbacks of the existing approaches and implement it to various load cases.

Our third aim was to provide insight to the failure envelopes of a single flexible pile and a 3x3 pile-group under combined M-Q-N loading, including the effects of soil-pile nonlinearities. The above-mentioned method was examined and compared with the existing approaches.

The important conclusions that were drawn from this thesis are presented below:

- A new macroscopic approach is developed under the Mohr-Coulomb i.e. Tresca failure criterion for simulating circular piles behavior. Its verification was focused in various concrete pile diameters (0.8m, 1m, 1.5m) with different reinforcements (1%, 1.5%, 2%), analytically and in finite element modelling. The results where more than satisfactory, as the approach is able to simulate the pile behavior in elastoplasticity, in terms of moment-curvature and to include the interaction between the external loads and the pile material properties, as well as the soil-pile interaction. The calibration of the approach can be easily be conducted through the following steps:

    1. Extraction of the failure envelope of the studied circular pile.

    2. Using the derived mathematical expressions and an optimization tool the calibration of the parameters of the model can be performed.

3. The variables are inserted in the finite element model in the appropriate soil model together with the other elastic pile parameters

4. Verification of the approach can be done by extracting the failure envelopes in the finite element program and comparing the moment-curvature diagrams.

- The new method of extracting pile forces is developed.The presentation of the pile response in terms of structural forces is an achievement of the beam theory and expresses the pile behaviour in a macroscopic level. However, this approach is subjected to the assumptions and simplifications of the beam theory (e.g. Bernoulli – Euler beam theory or Timoshenko beam theory). In view of this, the need of a tool is aroused, which incorporates the soil and pile behaviour and their interaction at an almost microscopic level and represents them in the same macroscopic terms of the beam theory: Axial and Shear force and Bending moment. On the contrary to any other existing method, this one takes into account the full pile geometry and every type of non-linearity of the soil – structure interaction i.e. the pile plastification, the soil non-linearity and non-linearities regarding the geometry of the model due to sliding and gapping. The pile is not treated as one-dimensional beam element and its response is not governed by the principals of beam theory. Instead, it stems from the continuous medium mechanics theory, because it manipulates the stresses that are extracted from the finite element simulation. This means that it is possible to take into account the interaction between the pile internal forces and the extent to which it influences the whole pile behaviour. Additionally, since the model takes into account the whole 3-D geometry of the soil – pile system, the pile-to-pile interaction is considered to its full extend. Hence, the actual pile behaviour is presented in a well-handled form and can be used for the design of the pile and its reinforcement.

- The failure envelopes of a single flexible pile in cohesive soil are derived. The pile is modeled by the previously derived approach. Various moment- lateral load combinations are applied under different safety factors against axial failure and the interaction diagrams are created. The correlation between the axial force and the bending capacity is examined among piles with same factor of safety and varying axial loading capacity.

- The interaction diagrams in 1x2 and 2x2 pile groups in cohesive soil are derived. From these two we make justifiable assumptions for the 3x3 pile-

group and examine its behaviour under different points of the failure envelope. First, the pile-group is examined in soft clay, where it cannot develop its axial capacity and minor differences between the stretched and the compressed pile response are noticed. On the contrary, the embedded pile-group in stiff clay, under the moment of failure, reveals a major difference to the stretched and compressed pile bearing capacity.

- The implementation of the new method gives an opportunity to examine the validity of the proposed Mohr-Coulomb failure criterion among varying types of loading and the extent to which, both of them correspond to each other and to reality as well.

Chapter 7

References

American Petroleum Institute (API), 2000, Recommended practice for planning, designing and constructing fixed offshore platforms-working stress design, API Recommended Practice 2A-WSD (RP 2A-WSD), 21st edn.

Broms, B. 1964. Lateral resistance of piles in cohesive soils. Journal of Soil Mechanics and Foundation Division, ASCE, 90(3): 27-63.

Comodromos EM and Papadopoulou MC (2012) "Response evaluation of horizontally loaded pile groups in clayey soils", Geotechnique, Vol. 62, No. 4, pp 329-39.

Correia A., Pecker A., Kramer S., Pinho R. 2012. A pile-head macro-element approach to seismic design of extended pile-shaft-supported bridges. 2nd International Conference on Performance-Based Design in Earthquake Geotechnical Engineering, Taormina, Italy, 28-30 May.

Crémer C, Pecker A, Davenne L. Cyclic macro-element for soil-structure interaction: material and geometrical non linearities. International Journal for Numerical and Analytical Methods in Geomechanics 2001; 25: 1257 – 1284.

Esmaeily A. 2001. USC-RC. Software for analyzing behavior of a single reinforced concrete member. Version 1.0.2, USC Civil Engineering Department.

Gerolymos N. & Gazetas G., Winkler model for lateral response of rigid caisson foundations in linear soil, Soil Dynamics and Earthquake Engineering, Volume 26, Issue 5, May 2006, Pages 347-361

Gerolymos N. & Gazetas G. 2005. Phenomenological model applied to inelastic response of soil–pile interaction systems. Soils and Foundations, 45(4): 119-132.

Gerolymos N., Papakyriakopoulos O., R. Brinkgreve 2014. Macroelement modeling of piles in cohesive soil subjected to combined lateral and axial loading

Giannakou, A., Gerolymos, N., Gazetas, G., Tazoh, T., and Anastasopoulos, I. (2010). ”Seismic Behavior of Batter Piles: Elastic Response.” J. Geotech. Geoenviron. Eng., 136(9), 1187–1199.

Hansen, J.B. (1970). "A revised and extended formula for bearing capacity." Danish Geotechnical Institute, Copenhagen, Denmark, Bulletin 28, pp. 5-11.

Harada T, Kubo K, Katayama T. Dynamic soil–structure interaction analysis by continuum formulation method. Report of the Institute of Industrial Science, vol. 29. The University of Tokyo; 1981 [issue no. 5].

Hill, R. 1950. The mathematical theory of plasticity. Clarenden Press, Oxford.

J.H. Atkinson (2007): “The Mechanics of Soils And Foundations”

Martin, C. M., Houlsby, G. T. 2000. Combined loading of spudcan foundations on clay: laboratory tests, Geotechnique, 50(4): 325-338.

Matlock, H. 1970. Correlations for design of laterally loaded piles in soft clay. Proc., 2nd Annual Offshore Technology Conference, Houston, Texas. 577-594.

Papakyriakopoulos O., Gerolymos N. (2013): Macroelement modeling of the non-linear response of piles and pile-groups subjected to combined lateral and axial loading, Diploma Thesis, NTUA

PLAXIS3D, 2012. Material Models Manual. Delft, The Netherlands: Plaxis b.v..

PLAXIS3D, 2012. Reference Manual. Delft, The Netherlands: Plaxis b.v..

PLAXIS3D, 2012. Scientific Manual. Delft, The Netherlands: Plaxis b.v..

PLAXIS3D, 2012. Tutorial. Delft, The Netherlands: Plaxis b.v..

Poulos H.G., Davis E.H., 1980, Pile Foundation Analysis and Design

Prager, W. (1959). An introduction to plasticity. Reading, MA: Addison-Wesley.

Randolph M.F. & Houlsby G.T. 1984. The limiting pressure on a circular pile loaded laterally in cohesive soil. Geotechnique, 34(4): 613-623.

Randolph, M. F. (1981): The response of flexible piles to lateral loading, Geotechnique, 31(2), 247-259

Reese LC, Cox WR, Koop FD (1974) Analysis of laterally loaded piles in sand. Proc., 6th annual offshore technology conference, Houston, Texas, pp 473–485

Roscoe KH, Schofield AN. The stability of short pier foundations on sand. British Welding Journal 1956; August: 343–354.

Roscoe, K.H. & Schofield A. N. 1956. The stability of short pier foundations on sand. Discussion. British Welding Journal, January: 12-18.

Schnabel PB, Lysmer J, Seed HB (1972) SHAKE—a computer program for earthquake response analysis of horizontally layered sites. EERC 72-12, Univ. of Calif., Berkeley

Sergey Edward Lyshevski, (2003): Rochester Institute of Technology Engineering and Scientific Computations Using MATLAB, John Wiley & Sons

Skempton, A.W. 1951. The bearing capacity of clays. In Proceedings of Building Research Congress, London. Vol. 1, pp. 180- 189

Tomilson M. J, Woodward J. (2007): “Pile Design and Construction Practice”

Varun, 2006. A simplified model for lateral response of caisson foundations, s.l.: s.n.

Walter Gander, Jiri Hrebicek (2004): Solving Problems in Scientific Computing Using Maple and MATLAB, Springer

APPENDIX

Slice method

```
clear
format long
P=xlsread('Plaxis_Mat.xlsx',3,'A3:E200');
P(:,3)=[];
CO_plaxis=unique(P(:,1:2),'rows','sorted');
last_plaxis = length(CO_plaxis);
X_plaxis=CO_plaxis(:,1);
Y_plaxis=CO_plaxis(:,2);
sigma_plaxis=zeros(size(X_plaxis));
shear_plaxis=zeros(size(X_plaxis));
for i=1:last_plaxis
    k=0;
    sum1=0;
    sum2=0;
    for j=1:length(P)
        if and(P(j,1)==CO_plaxis(i,1),P(j,2)==CO_plaxis(i,2))
            k=k+1;
            sum1=sum1+P(j,3);
            sum2=sum2+P(j,4);
        end
    end
    sigma_plaxis(i,1)=sum1/k;
    shear_plaxis(i,1)=sum2/k;
end
%
Xmax=round(max(P(:,1))*10)/10;
Xmin=round(min(P(:,1))*10)/10;
Ymax=round(max(P(:,2))*10)/10;
Ymin=round(min(P(:,2))*10)/10;
rad=linspace(0,1.999*pi,80)';
extsize=length(rad);
bounds=[((Xmax+Xmin)/2)+((Xmax-Xmin)/2+0.005)*cos(rad),
((Ymax+Ymin)/2)+((Ymax-Ymin)/2+0.005)*sin(rad)];
%
r=linspace(0,(Xmax-Xmin)/2,25);
theta=linspace(0,2*pi,80);
[r,theta]=meshgrid(r,theta);
x=(Xmax+Xmin)/2+r.*cos(theta);
y=(Ymax+Ymin)/2+r.*sin(theta);
F_sigma=scatteredInterpolant(X_plaxis,Y_plaxis,sigma_plaxis,'linear',
'nearest');
sigma=F_sigma(x,y);
%
F_shear=scatteredInterpolant(X_plaxis,Y_plaxis,shear_plaxis,'linear',
'nearest');
shear=F_shear(x,y);
%
x=reshape(x,[],1);
y=reshape(y,[],1);
sigma=reshape(sigma,[],1);
shear=reshape(shear,[],1);
Ptemp=[x,y];
[COtemp,ia,ic]=unique(Ptemp,'rows','sorted');
sigmatemp=zeros(size(ia));
for i=1:length(ia)
```

```
    sigmatemp(i)=sigma(ia(i));
end
sigma=[zeros(extsize,1); sigmatemp];
sheartemp=zeros(size(ia));
for i=1:length(ia)
    sheartemp(i)=shear(ia(i));
end
shear=[zeros(extsize,1); sheartemp];
CO=[bounds;COtemp];
last = length(CO);
X=CO(:,1);
Y=CO(:,2);
[v,c]=voronoin([X(:) Y(:)]);
figure;
voronoi(X,Y)
 plabels = arrayfun(@(n) {sprintf('P%d', n)}, (1:last)');
 Hpl = text(X, Y, plabels, 'FontWeight', ...
       'bold', 'HorizontalAlignment','center', ...
       'BackgroundColor', 'none');
 dA=zeros(last-extsize,1);
for i=(extsize+1):last
    dA(i)=polyarea(v(c{i},1),v(c{i},2));
end
A=sum(dA);
title(['Area = ' num2str(A)],'fontsize',14);
set(gca,'fontsize',14);
set(gcf, 'Position', get(0,'Screensize'));
dN=zeros(last-extsize,1);
for i=(extsize+1):last
    dN(i)=dA(i)*sigma(i);
end
N=sum(dN);
%
coeff=polyfit(X((extsize+1):last),sigma((extsize+1):last),1);
%To X_plaxis den exei extsize
x0=coeff(1,2)/(-coeff(1,1));
dM=zeros(last-extsize,1);
%
 for i=(extsize+1):last
     dM(i)=dA(i)*sigma(i)*((Xmax+Xmin)/2-X(i));
 end
 M=sum(dM);

dQ=zeros(size(X_plaxis));
dQ((extsize+1):last)=dA((extsize+1):last).*shear((extsize+1):last);
Q=sum(dQ);
NMQ=[N;M;Q]
```

Volume Method

```
clear all
format long
P=xlsread('Plaxis_Mat.xlsx',5,'D2:H6437');
COtemp=P(:,1:3);
sigmatemp=P(:,4);
sheartemp=P(:,5);
[CO_plaxis,ia,ic]=unique(COtemp,'rows','sorted');
%last_plaxis = length(CO_plaxis);
sigma_plaxis=zeros(size(ia));
shear_plaxis=zeros(size(ia));
for i=1:length(ia)
    sigma_plaxis(i)=sigmatemp(ia(i));
    shear_plaxis(i)=sheartemp(ia(i));
end
X_plaxis=CO_plaxis(:,1);
Y_plaxis=CO_plaxis(:,2);
Z_plaxis=CO_plaxis(:,3);

Xmax=round(max(X_plaxis)*10)/10;
Xmin=round(min(X_plaxis)*10)/10;
Ymax=round(max(Y_plaxis)*10)/10;
Ymin=round(min(Y_plaxis)*10)/10;
Zmax=round(max(Z_plaxis));
Zmin=round(min(Z_plaxis));
rad=linspace(0,1.999*pi,80)';
extsize=length(rad);
bounds=[((Xmax+Xmin)/2)+((Xmax-Xmin)/2+0.005)*cos(rad),
((Ymax+Ymin)/2)+((Ymax-Ymin)/2+0.005)*sin(rad)];

r=linspace(0,(Xmax-Xmin)/2,25);
theta=linspace(0,2*pi,80);
zeta=linspace(Zmax,Zmin,abs(Zmin-Zmax)+1)';
zeta1=zeta;
[r,theta,zeta]=meshgrid(r,theta,zeta);
xgrid=(Xmax+Xmin)/2+r.*cos(theta);
ygrid=(Ymax+Ymin)/2+r.*sin(theta);

F_sigma =
scatteredInterpolant(CO_plaxis,sigma_plaxis,'linear','nearest');
sigmagrid = F_sigma(xgrid,ygrid,zeta);
F_shear =
scatteredInterpolant(CO_plaxis,shear_plaxis,'linear','nearest');
sheargrid = F_shear(xgrid,ygrid,zeta);
NMQ=zeros(3,size(zeta,3));
for I=1:size(zeta,3)
    xloop=reshape(xgrid(:,:,I),[],1);
    yloop=reshape(ygrid(:,:,I),[],1);
    sigmaloop=reshape(sigmagrid(:,:,I),[],1);
    shearloop=reshape(sheargrid(:,:,I),[],1);
    Ploop=[xloop,yloop];
    [COloop,ia,ic]=unique(Ploop,'rows','sorted');
```

```
    sigmalooptemp=zeros(size(ia));
    shearlooptemp=zeros(size(ia));
    for i=1:length(ia)
        sigmalooptemp(i)=sigmaloop(ia(i));
        shearlooptemp(i)=shearloop(ia(i));
    end
    sigma=[zeros(extsize,1); sigmalooptemp];
    shear=[zeros(extsize,1); shearlooptemp];
    CO=[bounds;COloop];
    last = length(CO);
    X=CO(:,1);
    Y=CO(:,2);
    [v,c]=voronoin([X(:) Y(:)]);
    %figure;
    %voronoi(X,Y)
    plabels = arrayfun(@(n) {sprintf('P%d', n)}, (1:last)');
    Hpl = text(X, Y, plabels, 'FontWeight', ...
        'bold', 'HorizontalAlignment','center', ...
        'BackgroundColor', 'none');
    dA=zeros(last-extsize,1);
    for i=(extsize+1):last
        dA(i)=polyarea(v(c{i},1),v(c{i},2));
    end
    A=sum(dA);
    title(['Area = ' num2str(A)]);
    dN=zeros(last-extsize,1);
    for i=(extsize+1):last
        dN(i)=dA(i)*sigma(i);
    end
    N=sum(dN);
    coeff=polyfit(X(extsize+1:last),sigma(extsize+1:last),1);
    x0=coeff(1,2)/(-coeff(1,1));
    dM=zeros(last-extsize,1);

    for i=(extsize+1):last
        dM(i)=dA(i)*sigma(i)*((Xmax+Xmin)/2-X(i));
    end
    M=sum(dM);
    dQ=zeros(last-extsize,1);

dQ((extsize+1):last)=dA((extsize+1):last).*shear((extsize+1):last);
    Q=sum(dQ);
    NMQ(:,I)=[N;M;Q];
end
%Visualizations
subplot(1,3,1);
plot(NMQ(1,:),zeta1,'-b*','LineWidth',2,'MarkerSize',8);
hold on
plot([0 0],[Zmax Zmin], 'k:');
title('Axial Force (N)', 'FontSize', 20);
xlabel('(kN)','FontSize',16);
ylabel('Depth (m)','FontSize',16);
set(gca,'XAxisLocation','top','YAxisLocation','left','fontsize',14);
hold off
subplot(1,3,2);
plot(NMQ(2,:),zeta1,'-r*','LineWidth',2,'MarkerSize',8);
hold on
plot([0 0],[Zmax Zmin], 'k:');
title('Bending Moment (M)', 'FontSize', 20);
xlabel('(kNm)','FontSize',16);
ylabel('Depth (m)','FontSize',16);
```

```
set(gca,'XAxisLocation','top','YAxisLocation','left','fontsize',14);
hold off
subplot(1,3,3);
plot(NMQ(3,:),zeta1,'-g*','LineWidth',2,'MarkerSize',8);
hold on
plot([0 0],[Zmax Zmin], 'k:');
title('Shear Force (Q)', 'FontSize', 20);
xlabel('(kN)','FontSize',16);
ylabel('Depth (m)','FontSize',16);
set(gca,'XAxisLocation','top','YAxisLocation','left','fontsize',14);
set(gcf,'Color',[0.8,0.8,0.8],'Toolbar','none')
set(gcf, 'Position', get(0,'Screensize'));
hold off

%Stress distribution
[x_rec, y_rec, z_rec] =
meshgrid(linspace(Xmin,Xmax,100),linspace(Ymin,Ymax,100),linspace(Zma
x,Zmin,abs(Zmin-Zmax)/2+1));
sigma_rec = griddata(xgrid,ygrid,zeta,sigmagrid,x_rec,y_rec,z_rec);
shear_rec = griddata(xgrid,ygrid,zeta,sheargrid,x_rec,y_rec,z_rec);

figure;
slice(x_rec,y_rec,z_rec,sigma_rec,[],[],[Zmax:-1:Zmin]);
axis ([Xmin Xmax Ymin Ymax Zmin Zmax]);
axis equal
title('Normal Stress (kPa)');
set(gcf,'Color',[0.4,0.4,0.4])
colorbar
zoom (3)
pan on
set(gcf, 'Position', get(0,'Screensize'));
figure;
slice(x_rec,y_rec,z_rec,shear_rec,[],[],[Zmax:-1:Zmin]);
axis ([Xmin Xmax Ymin Ymax Zmin Zmax]);
axis equal
title('Shear Stress (kPa)');
set(gcf,'Color',[0.4,0.4,0.4])
colorbar
zoom (3)
pan on
set(gcf, 'Position', get(0,'Screensize'));
```